Roinn Cumarsáide, Gníomhaithe ar son na hAeráide & Comhshaoil
Department of Communications, Climate Action & Environment

Geological Survey
Suirbhéireacht Gheolaíochta
Ireland | Éireann

Research Programme
- Short Calls, Final Report -

Lead Applicant Name	Paul Doherty
Email	pdoherty@gdgeo.com
Host Organisation name	Gavin and Doherty Geosolutions Ltd.
Project Title	Scour Potential Evaluation of the Western Irish Sea Mud Belt (SCOPE)
Contract Number	2017-SC-035

Date: 31/05/2018

This report covers the period November 1st 2017 to May 31st 2018

2. (a) Project information:

Final project report (*max **2500** words, excluding figures and headings*):

(i) *Progress* of objectives and scientific/engineering targets beyond the state of the art & *methods* used

Gavin and Doherty Geosolutions Ltd. (GDG) has performed an evaluation of the potential for scour within the Western Irish Sea Mud Belt (WISMB). The WISMB is an area off the East coast of Ireland that has been identified for offshore wind development, which is likely to be exploited in the coming years as Ireland strives to achieve its renewable energy targets. It is estimated that 1000 MW of offshore wind energy will need to be installed in Irish waters by 2020 in order to meet a target of 40% electricity generation from renewable sources. Scour is the process of seabed erosion due to the imposed shear stress generated by the sea current and / or waves, which has been identified as a key feature of the Irish Sea (BGS, 2015). The placing of infrastructure, such as wind turbine foundations, on the seabed floor, typically results in increases in current velocities and, consequently, induced local scour. An accurate prediction of scour potential is important for marine developments, particularly for offshore wind farms since scour may compromise the structural stability of the turbine and foundation, and may also impact marine habitats. As such, scour represents a significant geological hazard from both an engineering and an environmental perspective.

This study has focused on a scour evaluation for the WISMB, which comprises an area of approximately 565 m^2 that extends from the East coast of Ireland to the Isle of Man and to Lambay Island to the south (see Figure 1). The WISMB is located along a distinct migratory pathway with strong tidal currents that lead to sediment transport. Since little or no information is currently available regarding the potential for scour within this region, the aim of this study was to provide a scour assessment for the WISMB that can be used to inform engineering activities in this region, supporting offshore wind development, whilst ensuring minimal environmental impact.

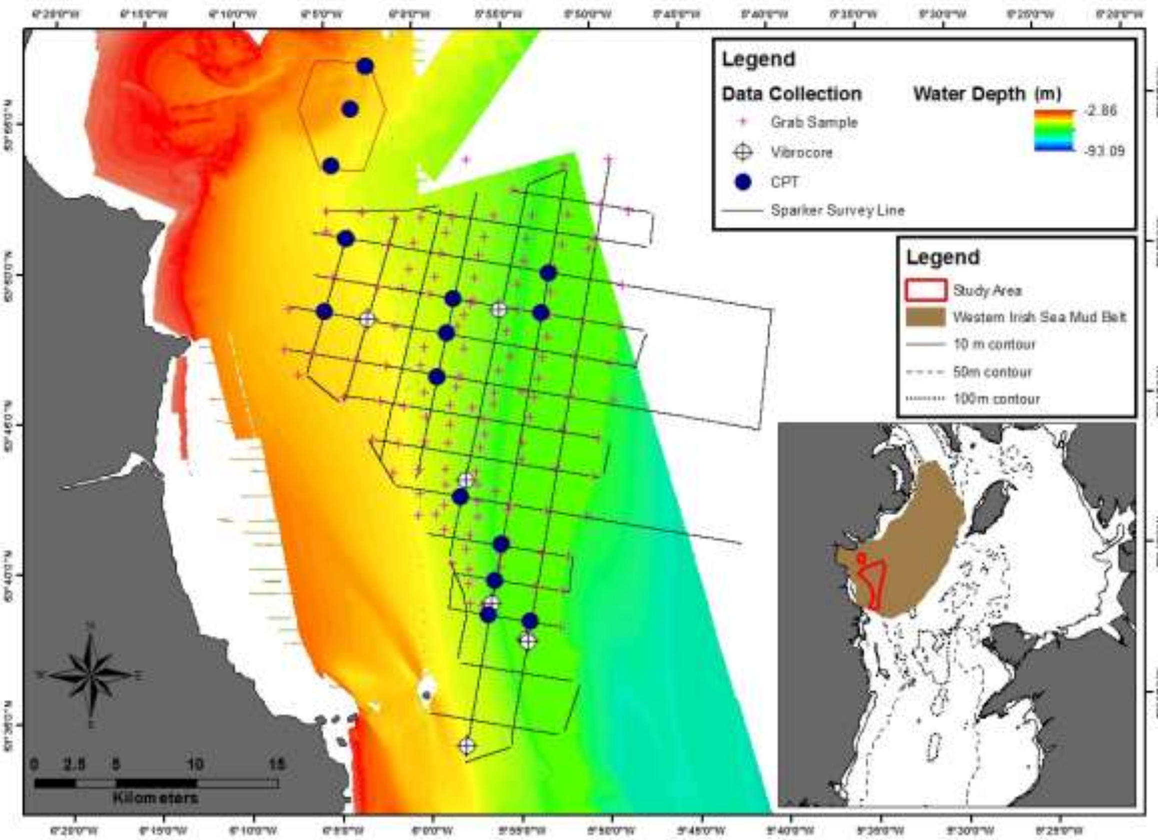

Figure 1 Inset map: Location of the WISMB in the Irish Sea. Also highlighted are the main study areas. Main map: highlighted study areas expanded showing data collection points.

This project has conducted a scour assessment specifically for the WISMB. A significant amount of data that was previously gathered for this region was analysed to identify the potential for scour occurrence in this region. Guidelines and recommendations for future scour assessments to support sustainable offshore wind development are also provided.

(ii) Implementation (please include any issues with timelines, milestones, management etc. or deviations from the original implementation plan)

An analysis of shipwrecks in this region highlighted that, despite being a low-energy environment with no natural scour, the introduction of an object to the seabed within the WISMB can induce scour. Furthermore, the suggested vectors of flow derived from these scour signatures would suggest that local conditions are more complex than the simplified model offered by Uehara et al. (2006). That said, there is a relatively decent correlation between the level of scour at a geographic location and the magnitude of bed stress suggested by Uehara et al. (2006) as evidenced by a propensity for more extensive scour in the south, diminishing heading north. Granted, this may also be a factor of the time the object has been resting on the seabed and the seabed sediment parameters. That considered, the majority of wrecks used in this study date from roughly the same year (early 1900s) and we have already demonstrated the homogenous nature of seabed sediment in the WISMB.

Whitehouse (1998) proposed a general framework to predict the likelihood of scour in the vicinity of marine structures, which was employed in this study. This methodology requires three environmental inputs: waves, currents and sediment. The methodology calculates bed shear stress for waves (τ_w), tidal currents (τ_c) and a combination of both (τ_{max}). These stress values are then compared to the critical stress threshold (τ_{cr}) for inducing sediment mobility. It assumes that scour occurs where shear stress amplification occurs adjacent to the structure and is defined by a shear stress amplification factor, M. M is defined as the ratio of local shear stress, $\tau_{0,\ local}$, to the ambient shear stress, $\tau_{0,\ ambient}$, a value generally varying between 4 and 9, depending on the shape and size of the structure.

A preliminary scour assessment was carried out according to the deterministic approach outlined by Whitehouse (1998). This involved the input of site data to determine the susceptibility of the seabed to wave- and/or current-induced scour. The analysis took into account the seasonal variability of the wave climate condition in the broader WISMB area (Table 1), as well as, spatial distribution of water depth and sediment size as obtained during previous ground truthing campaign at different core locations (Table 2).

Table 1 Seasonal averages for wave climate parameters (based on wave data from M2 buoy)

Year	Time of year	Wave Period (s)	Wave Height (m)
2013-2018	Jan - Mar	4.6	1.56
	Apr - Jun	4	0.86
	Jul - Sept	3.9	0.85
	Oct - Dec	4.5	1.48

Table 2 D50 sediment-size and water depth at core locations

Location	d50 (µm)	Water depth (m)
VC1a	62	29.5
VC1b	65	29.5
VC2	25	40
VC3a	59	36.4
VC3b	50	36.4
VC4a	109	41
VC4b	100	41

In order to assess the sediment mobility potential in the WISMB area, the values of critical bed shear stress, τ_{cr}, were first calculated at different core locations. The results were then compared against the wave-induced bed shear stress values, τ_w, to inform the susceptibility of the seabed to scour due to wave effects. The impact of currents was subsequently incorporated in the analysis by back-calculating the minimum (depth-averaged) current velocities, $\overline{U}_{cr}$, required to mobilise the sediments.

(iii) Outputs (please provide a short description *and* complete the table below)

The sediments of the Western Irish Sea Mud Belt can be divided, generally, into two units: a lower, highly heterogeneous, glacial deposit and a homogenous, fine-grained marine deposit. The latter of which was the primary focus of this study with respect to scour susceptibility. The fine-grained marine sediments are found at the surface and to a depth of between 0.8 and 26.5 mbsl. The sediments appear to be under-consolidated with relatively low shear strength. At the surface, sediments show a general trend of fining northward across the stud area.

Previously, it was suggested that the current speeds in the WISMB were insufficient to mobilise sediment and initiate scour without obstruction (Callaway et al., 2009; Holmes & Tappin, 2005). However, the analysis suggested that wave induced bed stresses are sufficient to generate sediment mobility without the necessity of relatively strong tidal currents.

The presence of obstacles on the seabed in the WISMB can generate significant amounts of scour with scour signatures revealing variations in localised seabed hydrodynamics, which, very often, are at odds with generalised regionalised modelled output. This suggests that local phenomena could have a strong effect on hydrodynamics and, hence, sediment mobility and scour. In this instance, the development of a seasonal gyre in the WISMB could be significant in variation in WISMB seabed hydrodynamics. The analysis suggested that the presence of wind turbine foundations would have a significant effect on lowering sediment mobility thresholds.

After previous qualitative studies (notably Callaway et al. (2009) and Caston (1975)), this study was the first attempt at quantifying the scour potential of sediments in the WISMB. Based on this summary, we conclude the following:

1. Sediments in the WIMSB are generally fine-grained and geotechnically relatively weak;
2. These sediments are generally not mobile within the area but can be susceptible to scour when seabed obstacles perturb the hydrodynamic regime;
3. The hydrodynamic regime in the WIMSB is more complicated than outlined in previous regional models with seasonal, local phenomena (e.g. a gyre) potentially having a strong effect;
4. There is significant scope for utilising shipwreck scour signatures in verifying future modelling efforts;
5. Wave induced bed shear stresses may play a more important role in seabed sediment mobility than previously noted by previous authors, reducing the necessity of (relatively) strong current velocities to initiate sediment mobility.

To these conclusions, we add the following caveats:

1. Due to the lack of information in the WIMSB, the metocean data used in this study involved a degree of spatial extrapolation, and therefore, may not fully represent the site conditions;
2. Grain-size parameters based on core analysis were taken from a limited geographic distribution across the study site and may not be fully representative of ground conditions.

While the current study provides valuable insights into the potential for sediment mobility in the WISMB area, the scour susceptibility predictions shall still be viewed as first estimates due to the limited site data available and the preliminary methodology adopted. It is therefore expected that the findings may be subject to alterations upon the availability of more accurate site specific data and the adoption of detailed scour modelling techniques.

Task No.	Deliverable description	Planned delivery (as per proposal)	Date of delivery
1	Desk Study Report	Month 2	Completed
2	Scour Assessment for WISMB (including maps and digital data set)	Month 4	Completed
3	Guidelines and Recommendations	Month 6	Completed

Publications to date:

None to date, however it is intended to publish the research outcomes at a later date.

4. Data/outputs submitted with final report *(please list the documents, presentations, datasets etc. submitted with this report)*

a. Detailed report of scour assessment for WISMB.

GDG
GAVIN & DOHERTY
GEOSOLUTIONS

Scour Potential Evaluation of the Western Irish Sea Mud Belt

Geological Survey
Suirbhéireacht Gheolaíochta
Ireland | Éireann

GAVIN AND DOHERTY GEOSOLUTIONS LTD
UNIT 2A NUTGROVE OFFICE PARK,
RATHFARNHAM, DUBLIN 14, D14 X627 IRELAND
Tel: +353 1 207 1000 | www.gdgeo.com

Project Title:	SCOPE: Scour Potential Evaluation of the Western Irish Sea Mud Belt
Report Title:	Scour Potential Evaluation of the Western Irish Sea Mud Belt
Document reference:	17120 – SCOPE Report - 2018

Document Control

Revision	Date	Authored:	Checked:	Approved:
01	30/05/2018	MC/JC/SJ	PD	PD

Table of Contents

List of Parameters

d	Grain size
D	Diameter of foundation
g	Acceleration of gravity
h_s	Height of Foundation
s	Relative unit weight of sediment grain
Smax	Maximum scour depth for cylinder
St	Scour Depth at time t
S_0	Equilibrium Scour Depth
t	Time
T	Time scale
T*	Non dimensional time
θ	Shields Parameter

1 Introduction

Gavin and Doherty Geosolutions Ltd. (GDG) has performed an evaluation of the potential for scour within the Western Irish Sea Mud Belt (WISMB). The WISMB is an area off the East coast of Ireland that has been identified for offshore wind development, which is likely to be exploited in the coming years as Ireland strives to achieve its renewable energy targets. It is estimated that 1000 MW of offshore wind energy will need to be installed in Irish waters by 2020 in order to meet a target of 40% electricity generation from renewable sources.

In order for Ireland to successfully exploit its offshore wind resource as a sustainable energy source, reliable designs must be provided that minimise the associated environmental impacts. One potential impact of offshore wind development on the environment is the development of scour. Scour is the process of seabed erosion due to the imposed shear stress generated by the sea current and / or waves, which has been identified as a key feature of the Irish Sea (BGS, 2015). The placing of infrastructure, such as wind turbine foundations, on the seabed floor, typically results in increases in current velocities and, consequently, induced local scour. An accurate prediction of scour potential is important for marine developments, particularly for offshore wind farms since scour may compromise the structural stability of the turbine and foundation, and may also impact marine habitats. As such, scour represents a significant geological hazard from both an engineering and an environmental perspective.

This project has conducted a scour assessment specifically for the WISMB. A significant amount of data that was previously gathered for this region was analysed to identify the potential for scour occurrence in this region. Guidelines and recommendations for future scour assessments to support sustainable offshore wind development are also provided.

1.1 Scour around Wind Turbine Foundations

Scour is the process of seabed erosion due to the action of water. Scour can occur in the absence of external structures (i.e. a dynamic or transitory seabed) but can also be triggered by the introduction of an obstacle to the flow path such as a substructure or a foundation. In this case, a localised lowering of the seabed around the structure may occur due to a change in the flow pattern in its immediate locality that leads to an increase in the local sediment transport capacity.

Figure 1 illustrates the process of scour for a vertical cylinder (e.g. a turbine foundation), highlighting the the main parameters that control the magnitude and rate of scour development. The field flow is defined by three phases: 1) downflow at the front of the cylinder, 2) a horseshow vertex at the junction of the cylinder and the seabed, 3) a wake vortex. These changes in the flow pattern surrounding the cylinder cause an increase in shear stress at the seabed, resulting in the removal and transportation of sediment particles from the seabed, and the development of a scour hole at the base of the structure. This local scour may develop over time since currents and waves are time-varying actions, and can pose a significant hazard to the structure as it may undermine the structural stability of the wind turbine due to exposure of the foundation. The key factors governing this process are, therefore, the metocean conditions, the seabed characteristics and the geometry of the structure. Where sediment transport occurs in the vicinity of a seabed structure but the rest of the seabed remains immobile, this is known as clear-water scour.

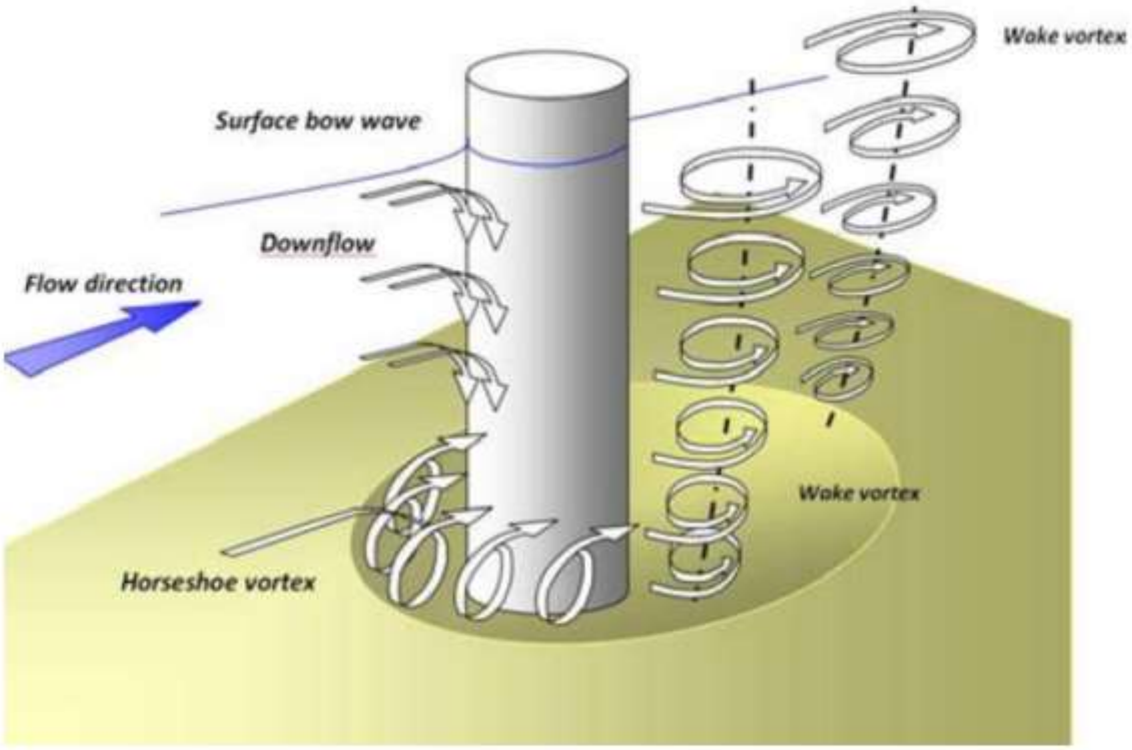

Figure 1 Schematic diagram of flow process and scour development around a vertical cylinder (Richard J. S. Whitehouse & Harris, 2014)

1.2 Scope of Study

This study has focused on a scour evaluation for the WISMB, which comprises an area of approximately 565 m^2 that extends from the East coast of Ireland to the Isle of Man and to Lambay Island to the south (see Figure 2). The WISMB is located along a distinct migratory pathway with strong tidal currents that lead to sediment transport. Since little or no information is currently available regarding the potential for scour within this region, the aim of this study was to provide a scour assessment for the WISMB that can be used to inform engineering activities in this region, supporting offshore wind development, whilst ensuring minimal environmental impact.

The study focused on a scour assessment for monopile foundations for offshore wind turbines, as these are currently the most commonly adopted foundation type and are generally suitable for the water depths in this region. Geological, geophysical and geotechnical data that was previously gathered as part of two INFOMAR surveys will be evaluated to identify existing occurrences of scour and to characterise the potential for scour in the case of offshore wind development.

1.3 Data Collection

1.3.1 Survey Work

Multibeam echosounder (MBES), sparker seismic data and vibrocores were acquired as part of the 2009 Irish Sea Marine Assessment (ISMA) survey (2009) on the *RV Celtic Voyager* (cruise number CV0926) (Wheeler et al., 2009). This survey covered part of the WISMB. The full inferred extent of the WISMB and the survey coverage within this area is shown in Figure 2.

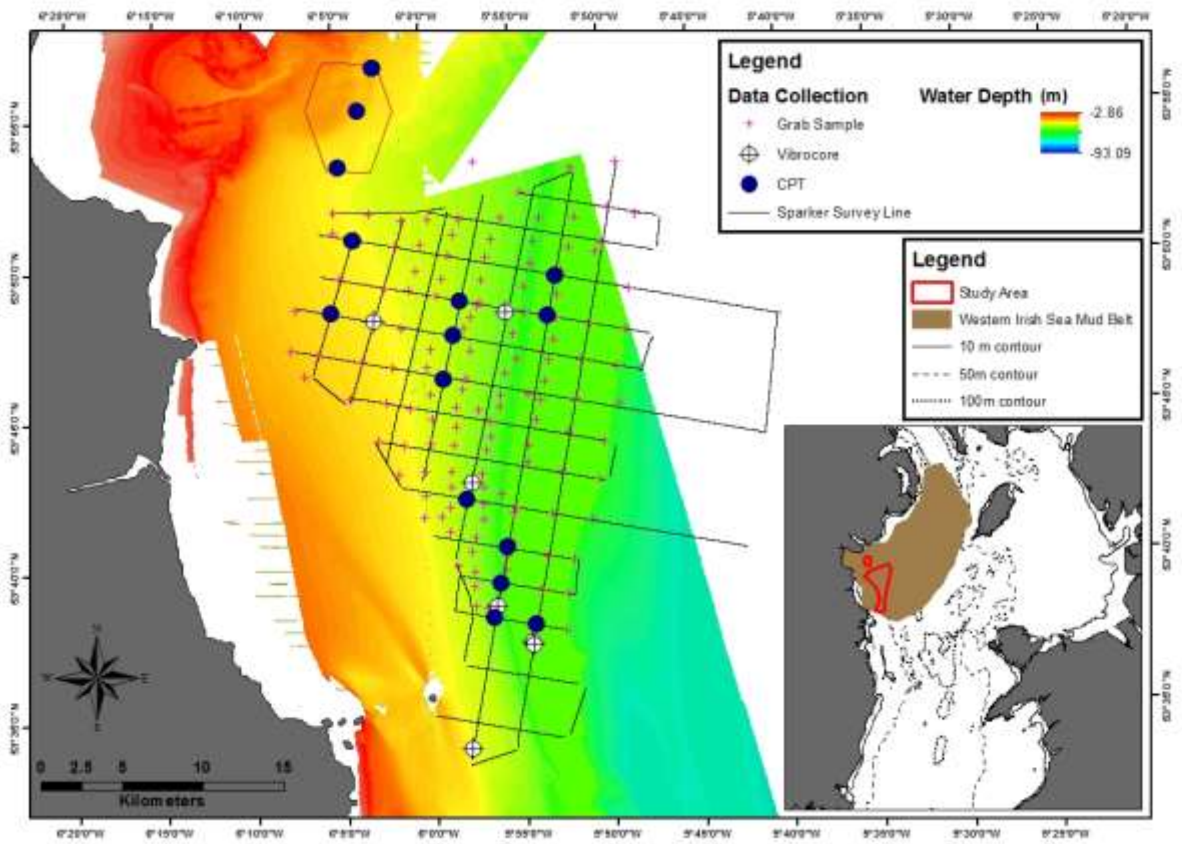

Figure 2 Inset map: Location of the WISMB in the Irish Sea. Also highlighted are the main study areas. Main map: highlighted study areas expanded showing data collection points.

The survey vessel was equipped with an EM3002D multibeam echosounder, acquiring bathymetry and backscatter data in the 300 kHz range using dynamically focused beams. The horizontal accuracy (x, y) was generally less than 50 cm with a vertical accuracy (z) of <15 cm obtained for the processed bathymetry data. Data processing was performed on board using CARIS HIPS and SIPS software packages to remove erroneous pings and to correct for tidal and water displacement offsets.

Sub-bottom data was gathered using a Geo-Source 400 sparker system. Roughly 415 km of sparker lines were collected in an area that measures approximately 565 km^2. The system consisted of a 6 kJ pulsed power supply operating at a frequency of between 0.5 and 2 kHz predominantly. The unfiltered return signal was picked up in a Geo-Sense single channel hydrophone array. A maximum penetration of 50 m below the seabed was achieved before signal attenuation with a vertical resolution of up to 30 cm. Direct samples from the uppermost decimetres of the seabed were taken using a Shipeck Day Grab. In total 269 samples were gathered. Furthermore, seven Geo-Resources 6000 vibrocores of up to 3 m length were collected to help groundtruth the seismic data (see Figure 2).

A further survey was undertaken in 2014, known as the Developing Geotechno-stratigraphies (Leg 2) survey, which was undertaken on board the *RV Celtic Explorer*. As part of this survey, the Geotechnical Offshore Seabed Tool (GOST), designed and developed at the MARUM Institute in Bremen Germany, was deployed at twelve sites within the original ISMA survey area (cruise number CE14001) (see Wheeler et al., 2014). The GOST is an innovative geotechnical tool used to characterise the unconsolidated sediment by means of "push-in tools" such as *in situ* Cone Penetration Testing (CPTu). The hardened stainless steel cone tip has a cross sectional area of 5 cm^2 recording tip resistance, sleeve friction, differential pore pressure, inclination and acceleration, and heat conductivity with a resolution of 0.06 MPa, allowing for a range up to 120 MPa. Exact control on push velocity during penetration allows for data to comply with the highest international standards including DIN 4904 requirements. The digital interface is a RS485 BUS using direct A/D conversion of a measured variable with overvoltage and reverse protection.

Based on a review of the seismic data from the ISMA survey, twelve site locations were selected for GOST *in situ* CPT investigations (see Figure 2). In total, 17 Cone Penetration Tests were undertaken across the site as part of the Phase 1 Geotechnical Survey. The CPT traces penetrated from between 3.12 m below mudline (bml) to a maximum penetration depth of 30.05 m bml (see Table 1).

Table 1 CPT data

Station No.	Latitude (Deg)	Latitude (DecMin)	Longitude (Deg)	Longitude (DecMin)	Water Depth (m)	Depth of penetration (m)
1	53	46.2545	5	59.0872	31.6	30
2a	53	56.6689	6	2.658	22.1	3.3
2b	53	56.669	6	2.659	21.3	0.75
2c	53	56.682	6	2.652	20	3.3
3	53	55.261	6	3.551	21.4	3.75
4	53	53.375	6	47.091	29.1	3.65
5a	53	50.937	6	4.015	28.6	10
5b	53	50.9346	6	4.01	27.1	8.7
6	53	37.994	5	54.266	48.8	21.2
7	53	38.284	5	56.577	36.8	16
8	53	39.418	5	56.158	37.7	19
9	53	40.573	5	55.768	43.4	19
10	53	42.248	5	57.914	37.5	20
11	53	47.706	5	58.502	32.7	26.5
12	53	48.819	5	58.045	35.3	26
13	53	48.309	5	58.231	43.9	30
14	53	49.58	5	52.701	44.1	26.7
15	53	48.491	6	5.373	24.3	18.32

1.3.2 Supplementary Data

Supplementary MBES data was provided by Ms. Charise McKeon of the GSI, which comprised data for selected shipwreck sites relevant to this study. A characteristic description of each shipwreck site is provided in Section 3.3. In addition, oceanographic data was garnered from the Marine Institute M_2 weather buoy, which is located at 53.4800°N 05.4250°W, and represents the closest *in-situ* oceanographic data collection site to the selected study area.

1.3.3 Geophysical Data Processing

1.3.3.1 Sparker data processing

Seismic sparker data was incorporated into IHS Kingdom software in SEG-Y format and merged with ASCII navigation data before being processed. A trapezoid bandpass filter was applied (low pass value 0.9 - 1.2 kHz, high pass value 5 - 6 kHz) and an automatic gain control of 50 and 100 ms. Seismic interpretation was also performed in IHS Kingdom. Horizons were picked manually and seismic depths were converted from two-way travel time to metres using an acoustic internal velocity of 1600 ms^{-1}.

1.3.3.2 MBES data processing

The output from the CARIS HIPS and SIPS software consisted of ungridded, tidally corrected XYZ data that was subsequently gridded using QPS Fledermaus v.7 to a 5 x 5 m cell resolution. Gridded raster data was then exported to ArcGIS v10.2 for use in groundtruthing and morphological analysis.

1.3.4 Particle Size Analysis

Samples from cores weighing roughly 2 g were taken every 5 cm for particle size analysis. A Beckman Coulter LS 13 320 laser diffraction particle size analyser at MARUM provided information about downcore grain size distributions for all cores. The laser is equipped with an Aquous Liquid Module and an Auto Prep Station and determines grain sizes from 0.4 to 2000 mm. No grain sizes were greater than 2000 mm. For surface grab-samples, the particle size distribution of the siliciclastic fraction was measured on a Malvern Mastersizer 2000 laser-granulometer with Autosampler and Hydro G dispersion unit at the National Oceanography Centre in Southampton. The siliciclastic fraction was obtained through the removal of organic matter and the carbonate phase by oxidation (10% H2O2) and dissolution (10% HCl), respectively. Adding a 5% Calgon (Sodium Hexametaphosphate) solution and mechanically shaking the sample enabled particles to disaggregate and disperse.

1.3.5 Geotechnical Data Analysis

Raw CPT data was calibrated using standard methods (Lunne et al., 1997) for each input signal, according to Equation 1, where a is the gradient and b is the intercept.

$$y = ax + b \quad \textbf{Equation 1}$$

All data was calibrated prior to each test. Double depth values were averaged to get a mean value and artificial outliers were manually removed (e.g. due to deceleration and acceleration effects at the start and end of each push). To allow for vertical shifts in sleeve data, the data was interpolated to a depth interval of 1 cm. The sleeve data values were shifted 7 cm upward, which is the distance between the theoretical cone and the sleeve centre. The apparent depth was corrected by the measured inclination for each data point. Where temperature data was available (i.e. compression cones), the data values were corrected for temperature effects.

2 Background

A desk study was initially conducted to evaluate the underlying mechanisms associated with the development of scour around seabed structures. A review of recorded instances of scour around wind turbine foundations was also conducted. In addition, an evaluation of existing methodologies to predict scour development over time for offshore wind turbines was conducted, and the associated data requirements were identified.

2.1 Review of Scour Assessment Methodologies

Where sediment transportation occurs in the vicinity of a seabed structure but where the rest of the seabed remains immobile, 'clear-water' scour is said to occur. This is in contrast to 'live-bed' scour which exists when there is general sediment transport taking place across the seabed. In such cases, the ambient seabed shear stress, τ_0, is less than the critical value for sediment motion, τ_{cr}, but is greater than τ_{cr}/M in the vicinity of the seabed structure, where M is the shear stress amplification factor due to the structure's presence (Whitehouse, 1998). Whitehouse (1998) proposed a general framework to predict the likelihood of scour in the vicinity of marine structures. Whitehouse et al. (2011) proposed a conceptual model to predict scour depths for offshore turbine foundations under normal prevailing conditions as well as under extreme conditions (Figure 3).

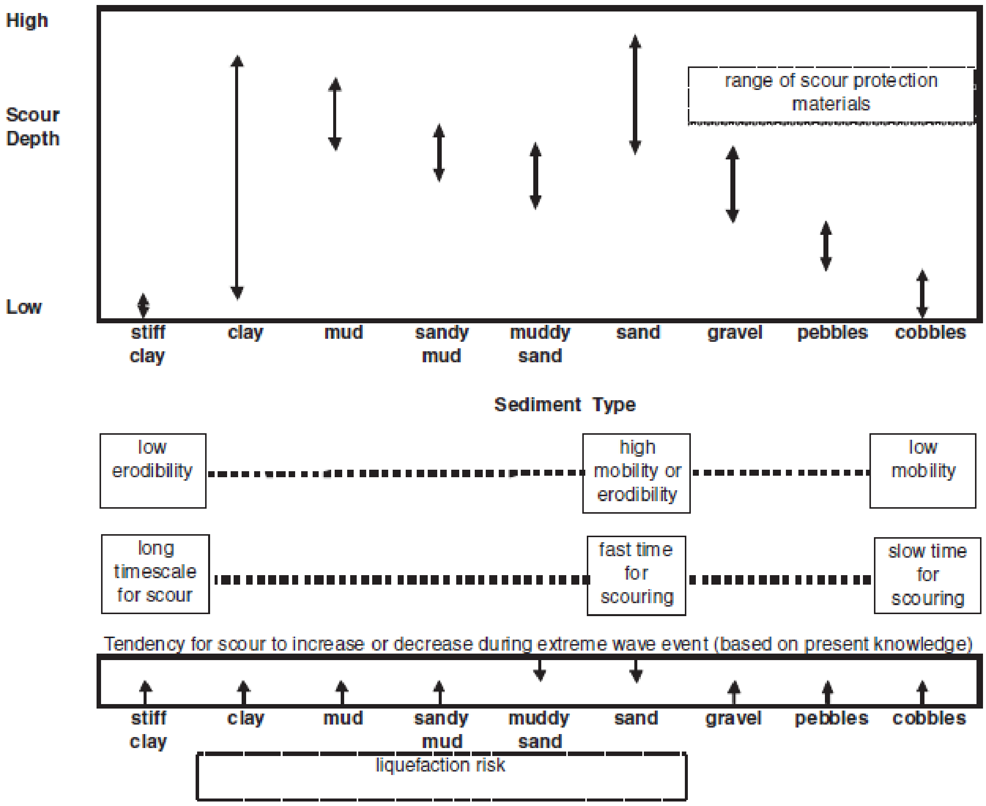

Figure 3 Conceptual model for scour development around marine foundations (R J S Whitehouse, Sutherland, & Harris, 2011)

The conceptual model put forward by Whitehouse et al. (2011) in Figure 9 is linked to the Folk diagram so that a site specific classification of sediment can be made (Figure 4). The conceptual model takes the Folk type Mud: Gravel: Sand classification of soil types as its starting point.

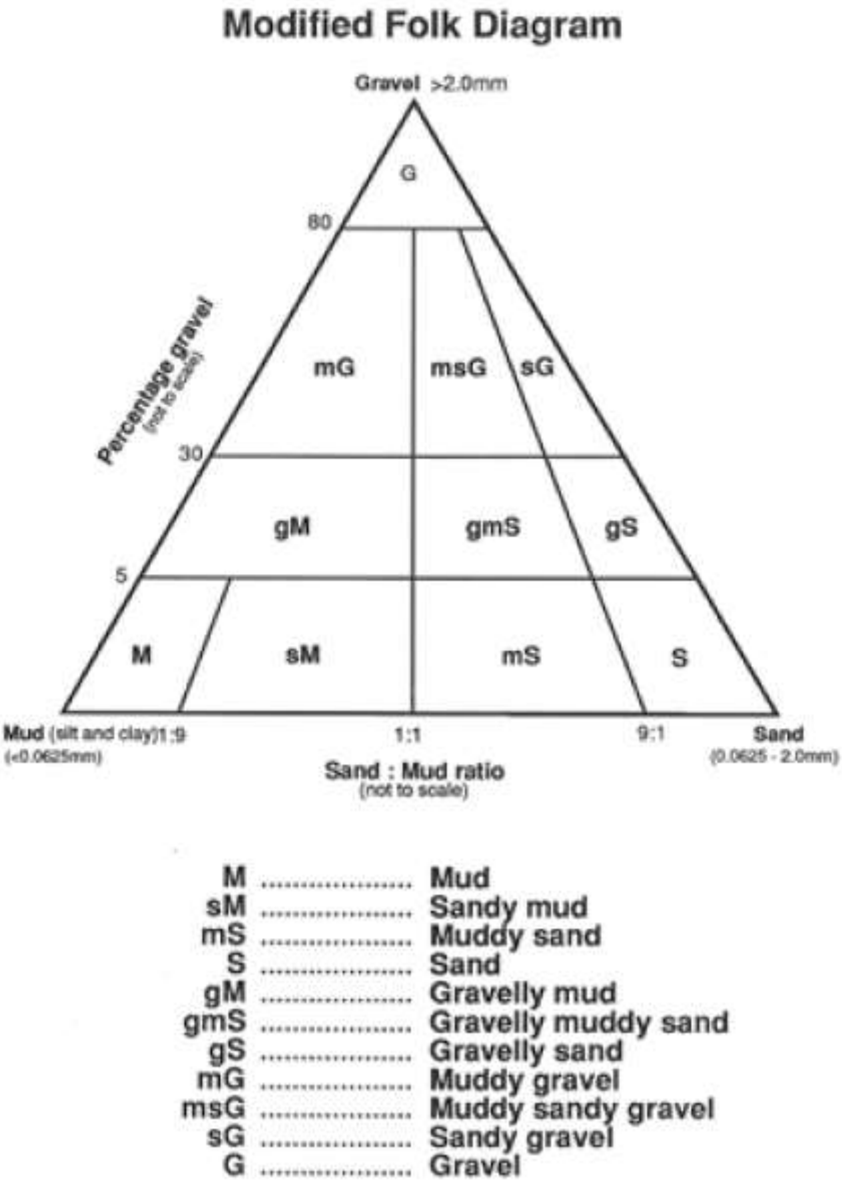

Figure 4 Modified Folk sediment classification diagram

Whitehouse and Harris (2014) proposed a life cycle scour management plan, which incorporates prediction, monitoring and remediation steps (Figure 5).

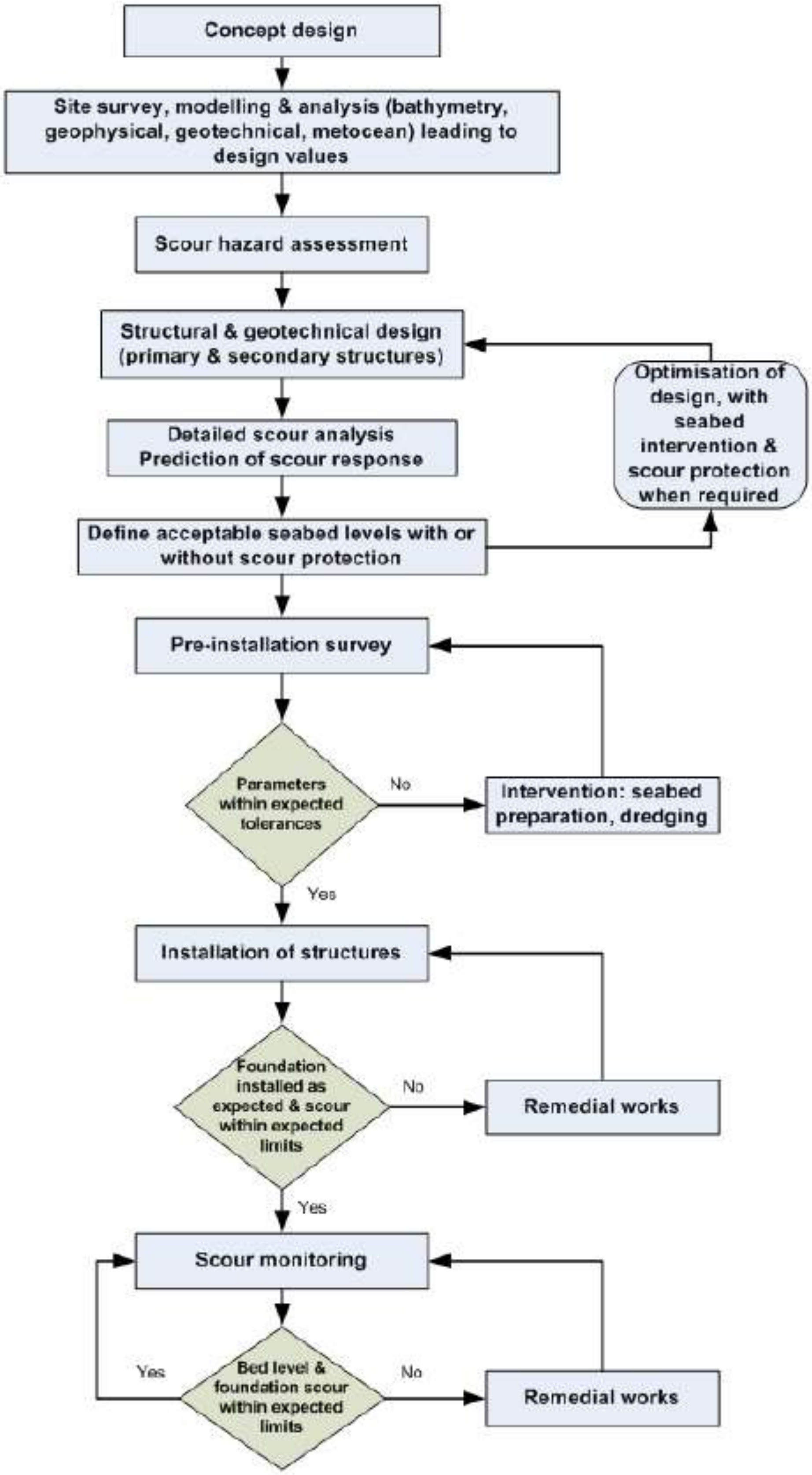

Figure 5 Life-cycle scour management plan (from: Whitehouse and Harris (2014))

2.1.1 Equilibrium Scour Depth

The equilibrium scour depth, S_e, is said to occur when the resistive force of the seabed sediment (τ_0) is equal or greater to the flow velocity (U_f). Existing design guidance (Det Norske Veritas, 2014) have adopted a mean value of the equilibrium scour depth equal to 1.3 times the diameter of the substructure based on an empirical study, which agrees with experimental data reviewed by Sumer et al. (1992). By contrast, the International Organisation of Standardization (ISO) has adopted a scour depth of 1.5 times the diameter in their 2007 recommendations.

The equilibrium scour depth was studied by Breusers et al. (1977) for steady currents impacting on a circular cylinder, who postulated the following equation:

$$\frac{S_{\infty,c}}{D} = \propto \tanh\left(\frac{h}{D}\right) \qquad \textbf{Equation 2}$$

Where α is the depth independent equilibrium scour depth and h is the water depth. This equation was subsequently modified by den Boon et al (2004) based on the results of the physical model testing for the Q7 offshore wind farm in the Netherlands, by introducing correction factors, K1 and K2 to deal with depth limitation and sediment grading respectively:

$$\frac{S_{\infty,c}}{D} = \propto K1\tanh\left(K2\,\frac{h}{D}\right) \qquad \textbf{Equation 3}$$

For the current alone case, the time scale is found from equation 4 (from Sumer & Fedose (2002)):

$$T^* = \theta^{-2.2}\delta/(2000D) \qquad \textbf{Equation 4}$$

Where T* is a dimensionless timescale related to real time T, according to (Sumer et al. 1992) and Fredsoe et al. (1992):

$$T = \frac{D^2}{\sqrt{g(s-1)d^3}}T^* \qquad \textbf{Equation 5}$$

where s is the relative density of the soil, h is the water depth, D is the outer diameter of the foundation, and g is the acceleration due to gravity. The timescale above is valid for a circular cylinder, whereas when the scour is generated from turbulence due to additional geometric appurtenances, the scour may be drastically accelerated (up to a factor of 3 times faster).

For gravity base foundations (GBF), Whitehouse et al. (2011) reviewed existing empirical methods to predict scour and compared them to laboratory and field measurements. The empirical methods included Hoffmand and Verheij (1997);

$$\frac{S}{D_c} = 8.96\left(2\,\frac{0.5\alpha_{C\,U}}{U_{cr}} - 1\right)\left(\frac{h_c}{D_c}\right)^{1.43}\left[\frac{(0.5\alpha_c U)^2}{gh}\right]^N \qquad \textbf{Equation 6}$$

where S = scour depth, D_c = average of the length and breadth of the GBF, α_c = 2 for a circular GBF and α_c = 2.3 for a rectangular GBF, U_{cr} is he depth-averaged flow velocity for initiation of sediment motion, h_c is the flow depth, h_c is the GBF height and g is gravitational acceleration.

In their study, Matutano et al. (2013) analysed different methods used in predicting maximum scour depth and scour extension. By collecting information from different windfarms, including scour extent, they were able to assess different formulations and their applicability. For this they considered the most important formulations developed for predicting maximum scour depth (Figure 6).

Scour depth prediction, main formulae. Own research.

Authors	Year	Flow conditions	Maximum scour depth prediction
Breusers et al. [6]	1977	Steady current	$\frac{S}{D}max = 1.5 \cdot D \cdot \tanh\left(\frac{h}{D}\right)$
Zanke [16]	1982	Steady current or waves	$\frac{S}{D}cmax = 2.5 \cdot \left(1 - 0.5 \cdot \frac{uc}{u}\right)$ $\frac{S}{D}wmax = KC - 6$
Melville et al. [17]	1988	Steady current	$\frac{S}{D}cmax = 2.4$
Sumer et al. [18]	1992	Steady current or waves	$\frac{S}{D}cmax = 1.3$ $\frac{S}{D}wmax = 1.3 \cdot (1 - \exp(-0.03(KC - 6)))$
Richardson and Davis (HEC-18) [19]	1995	Steady current	$\frac{S}{h}cmax = 2 \cdot K1 \cdot K2 \cdot K3 \cdot \left(\frac{b}{h}\right)^{0.65} \cdot Fr^{0.43}$
Sumer et al. [5]	2002	Steady current and waves	$\frac{S}{D}cwmax = 1.3 \cdot (1 - \exp(-A(KC - B)))$
Zanke et al. [20]	2011	Steady current and waves	$\frac{S}{D}cwmax = 2.5 \cdot \left(1 - 0.5 \cdot \frac{uc}{u}\right) \cdot xrel$

Figure 6 Scour depth prediction formulae (From Matutano et al. (2013))

The formula developed by Breusers et al. (1977) was used with a coefficient of 1.25 to obtain a best-fit using Scroby Sands data. Subsequently this formula was applied, along with the DNV standard, and the results compared with available scour data. They found that the maximum scour was less than estimated in most offshore wind farms, with only two displaying greater scour (Table 2).

Table 2 Values of maximum scour estimation on available scour data on European wind farm sites (from: Matutano et al. (2013))

Site Location	Monopile diameter (m)	Estimated scour (S_{max}, m)		Available scour data (S_{max}, m)	
		Breusers et al.	DNV		
N7	6	7.41	7.80	1.05D	6.30
Scarweather Sands	2.2	3.30	2.86	0.59D	1.30
Otzumer balje inlet	**1.5**	**2.25**	**1.95**	**1.47D**	**2.21**
North Hoyle	4	5.87	5.20	0.125D	0.50
Scroby Sands	**4.2**	**5.96**	**5.46**	**1.66D**	**6.97**
Arklow Bank	5	6.25	6.50	0.86D	4.00
Kentish Flats	5	7.10	6.50	0.46D	2.30
Barrow	4.75	7.10	6.18	1.21D	5.74
Egmond aan Zee	4.6	6.90	5.98	0.48D	2.2
Princess Amalia	4	6.00	5.20	1.075D	4.30

2.1.2 Current alone

In the case of a current only scenario, a smooth seabed can de assumed if the viscous sublayer thickness, δ, is larger than the seabed roughness, k.

$$\delta = 11.7\frac{v}{U_f}$$ **Equation 7**

where v is the kinematic viscosity value ~10^{-6} m^2/s.

$$k = 2.5d$$ **Equation 8**

where d is the mean soil particle diameter.

In the smooth wall case, the mean flow velocity, V, is related to the shear velocity (friction velocity) according to Equation 5. Therefore, the resulting shear velocity can be derived for any flow velocity.

$$\frac{V}{U_f} = 3.2 + 2.5\ln\left(\frac{h}{v}U_f\right)$$

Equation 9

It should be noted that due to the dependency of the smooth wall condition on the flow velocity, it may be the case that for larger flow velocities, the behaviour may transition to a rough wall case (as governed by the viscous sublayer thickness). In these circumstances, the shear velocity should be recalculated for the rough wall condition as outlined in Equation 6.

$$\frac{V}{U_f} = 6.1 + 2.5\ln\left(\frac{h}{\frac{k}{30}}\right)$$

Equation 10

For the purposes of scour analysis, it is necessary to determine both the magnitude of the scour and the time taken for the scour to develop. In most circumstances, current-alone creates the largest scour hole, where the presence of waves will inhibit the scour development somewhat and reduce the scour depth. For example, Figure 7 highlights the beneficial impact of the presence of waves as measured in lab experiments where perpendicular waves (to the primary current direction) are shown to impede scour development.

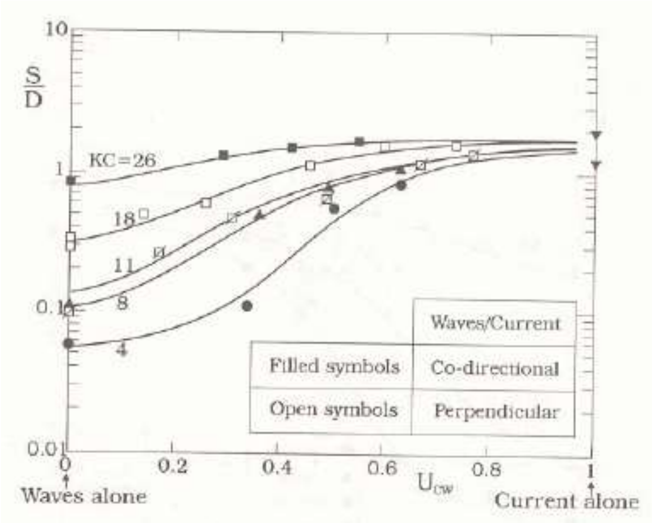

Figure 7 Variation in scour depth with waves and current (Sumer & Fredsoe, 2002)

2.1.3 Impact of Waves

The co-existence of waves together with the current usually implies a reduction in the potential scour depth. The Keulegan-Carpenter number, KC, is an important parameter in assessing the wave induced impact on scour development, and is defined according to;

$$KC = \frac{U_m}{D} T_w \qquad \textbf{Equation 11}$$

where U_m is the maximum orbital velocity from the waves and T_w is the wave period, D is the diameter of the foundation. This can be seen in Figure 8 where the variation in scour depth around a circular cylinder is shown.

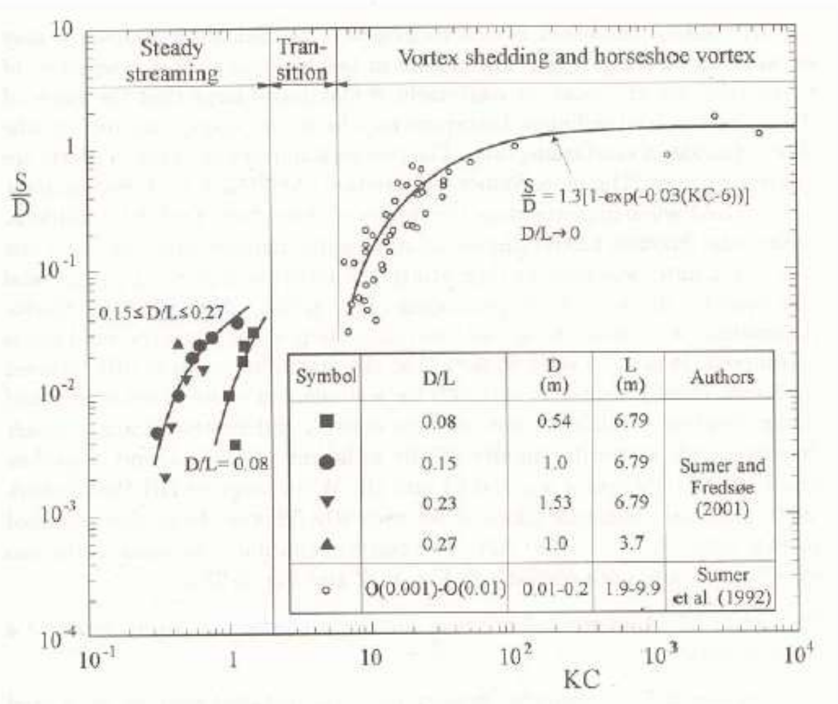

Figure 8 Detailed scour diagram in the diffraction regime

While the maximum magnitude of the scour development may be curtailed due to the presence of waves, the timescale for the scour to develop is accelerated because the erosion mechanism is enhanced in the combined wave-current motion. Adding the bed shear stress from the current with that from the waves and once more calculating the timescale for erosion can obtain a rough estimate of this increased rate. The waves enhance the rate of scour, so the time scale for the scour development becomes much smaller for large waves, the erosion will occur during a few hours, or, with slightly smaller waves, during a couple of days.

The friction factor in waves is much larger than in the current only case (because the small thickness of the wave boundary layer), this is reflected in the bed shear stress, τ_b, responsible for sediment mobility. Waves generate much larger shear stresses than current alone. For the wave alone case, Equation 12 can be used to derive the friction factor, f_w.

$$f_w = 0.04\left(\frac{\alpha}{k}\right)^{-0.25}$$ **Equation 12**

where k is the roughness factor, which is usually taken as equal to 2.5 times the grain diameter of the bed sediment or 0.5mm.

Komar and Miller (1973) describe how to calculate the threshold orbital velocity under waves:

$$U_{wcr} = [0.118g(s-1)]^{\frac{2}{3}} d_{50}{}^{\frac{1}{3}} T^{\frac{1}{3}}$$ **Equation 13**

Where g is the acceleration due to gravity, s is the ratio of densities of grain and water, d_{50} is the mean grain size and T is the dominant wave period.

2.1.4 Time Effects

Scour does not occur instantaneously with variance in hydraulic conditions over time (i.e. waves, current and water depth) generating new equilibrium scour depths.

Sumer et al. (1992) demonstrated that the increase in the depth of the scour pit over time for a vertical pile subject to a steady current and wave action may be defined by $\boldsymbol{S(t) = S_e\left(1 - \exp\left(-\frac{t}{T}\right)^p\right)}$ Equation 14 14 where t is time, T is the characteristic time-scale for scour and p is a fitting coefficient relating to the shape of the $S(t)$ curve, which is generally taken as equal to 1.

$$\boldsymbol{S(t) = S_e\left(1 - \exp\left(-\frac{t}{T}\right)^p\right)} \qquad \textbf{Equation 14}$$

2.2 Methodology Adopted for this Study

To date, a number of studies have attempted to develop methodologies to predict the development of scour around marine foundations. However, there is generally a high level of uncertainty associated with the prediction of scour depths for offshore wind turbines.

Whitehouse (1998) provides a general framework to predict the likelihood of scour in the vicinity of marine structures (Figure 9).

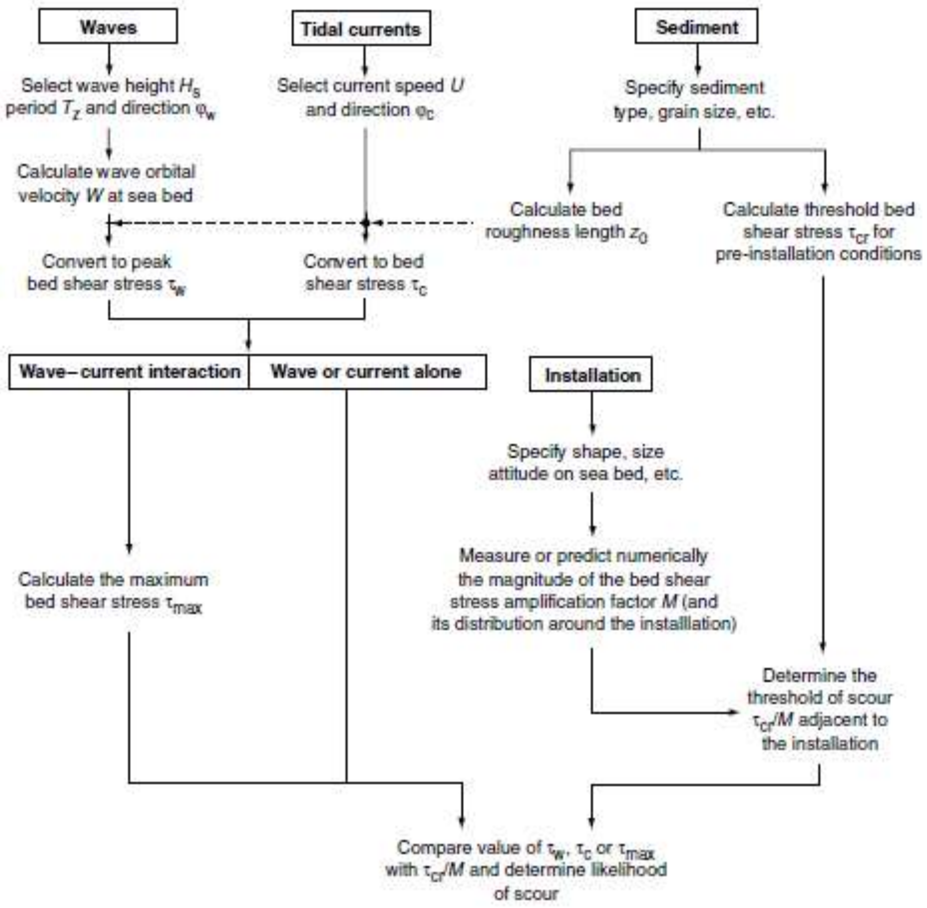

Figure 9 Flow chart for calculating sedimentary mobility (from Whitehouse (1998))

This methodology requires three environmental inputs: waves, currents and sediment. The methodology calculates bed shear stress for waves (τ_w), tidal currents (τ_c) and a combination of both (τ_{max}). These stress values are then compared to the critical stress threshold (τ_{cr}) for inducing sediment mobility. It assumes that scour occurs where shear stress amplification occurs adjacent to the structure and is defined by a shear stress amplification factor, M. M is defined as the ratio of local shear stress, $\tau_{0,\ local}$, to the ambient shear stress, $\tau_{0,\ ambient}$, an value generally vary between 4 and 9, depending on the shape and size of the structure.

Given its simplicity, and adaptability, we adopted the framework of Whitehouse (1998) in this study to assess the potential for sediment mobility in the WISMB.

2.2.1 Calculation of wave related shear stress

Wave–driven near bed orbital velocities can be estimated using Equation 15 according to Whitehouse (1998):

$$U_w = \frac{\pi H}{T} \frac{1}{\sinh(kh)}$$ **Equation 15**

Where *H* is the wave height, *T* the wave period, *k* the wave number (k = 2π/L, L = wave length) and *h* is the water depth. In turn, wave oribital velocitities can be converted to wave related bed shear stress (τ_w) using Equation 16:

$$t_w = 0.5 p f_w U_w^2$$ **Equation 16**

Where f_w is the wave friction factor, calculated as:

$$f_w = 1.39(A/z_0)^{-0.52}$$ **Equation 17**

Where *A* is the amplitude of the orbital wave motion at the bed and z_0 is the median grain-size value (d_{50}). A is calculated by:

$$A = \frac{U_w T_p}{2\pi}$$ **Equation 18**

where T_p is the wave period.

2.2.2 Calculation of current related shear stress

To calculate the current related bed shear stress, Whitehouse (1998) prescribe the following equation:

$$t_c = p C_D \overline{U}^2$$ **Equation 19**

where p is the water density, C_D the drag coefficient and Ū the depth averaged current speed. The drag coefficient (C_D) is a function of the water depth and median grain-size (d_{50}) expressed as:

$$C_D = \left[\frac{0.40}{\ln(\frac{h}{z_0}) - 1}\right]^2$$ **Equation 20**

where *h* is the water depth and z_0 the hydraulic roughness (or d_{50}/12, d_{50} = median grain-size).

2.2.3 Calculation of combined shear stress (wave and current)

Having calculated bed shear stress values for for waves (τ_w) (Equation 16) and tidal currents (τ_c) (Equation 19), the next step in the work flow chart of Whitehouse (1998) is to calculate the combined maximum stress of wave and current together (τ_{max}). This is done according to the equation:

$$\tau_{max} = \left[(\tau_m + \tau_w \cos ø)^2 + (\tau_w \sin ø)^2\right]^{0.5}$$ **Equation 21**

where ø is the angle (°) between the wave and current shear stresses (assumed to be 45).

T_m is the mean shear stress calculated by the following:

$$\frac{\tau_m}{\tau_c} = 1 + 1.2\left(\frac{\tau_w}{\tau_c + \tau_w}\right)^2$$ **Equation 22**

where τ_w us calculated from Equation 16 and τ_c from Equation 19.

2.2.4 Calculation of critical shear stress

The potential mobility of sediment can be assessed by comparing the values for bed stress calcauted per the above with the critical shear stress (τ_{cr}), as defined by:

$$\boldsymbol{\tau_{cr} = \theta_{cr}.\, g(p_s - p)d_{50}} \qquad \textbf{Equation 23}$$

where Θ_{cr} is the critical Shields parameter, which, in this instance is averaged at 0.0905 for the range of sediments, identified in this study and in accordance with U.S. Geological Survey investigation reports[1]. g is acceleration due to gravity (9.81 m s^{-2}), p_s and p are densitites of sediment and water respectively and d_{50} is the median grain-size.

2.3 Recorded Instances of Scour around Offshore Wind Turbines

Whitehouse et al. (2008) reported scour measurements for five offshore wind farm sites in the UK and Ireland for wind turbines founded on monopiles. The study demonstrated that for sites underlain by a marine clay stratum, the development of scour was limited. However, for sites comprised of unconstrained depths of sandy sediments, scour depths were significant. Whitehouse et al. (2011) analysed the occurrence of scour at foundations for a number of offshore wind farms, and other monopole foundations, in the Irish Sea and the North Sea (Table 3). The paper takes the scour depth, *S*, and water depth, *h*, and makes them non-dimensionalised with the pile diameter, *D*. By doing so, the data can be used to show whether the water depth for a specific structure is shallow, with relative values of *h/D* of 3.5 generally used to indicate shallow water. This allows data from various sites to be compared in a clear and consistent fashion. The controlling influence of sediment type on scour depth was most evident at the Barrow site where near-zero scour depths occur in till bed material or at locations where surficial layer thickness had a limiting effect. They demonstrated that 95% of measured scour depths were less than less than or equal to the value of 1.3D provided in the guidance for offshore windfarms (Det Norske Veritas, 2007) based on laboratory data. Overall, the extent of scour in a bed was typically found to be 4-5D without placement protection.

In the Irish context, scour has been recorded at Ireland's only offshore wind farm, Arklow Bank. Scour was measured following installation and prior to the deployment of scour protection measures. The scour hole was fairly symmetrical with smooth sides and was about 0.8D deep. It had a similar depth and shape to lab tests previously carried out. Consequently, rock with a median eight of 200 kg was installed around the 5 m diameter monopoles. Subsequent diver investigation found some secondary scour around this protection.

[1] https://pubs.usgs.gov/sir/2008/5093/table7.html

Table 3: Documented instances of scour (Whitehouse et al., 2008; Whitehouse et al. 2011)

Location	Site Description	Geological Conditions	Wind Farm Development	Scour Depth
Barrow, north-east Irish Sea	Moderately exposed to waves, moderate currents. Deep water.	Gravelly sand, sand and sandy clay. Stable seabed environment.	Thirty turbines founded on 4.75m diameter (D) monopiles.	0.44D in sandy deposits, increasing to 1.21D over time. Scour depths limited to 0.5D where superficial cover of sand was overlying glacial till.
Kentish Flats, outer Thames Estuary	Moderately exposed to waves, moderate currents.	Superficial fine sand overlying clay. Stable seabed environment.		0.28D, increasing to 0.46 over time.
Scroby Sands, southern North Sea	Strong currents, exposed to waves. Shallow water.	Sand, dynamic sandbank environment, presence of mobile bedforms.	Thirty turbines founded on 4.2m diameter (D) monopiles.	0.95D – 1.38D in the unlimited thickness of sandy sediment.
North Hoyle, southern Irish Sea	Moderately sheltered from waves, moderate currents. Deep water.	Gravels and sandy gravels underlain by compact gravelly clay. Stable seabed environment.	Thirty turbines founded on 4.0m diameter (D) monopiles.	0.125D following installation, which reduced to nothing over time.
Arklow Bank, Irish Sea	Exposed to waves, strong currents.	Sandy gravel. Dynamic seabed environment.	Seven turbines founded on 5.0m diameter (D) monopiles.	0.8D. Scour protection – secondary scour observed. 0.55D deep after 9 months, showing a progressive increase with time to 1.05D after 5 years.
Scarweather Sands	Wind turbines very exposed to waves, strong currents. 2.2m monopile for met mast.	Medium sand, dynamic seabed environment.		0.27D - 0.59D depth scour that varied according to the strength of the current and tidal action.
Otzumer Balje, Northwest coast of Germany.	1.5m diameter monopile.			1.47D with variation between spring and neap tides.

2.4 Western Irish Sea Mud Belt Geological Setting

Based on the best available seismic data, Belderson (1964), Pantin (1977) and Yuan et al. (1992) all present a basic model for the WISMB consisting of a heterogeneous, lower glacial layer deposited during the last glaciation by the BIIS that rests on undulating Palaeozoic bedrock (Figure 10) . From the BGS borehole 89/15, Dickson and Whatley (1993) describe glaciomarine Late Devensian silty muds, overlain by a thin (1 m) sandy layer above an erosive surface. Subsequently, Jackson et al. (1995) distinguished the lower glacial layer as consisting of the Upper Till Member. Above this glacial layer, Belderson (1964), Pantin (1977) and Yuan et al. (1992) report a upper mud layer, marked by an erosive base, and associated with the Holocene marine transgression.

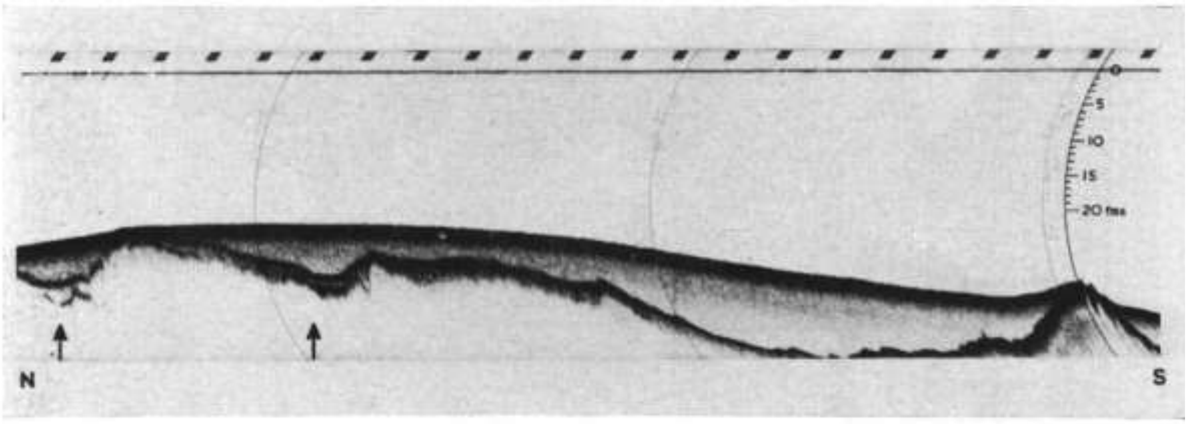

Figure 10 Echogram showing Holocene marine muds resting on presumed glacial deposits (Belderson, 1864)

Initial studies in the WISMB found that thicknesses of the upper mud layer ranged up to 33 m from seismic profiles (Belderson, 1964) and 39.3 m from borehole cores (Dickson & Whatley, 1993). Deposits were thickest in depressions and no intermediate reflecting horizons between the seafloor and the strongly reflecting surface on which the muds rested (Late Devensian glacial till) recognized. Subsequently, Belderson (1964) deduced that the muds, as a whole, were either uniform or with slight progressive vertical variations in composition as had been shown in core profiles. From this, he surmised that past conditions were not radically different from the present day. Thinner deposits of these muds were noted at the margins of the WISMB and to the south where the reflected horizon at the base became progressively shallower before becoming lost beneath sediment waves. Shell rich horizons are also recorded in cores from this unit consisting of the gastropod *Turitella communis* (Belderson, 1964; Kershaw, 1986; Coughlan et al., 2015). Previous AMS ^{14}C datings of shells from this unit have returned Holocene ages for these sediments (Kershaw, 1986; Coughlan et al., 2015).

At depth, areas of acoustic turbidity in the WISMB have long been recognized on seismic profiles and attributed to the presence of shallow gas accumulation (Pantin, 1977; Yuan et al., 1992; Figure 11). Such gas-charged sediments were delineated on seismic profile by enhanced internal reflectors with all reflectors stratigraphically below these sediments suppressed acoustically by a "blanking effect" (Pantin, 1977). As a result, the penetration of seismic surveying was limited and, therefore, forming a coherent image of sub-bottom conditions was difficult due to this acoustic blanking (Pantin, 1977; Williams et al., 1981; Yuan et al., 1992; Jackson et al., 1995).

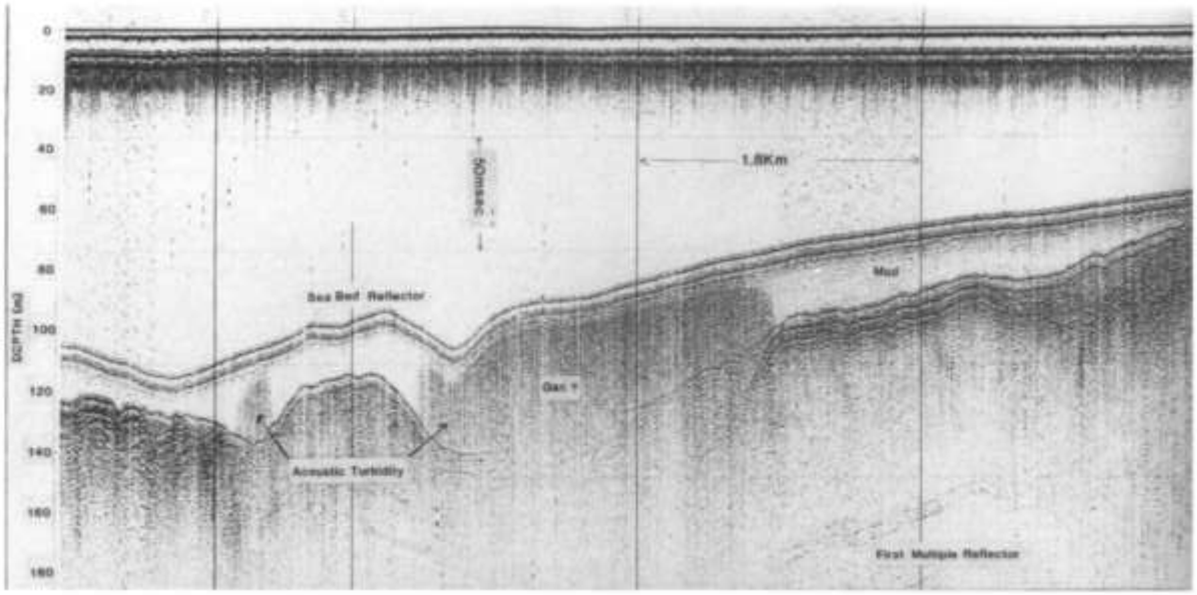

Figure 11 From Yuan et al. (1992). Seismic sub-bottom record displaying some typical gas signatures

Based on dating of the sediment, it is generally accepted that the WISMB is an area of active sedimentation (Coughlan et al., 2015; Kershaw, 1986; Mitchell, Condren, Leo, & Mcmahon, 1999). However, potential sources for the supply of fine-grained sediment have not been established definitively (Kirby, Parker, Pentreath, & Lovett, 1983). Belderson (1964) postulated that much of the material deposited in the WISMB originated further south as reworked glacial deposits with transport driven by the predominately northward flow within the Irish Sea. Despite close similarities in the sub-sand fraction of samples taken from the north Irish Sea, including WISMB, Johnson(1983) was sceptical of a uniform source material for the sediments found in the WISMB suggesting flocculation had a significant influence on sorting and sediment distribution.

2.5 Irish Sea Hydrodynamics and WISMB Conditions

The Quaternary sediments in the Irish Sea generally form a drape over the underlying bedrock. These sediments mainly consist of reworked glacial and post-glacial sediments that form a complex distribution of various sediment types (Belderson, 1964; Dobson, Evans, & James, 1971; Jackson et al., 1995). The present day distribution of seabed sediments is related to bed stress conditions. These bed stress conditions are a reflection of tidal dynamics which are primarily determined by the geometry of the Irish Sea basin. Bathymetrically, the Irish Sea can be divided into five zones (Belderson & Stride, 1966; Jackson et al., 1995):

- Estuaries and coastal embayments with depths of high water mark to 10 m;
- Inner shelf platforms with depths of 10 to 60 m;

- The Western Trough which runs sinuously from the North Channel to St. George's Channel forming a zone up to 80 km wide and between 60 to 140 m water depth;
- Enclosed deeps that are generally 30 km long and from 10 to 165 m deeper than the general seafloor. These are glacially formed tunnel valleys which have not been infilled by sediment;
- Rocky prominences including outcrops of rock at headlands, islets and shoals and can occur at depths of 75 up to 130 m depth.

At present, the sea has access to the Atlantic Ocean through the North Channel to the north and St. George's Channel in the south with a central trough connecting the two running through the Irish Sea. It is through these two channels that tides enter the Irish Sea with the two tidal branches meeting to the southwest of the Isle of Man to form a standing wave field (Belderson & Stride, 1966). From the dengenerate amphidrome (where a bedload parting zone has been inferred) at the Wicklow-Cahore Point interval of the Irish Coast, tidal ranges increase away from this location in a northerly and southerly direction (Robinson, 1979; Van Landeghem, Uehara, Wheeler, Mitchell, & Scourse, 2009). For the most part, the bed stress conditions created by these residual tidal currents exceed the energy thresholds that allow sediment to be actively eroded or induced to transport with the result that their direction are marked by migratory sediment-wave fields ending in areas of sediment accumulation; the Eastern and Western Irish Sea Mud Belt (EISMB and WISMB) in the north and Celtic Sea in the south (Belderson, 1964; Van Landeghem et al., 2009). As a result, seafloor sediments of the Irish Sea can be divided into three types; lag or modern day erosion, sediments in transport and present day deposits (Holmes and Tappin 2005; Figure 12)

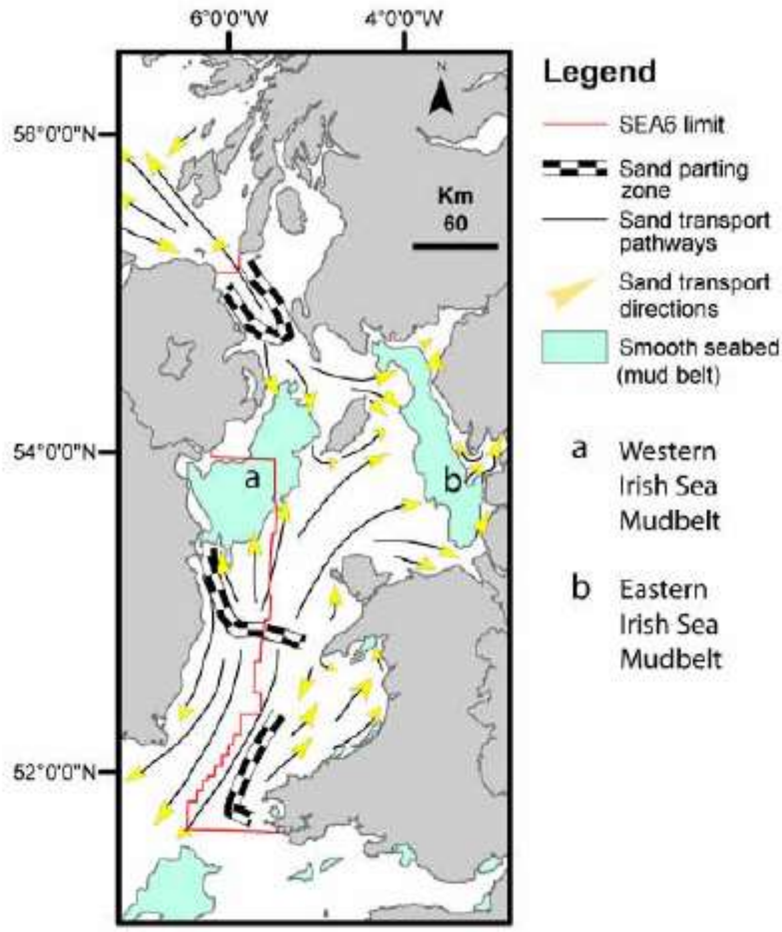

Figure 12 Map of the Irish Sea including the Western Mud Belt and generalised transport paths (from Holmes and Tappin (2005))

Unlike the rest of the Irish Sea, which is well mixed by strong tides, the WISMB stratifies in Spring and Summer of each year. This is the result of a combination of weak tides and relatively deep water producing insufficient mixing usually generated by tides and so fails to overcome the input of surface buoyancy created by solar heating (Hill, Brown, & Fernand, 1997). Bed stress current velocities within the area generally do not exceed the 0.5 ms^{-1} to mobilize the class of sediment found there and tidal currents are largely weak at < 0.3 ms^{-1} (Hill et al., 1997; Holmes & Tappin, 2005). A seasonal gyre is known to develop in the area which increases near surface water current velocities and has been noted to have an effect on seafloor sediment and its dynamics (Callaway et al., 2009; Horsburgh et al., 2000). This is particularly true in the case of Callaway et al. (2009) who noted the formation of scour hollows at the base of bedrock structures of approximately 40 m against the average seabed level. They concluded that significant amounts of scour around the reef were generated by obstacle flow induced current acceleration with subsequent vortex evolution and shedding. Their data suggested the currents in the area were responsible for the development of scour, often enhanced by the development of the gyre in addition to perturbations to the bottom current regime brought about by the obstacle of the bedrock. Furthermore, hydrogeographical modelling work carried out by Olbert et al. (2012) based on climatic changes predict a strengthening of the western Irish Sea gyre in time. Belderson (1964) also postulated that continued deposition in the area could result in a shallowing of water which would in turn cause a gradual increase in the near-bottom current velocity until the deposition of mud eventually becomes inhibited resulting in a "sand over mud" sequence. Scour Assessment for Western Irish Sea Mud Belt

3 Scour Assessment for the Western Irish Sea Mud Belt

3.1 Geophysical Survey Results Summary

From seismic profiles two major seismic reflectors (R1 and R2) were recorded which could be traced laterally across the study area. These reflectors in turn marked the base of two dominant seismic facies (S1 and S2). R2 was inferred as the top of bedrock. However, in many areas certainty of R2 was low due to acoustic turbidity. Generally, depth to bedrock was shallowest in the north and southern most aspects of the area showing its greatest depths (up to 45 m) towards the centre. The first strong reflector (R1) after seabed varied in depth from 0.8 to 26.5 metres below seafloor (mbsf). It is largely horizontal in nature and shows greatest depth towards the centre of the WISMB. Lying above R1 is seismic facies 1 (S1) (Figure 13).

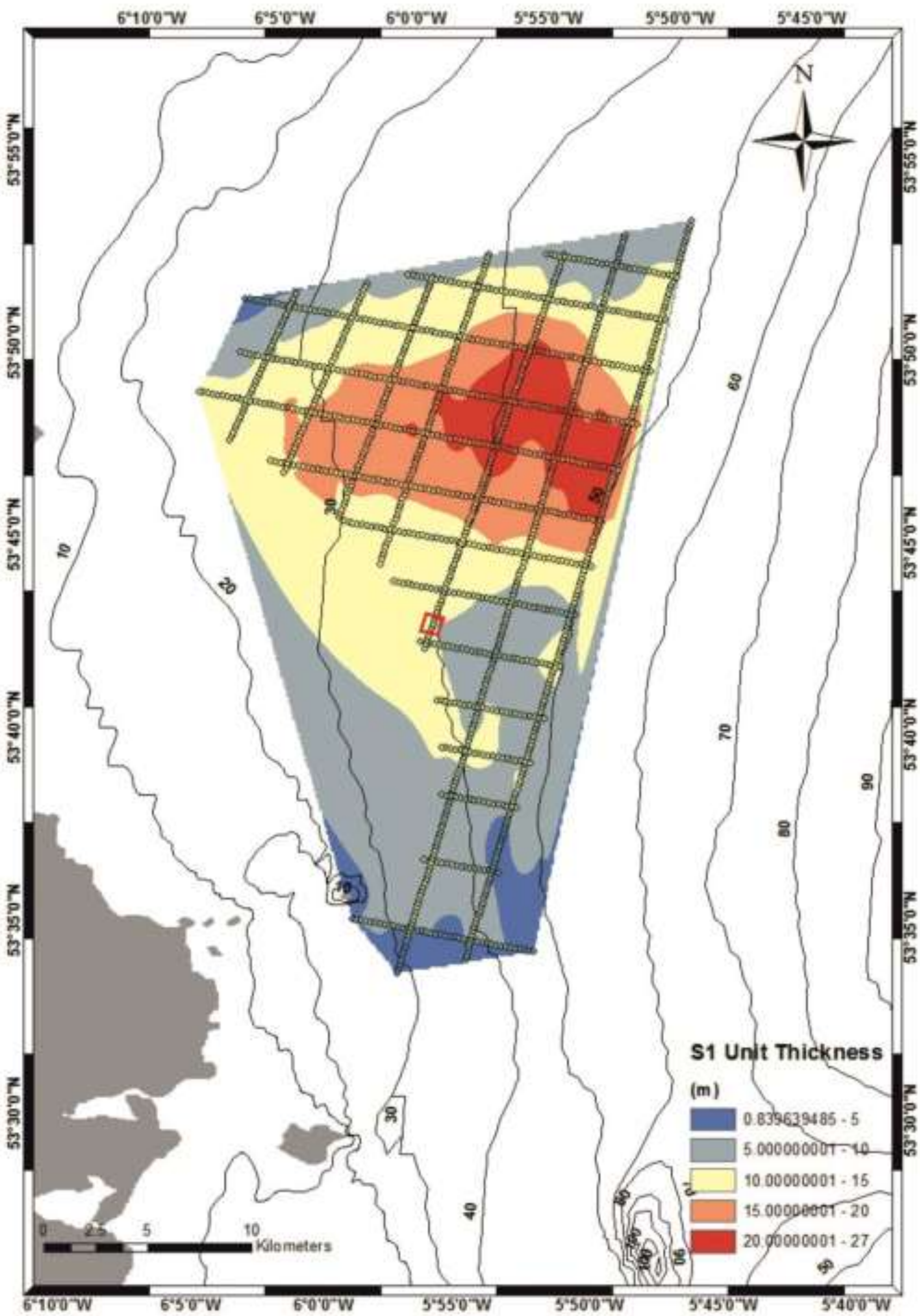

Figure 13 Isopach distribution (in metres) of S1. The seismic line segment highlighted by the red box is presented in Figure 14.

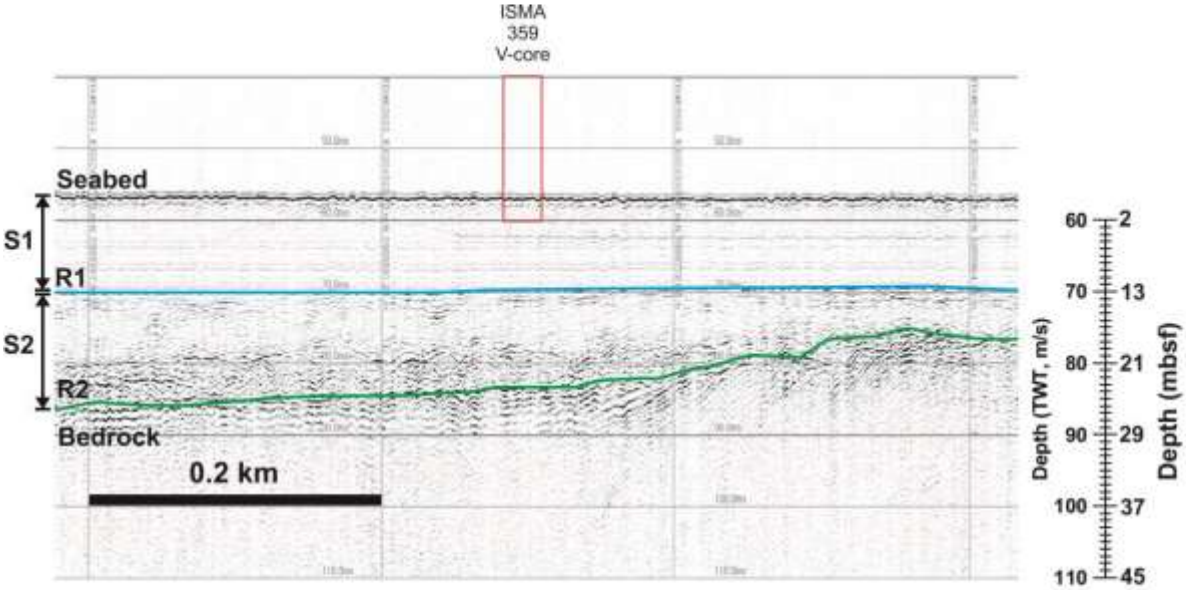

Figure 14 Seismic profile highlighted in 13 with interpretations.

Overlying R2 is S2, a unit lacking internal horizontal laminations. For the most part the unit exhibits an amorphous structure (Figure 14). However, in some places clear and laterally continuous structures were identified, mostly in the upper part of S2. This is likely to indicate erosive horizons and, thus, two stages of deposition. Thickness of this unit ranged from 1.5 to 24 m with variation depending on the undulating nature of underlying bedrock. Often the base of the unit was synchronous with R1 indicating the unit may be relatively shallow and close to the seabed in places.

3.2 Seabed Sediment Distribution

Backscatter data revealed a generally homogenous sediment distribution across the study area consisting overwhelmingly of low-return, soft sediment (Figure 15). Particle-size analyses on grab samples confirmed the fine-grained nature of seafloor sediment with all samples graded as poorly to very poorly-sorted and classified as Muddy Sand, Sandy Mud, Slightly Gravelly Mud or Slightly Gravelly Sandy Mud according to (Folk and Ward (1957). Generally, median (d_{50}) grain-size ranged from <10µm to roughly 241µm. A subtle change in sediment distribution shows a progressive northward decrease in median (d_{50}) grain-size (Figure 15).

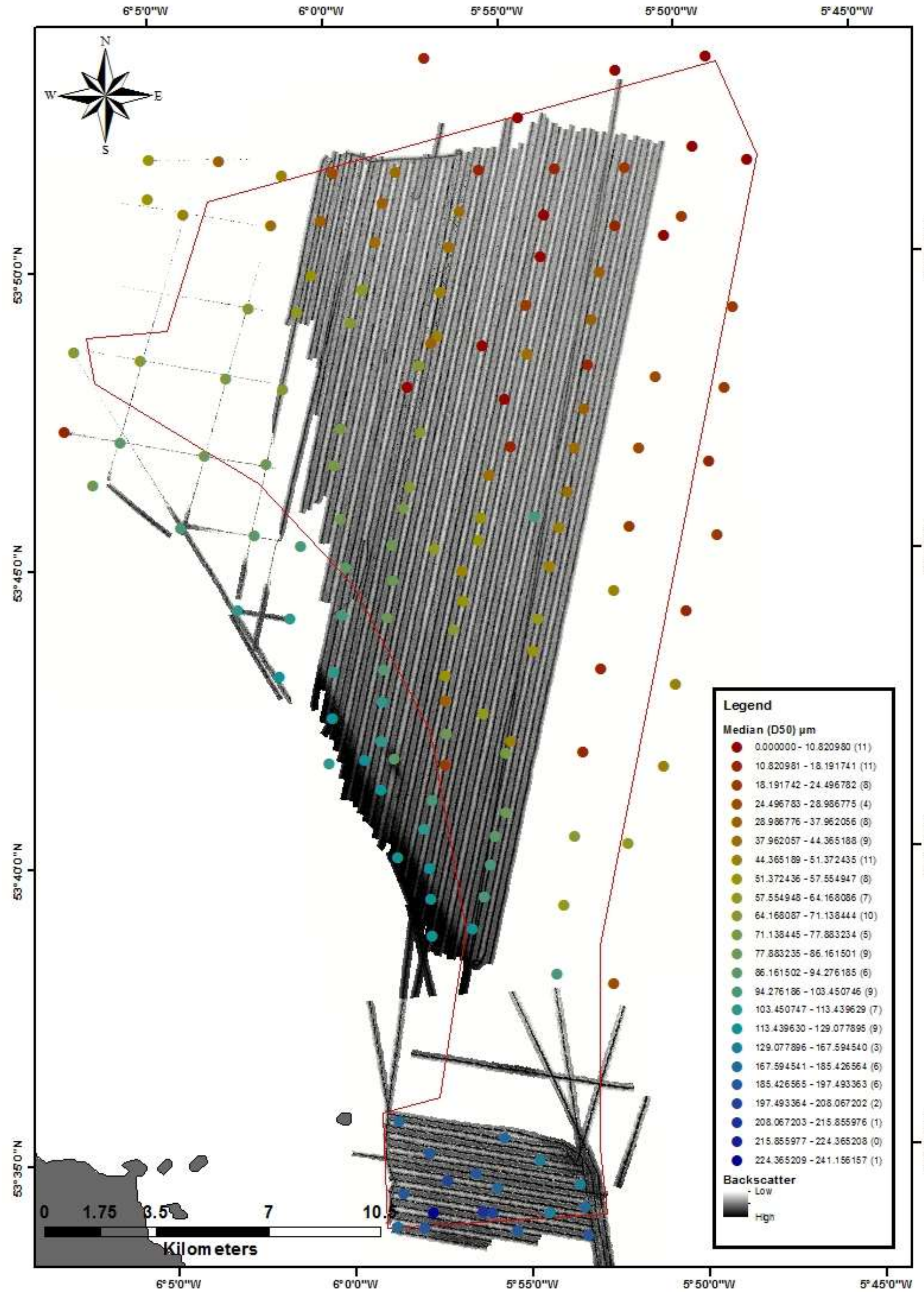

Figure 15 Surface sediment distribution

3.3 Recorded Instances of Scour in the Western Irish Sea Mud Belt

Interpretation of the MBES data reveals a relatively uniform seabed within the study area which slopes gently eastward to a maximum water depth of 55 m. No significant natural scour was noted within the dataset although significant scour has been recorded at shipwreck sites in the WISMB (Figure 16).

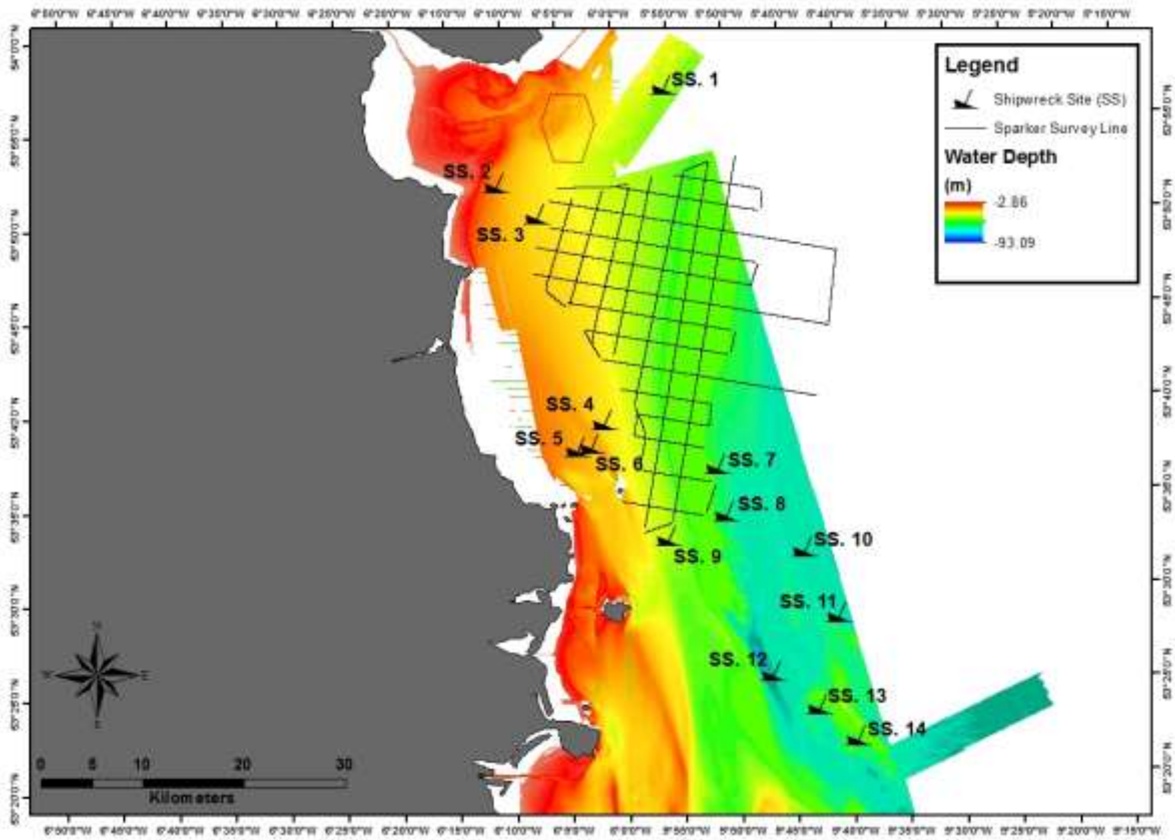

Figure 16 Selected shipwreck sites used in this study.

3.3.1 Shipwreck site 1

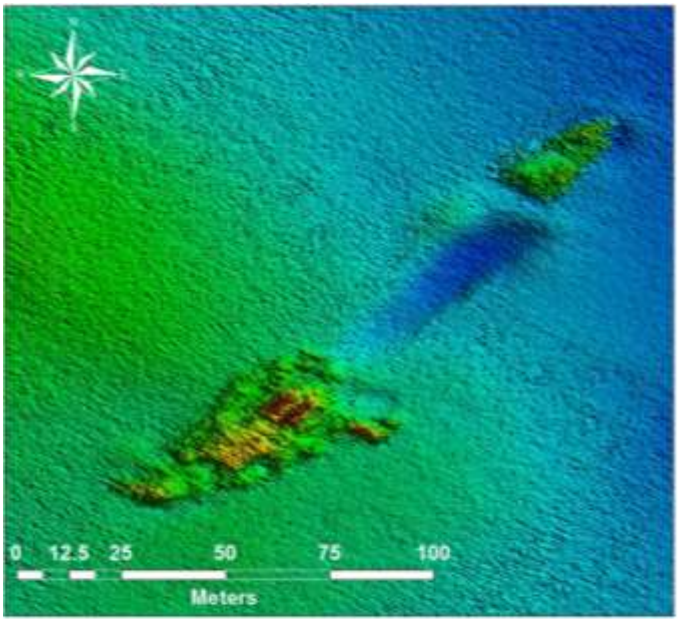

Shipwreck site 1 is located to the north of the study area, approximately 8 km northeast of the Oriel Windfarm site and 13 km southeast of Carlingford Lough. It is located in water depths of up to 34 m. Identified as the *Crusader* in the INFOMAR inventory; it is a barque type vessel with a length of 112 m and breadth of 20 m. It sailed in February 1892 from Birkenhead and was never heard of again. On the seabed it is orientated in a NE-SW direction and consists of two dominant features separated by a depression 41.5 m long. There are no significant levels of scour surrounding the wreck aside from this central depression.

3.3.2 Shipwreck site 2

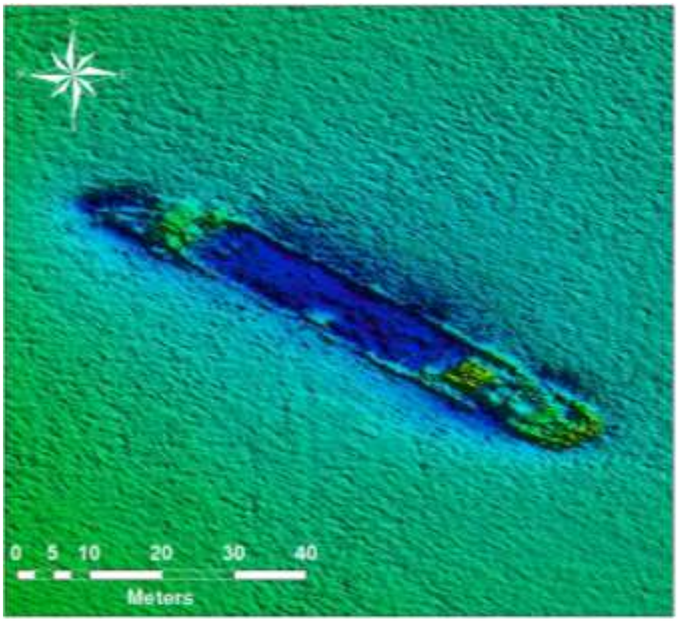

Shipwreck site 2 is located 4 km northeast of Dunany Point, in water depths of approximately 16.5 m. It is identified in the INFOMAR inventory as the *SS Topaz*,which sank on 28th December 1891 having struck Dunany reef. On the seabed the wreck measures roughly 50 m long with a breadth of about 8 m. It is orientated in a NW-SE direction with no significant levels of scour present, aside from some minor (approximately 1m) towards the northwest end.

3.3.3 Shipwreck site 3

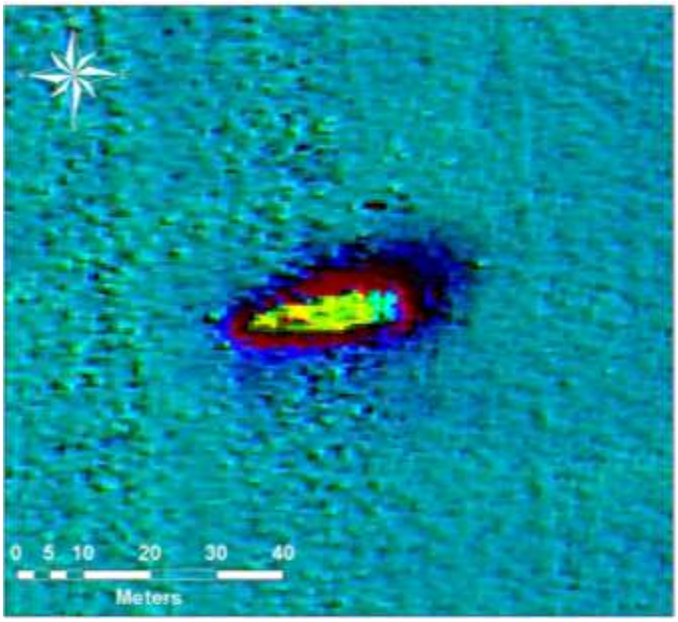

Shipwreck site 4 is located 8 km to the east of Dunany Point, Co. Louth. Based on the INFOMAR shipwreck database, we identify this wreck as the *Samaria*: a fishing vessel sunk on 23rd June 2000 after a collision with another vessel with no loss of life. The wreck lies in water depth of 26.9 m, has a length of 13.5 m and a width of 4.5 m. Scour occurs around the entire wreck site to a depth of 1 m below the general seabed level, but, is most prominent to the north-east. This scour morphology would indicate a relatively uniform flow regime with a slight propensity towards the north-east.

3.3.4 Shipwreck site 4

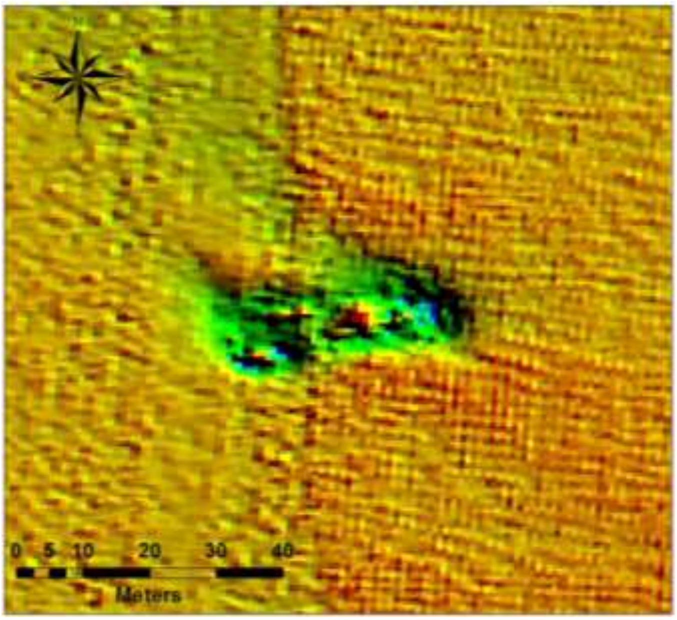

Shipwreck site 4 lies further 21 km to the south of Shipwreck site 3. The identity and timing of this wreck is unknown. From the MBES data, it would appear that the wreck is poorly preserved and extensively disintegrated. The wreck is spread across an area of approximately 108 m^2 with an overall length of 18 m in an E-W orientation. The seabed is at an average depth of 27.5 mbsf at this site. The scour signature is, on average, 1 m below the regular seabed level and extends towards the north and northeast of the wreck indicating dominant bottom flow to the north-west.

3.3.5 Shipwreck site 5

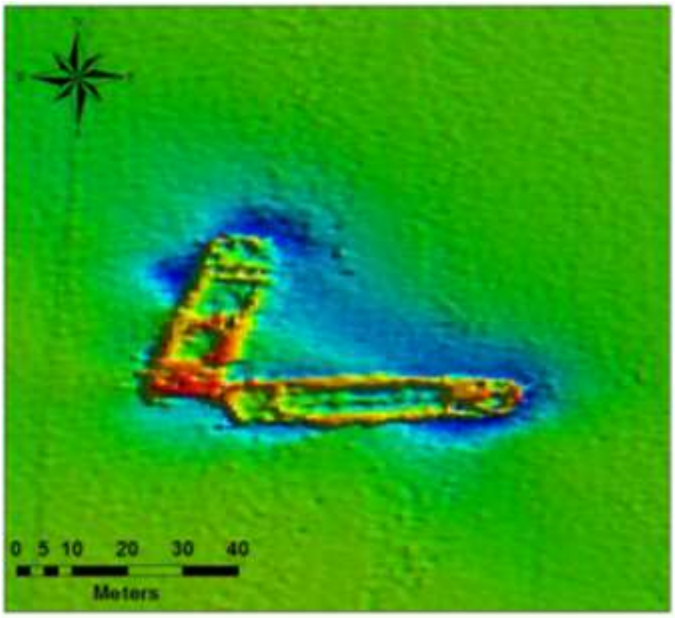

Shipwreck site 5 is located 6 km north-east of Skerries, Co. Dublin and is composed of two separate wrecks. Their identities and when they were sunk is unknown. The first wreck is 30 m long with a width of 8 m and orientated in a NNE-SSE direction. The second wreck has a length of 31 m, a width of 7 m and is orientated E-W. The southernmost tip of the first wreck and the western most tip of the second appear to meet, and there is a gap of 40 m between their alternate ends. It is in this 40 m area between the two ends that the vast majority of scour is located indicating dominant bottom flow to the north. The surrounding seabed in this area is generally 20 mbsl with scour depth around both wrecks on generally 0.5 m below this with a maximum of 1.5 m. The tidal-parallel scour tail is roughly 80 m long.

3.3.6 Shipwreck site 6

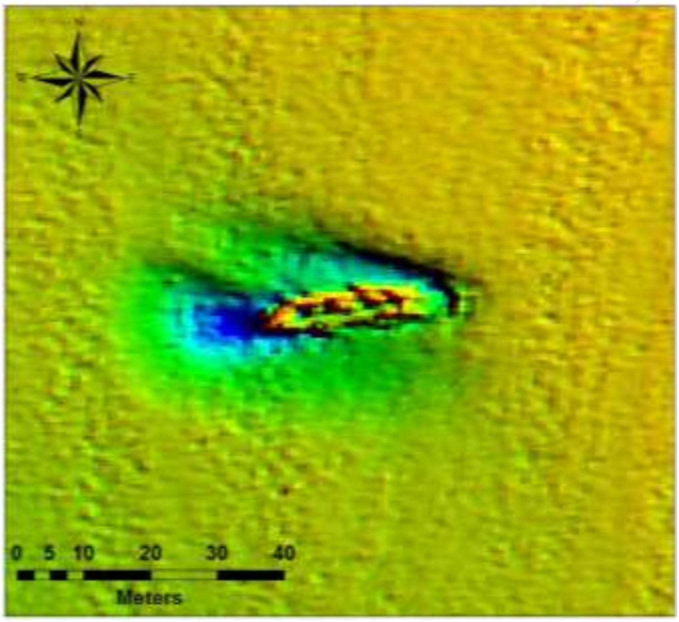

Shipwreck site 6 is located 1.4 km to the east of Shipwreck site 5. The origin of this wreck is also unknown. The wreck has a length of approximately 15 m and a maximum width of 6 m. It is orientated E-W at a general water depth in this area of 20 m. The most pronounced scour signature is to the west of the wreck and has a maximum depth of 2.2 m below the general seabed level. Significant scour can also be seen to the north of the wreck. These two lobes of scour indicate dominant bottom flow in a predominately alternating south-east to north-west and east to west direction.

3.3.7 Shipwreck site 7

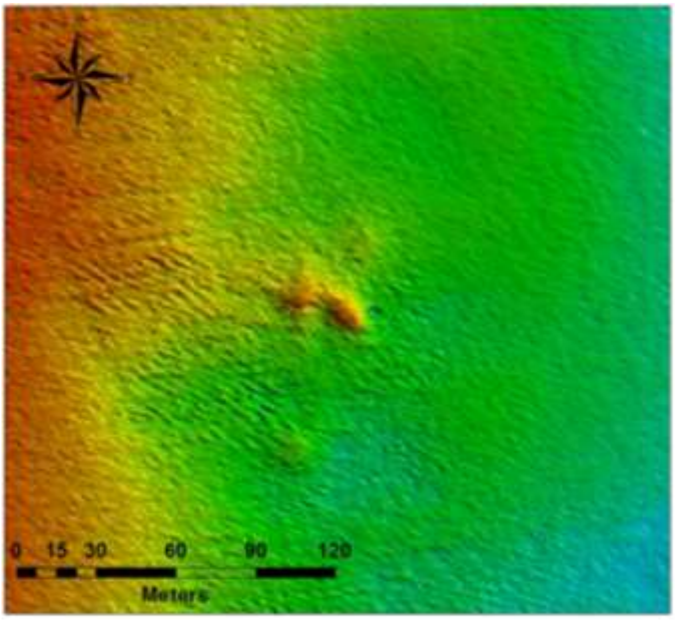

Shipwreck site 7 is located approximately 13 km to the east of shipwreck site 6 and is located in water depths of roughly 56 m. The wreck is not readily identifiable and appears to be partially covered by sedimentation even. It comprises and area of approximately 485 m^2. The surrounding seabed is slightly undulatory although no scour marks are noted at the site.

3.3.8 Shipwreck site 8

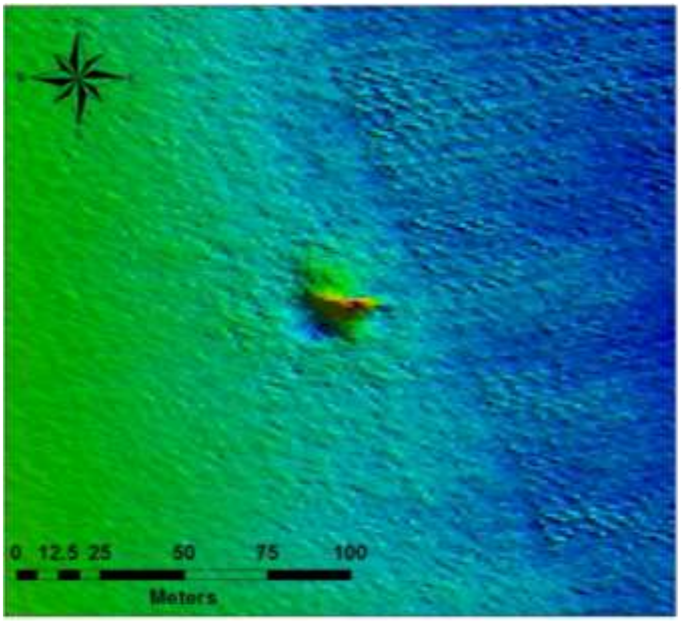

Shipwreck site 8 is located approximately 4.6 km to the south of shipwreck 7 in water depths of up to 60 m. The main body of the wreck is approximately 15 m in length orientated in an E-W direction. From the MBES it appears that is some degree of sediment accumulation to the northwest and southeast of the wreck with a minor scour pit to the southwest. This would indicate a dominant flow at this site towards the southwest.

3.3.9 Shipwreck site 9

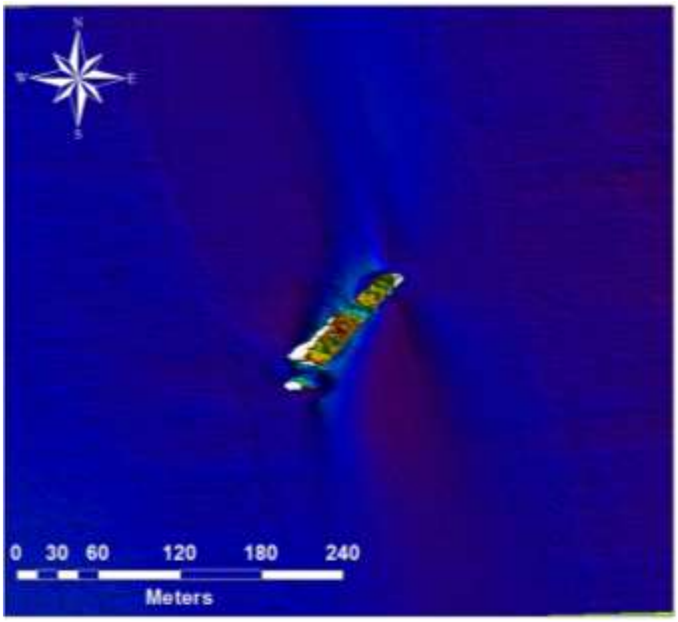

Shipwreck site 9 is located approximately 8 km northeast of Lambay Island and 6 km southeast of shipwreck site 8. According to the INFOMAR inventory this wreck is the SS Polwell; a steam collier that was sunk by a German U-boat in June 1918. On the seabed, the wreck has a length of about 96 and a width of 12 m. It rises above the average seafloor by approximately 8 m and sits in water depths of, on average, 35 m. The scour signature at this wreck exhibits a striking feature both to the north and south. The scour is deepest directly adjacent to the wreck (approximately 1.5 m below regular seafloor level) in both directions and extends out for a distance of roughly 220 m to the north and 200 to the south. This sort of signature would suggest that the wreck lies at roughly 90° to a bi-directional flow regime.

3.3.10 Shipwreck site 10

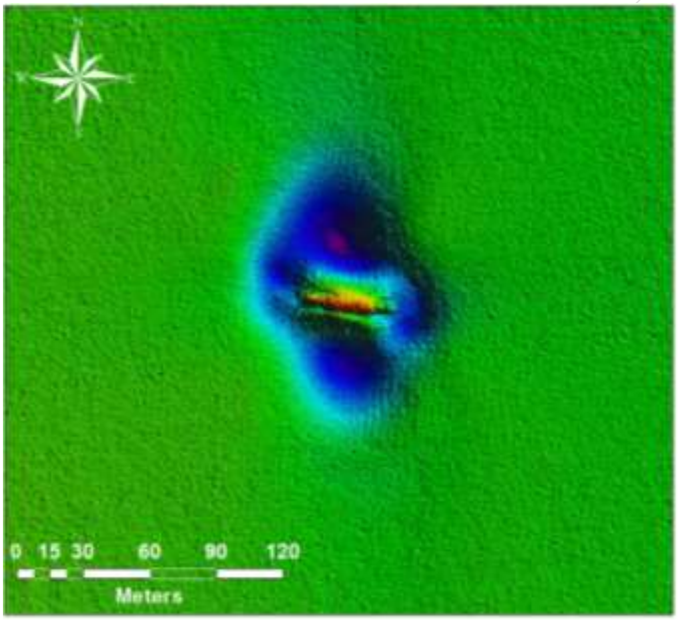

Shipwreck site 10 is located 13.5 km to the east of shipwreck site 9. According to the INFOMAR inventory, it is the *St. Michan, which* was sunk in March 1918. The wreck is approximately 23 m long and orientated E-W on the seabed in water depths of roughly 73 m. The scour signature at this wreck consists of a series of individual lobes to the north, east, south and east. The most pronounced lobes occur to the north and south, extending to a length of 65 m and 56 m respectively with scour depths of up to 2 m. This signature would suggest a generally uniform flow regime with a bi-directional element 90° to the wreck orientation.

3.3.11 Shipwreck site 11

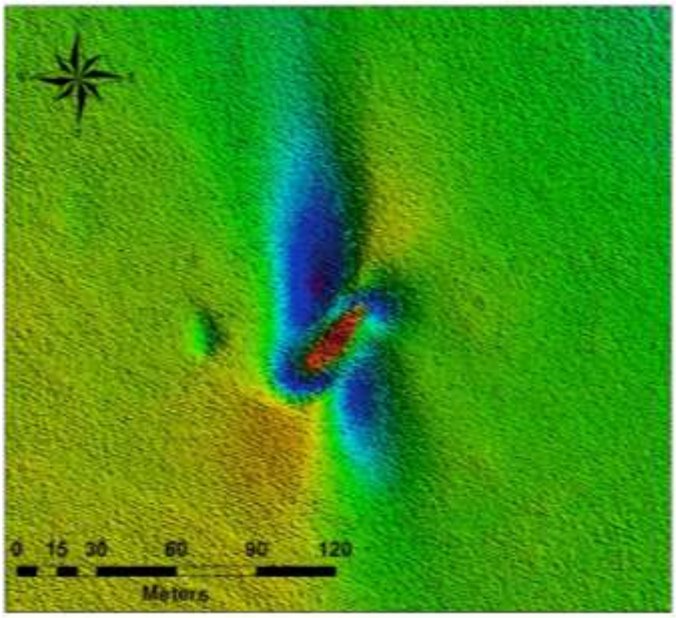

Shipwreck site 11 is located 7 km to the south of shipwreck site 10. Located in a water depth of approximately 66.5 m, the origin of the wreck is unknown. The wreck was a length of approximately 27 m and is orientated on the seafloor in a NE-SW direction. Scour at this site occurs all around the wreck and consists of four lobes. An apparently fifth scour lobe occurs 23 m to the west of the wreck. The largest lobes occur to the north and south of the wreck with a length of 74 m and 43 m respectively. This signature would suggest a uniform flow regime with a bi-directional element 90° to the wreck orientation.

3.3.12 Shipwreck site 12

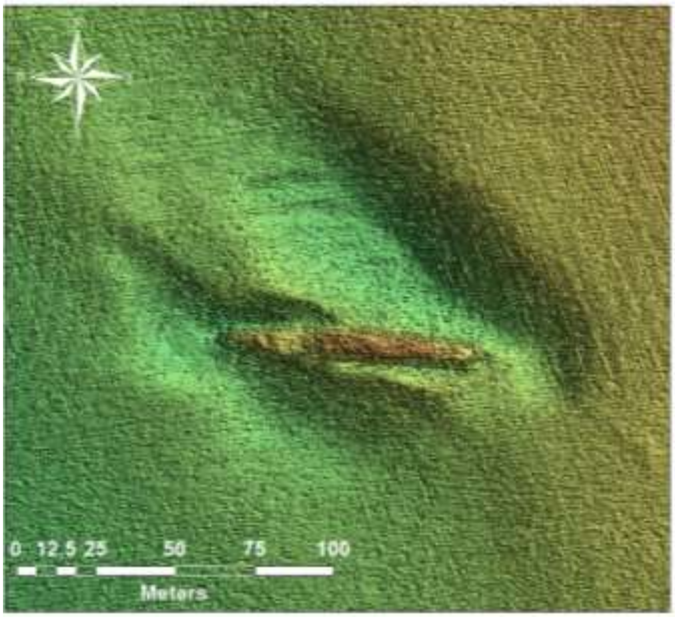

Shipwreck site 12 is located 20 km east of Irelands Eye and 8.7 km to the southwest of shipwreck site 11. According to the INFOMAR inventory it is recorded as the *SS Fern*; a passenger ship sunk in April 1918. On the seabed, the vessel measures 54 m long, 8.8 m wide with a height of about 7 m above the regular seafloor and is orientated roughly E-W. It is located in water depths of up to 79 m. Scour occurs around the wreck with the most prominent signature to the northeast of the wreck with a length of 98 m. A separate scour signature occurs to the southwest and is 74 m in length. The signature in this instance would suggest and alternating directional flow.

3.3.13 Shipwreck site 13

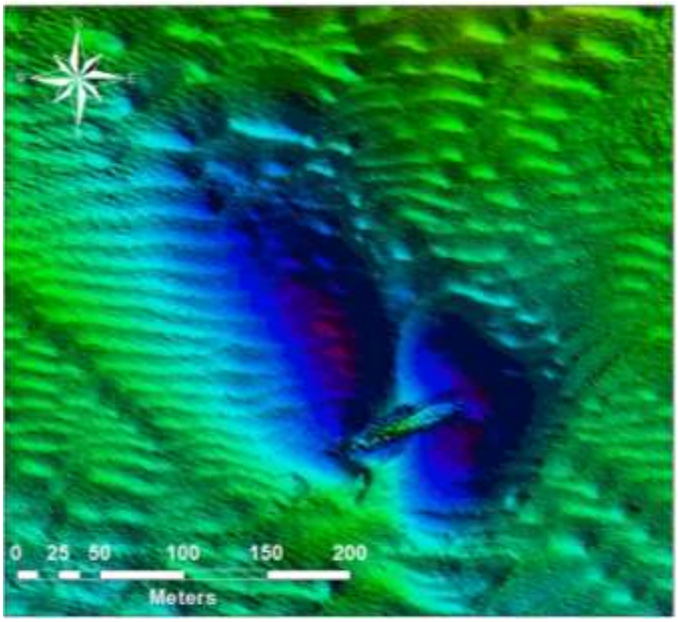

Shipwreck site 13 is located approximately 5.6 km to the southeast of shipwreck site 12. It is located in a highly dynamic area of seabed consisting of prominent sediment waves. It is identified as the *SS Hare* in the INFOMAR inventory; a merchant ship sunk in December 1917. It is located in water depths of generally 60 m and is roughly 45 m long orientated SW-NE on the seabed. Two significant scour tails have formed to the east of northwest of the wreck.

3.3.14 Shipwreck site 14

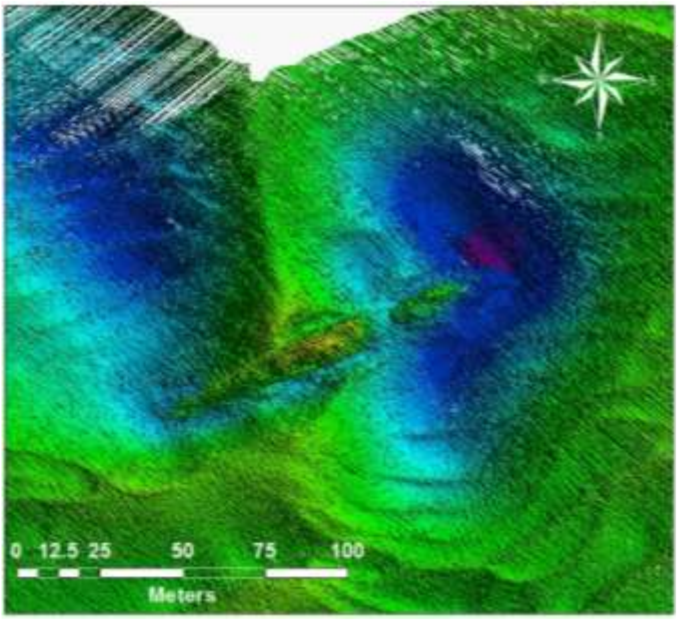

Shipwreck site 14 is located 5 km to the southeast of shipwreck site 13. Similarly, it is located in an area of strong sediment dynamics. The ship is identified as the *W.M Barkley* by the INFOMAR inventory and was sunk in October 1917. Water depth at the site is approximately 56 m and is approximately 59 m, orientated SW-NE on the seabed. Two distinctive scour tails have formed to the east and northwest of the wreck.

3.4 Existing Scour Summary

From the shipwreck sites analysis outlined in Section 3.3, the bottom-current vectors for each site were derived that predominantly influenced scour direction. These vectors were then plotted against present day bed shear stress vectors from tidal model outputs created by (Uehara, Scourse, Horsburgh, Lambeck, & Purcell, 2006) (Figure 17). Ten of the fourteen sites (SS1 – SS10) are located within the broad geographic extent of the WISMB, whilst the remainder (SS11 – SS14) were included by way of a comparison.

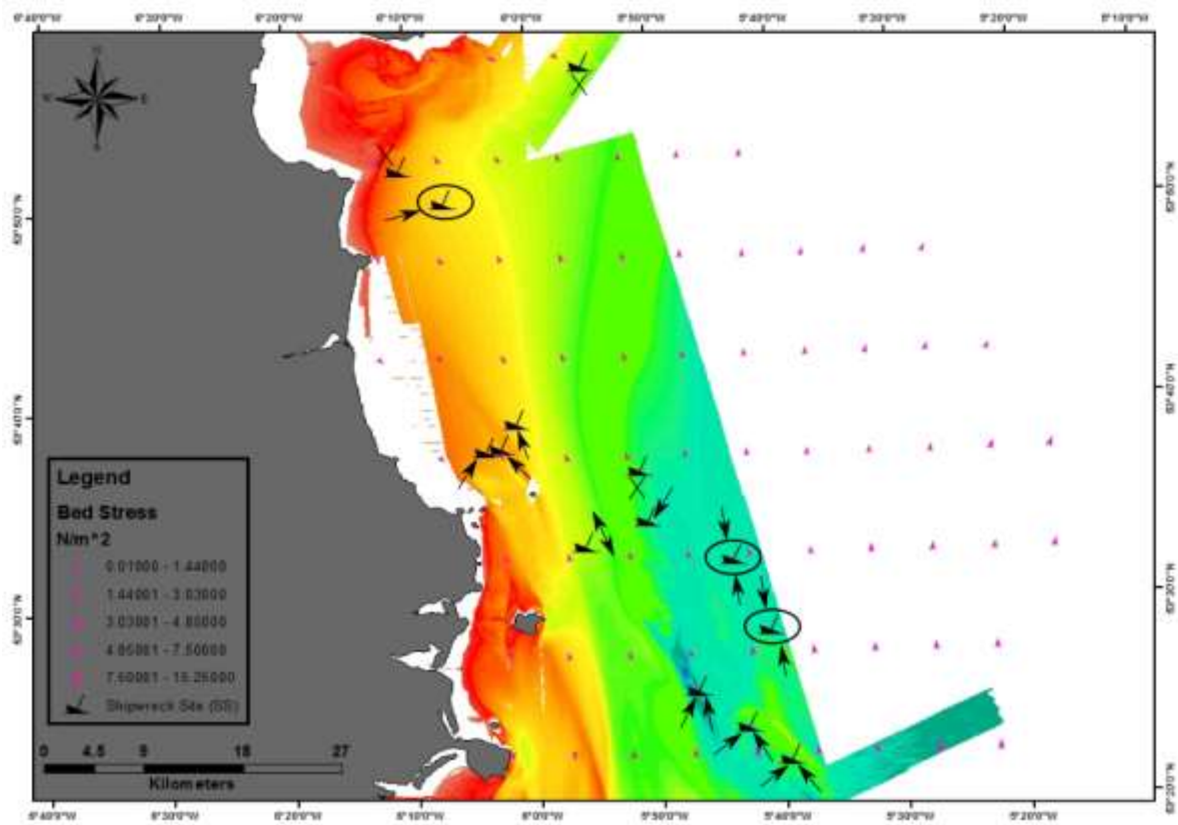

Figure 17 Bottom current vector plot. The pink arrows represent tidal model outputs from Uehara et al (2006) with bed shear stress magnitude (in N/m²) and direction (denoted by arrow direction). For each shipwreck site a dominant current vector-influencing scour is denoted by a black arrow, with a circle indicating a dominant uniform flow regime and a cross denoting no significant scour at the site.

Generally, the bed shear stresses in the study area are low (<2 N/m^2) and with a northerly flow direction. From the bed stress vector plot, shear stress magnitude decreases towards the north of the study area. This corroborates with the scour signatures seen at the three most northerly shipwreck sites where either no significant scour (SS1 and SS2) or minor levels of scour are seen (SS3). At SS3 the scour signature suggests a uniform flow regime with a slight inclination towards scour propagation in the north-western directing, which is slightly at odds with the dominant northerly flow according to Uehara et al. (2006).

Further south, sites SS3, SS4 and SS5 generally suggest a controlling northerly current vector. The Uehara et al. (2006) modelled bed stress vectors for this area suggest a varying flow regime with a more dominant southerly aspect closer to shore and northerly heading east.

At SS7 no significant scour was recorded, whilst at SS8 minor scouring indicated a strong south-westerly flow dynamic contrary to the dominant northerly aspect suggested by the Uehara model. Some evidence for sediment deposition at SS8 would further suggest a complex hydrodynamic regime at the site. Significant scour to the north and south at SS9 suggests a strong bi-directional element here, again counter to the dominant northerly aspect of Uehara et al. (2006), further emphasising the possible complexity in this particular area of the WISMB.

Both SS10 and SS11 display similar scour signatures consisting of lobes around the wreck with a propensity for extended tails in an N-S orientation. This would indicate a general uniform flow regime, but with a strong N-S, bidirectional component. The location of these sites towards the southern extent of the WISMB also highlight the increasing bed stresses as suggested by the Uehara et al. (2006) model.

SS12, SS13 and SS14 are found in dynamic environments outside the WISMB as highlighted by their much more extensively developed scour signatures.

This analysis has highlighted that, despite being a low-energy environment with no natural scour, the introduction of an object (in this case a shipwreck) to the seabed within the WISMB can induce scour. Furthermore, the suggested vectors of flow derived from these scour signatures would suggest that local conditions are more complex than the simplified model offered by Uehara et al. (2006). That said, there is a relatively decent correlation between the level of scour at a geographic location and the magnitude of bed stress suggested by Uehara et al. (2006) as evidenced by a propensity for more extensive scour in the south, diminishing heading north. Granted, this may also be a factor of the time the object has been resting on the seabed and the seabed sediment parameters. That considered, the majority of wrecks used in this study date from roughly the same year (early 1900s) and we have already demonstrated the homogenous nature of seabed sediment in the WISMB.

3.5 Design Inputs

3.5.1 Water Depths

Water depth at the study site derived from MBES data reveal a relatively uniform seabed that slopes gently eastward from water depth of approximately 10 m to a maximum of 55 m (Figure 2).

3.5.2 Oceanographic Conditions

The Irish Sea is generally influenced by the southern tidal current influx. The tide principally results from the M_2 (principal lunar) forcing. Unlike the rest of the Irish Sea, which is well mixed by strong tides, the WISMB stratifies in Spring and Summer of each year. This is the result of a combination of weak tides and relatively deep water producing insufficient mixing usually generated by tides and so fails to overcome the input of surface buoyancy created by solar heating (Hill et al., 1997). Bed stress current velocities within the area generally do not exceed the 0.5 ms^{-1} to mobilize the class of sediment found there and tidal currents are largely weak at < 0.3 ms^{-1} (Hill et al., 1997; Holmes & Tappin, 2005). Peak spring tide current velocities are also modelled to be low (Lewis et al., 2015; Figure 18). A seasonal gyre is known to develop in the area which increases near surface water current velocities and has been noted to have an effect on seafloor sediment and its dynamics (Callaway et al., 2009; Horsburgh et al., 2000).

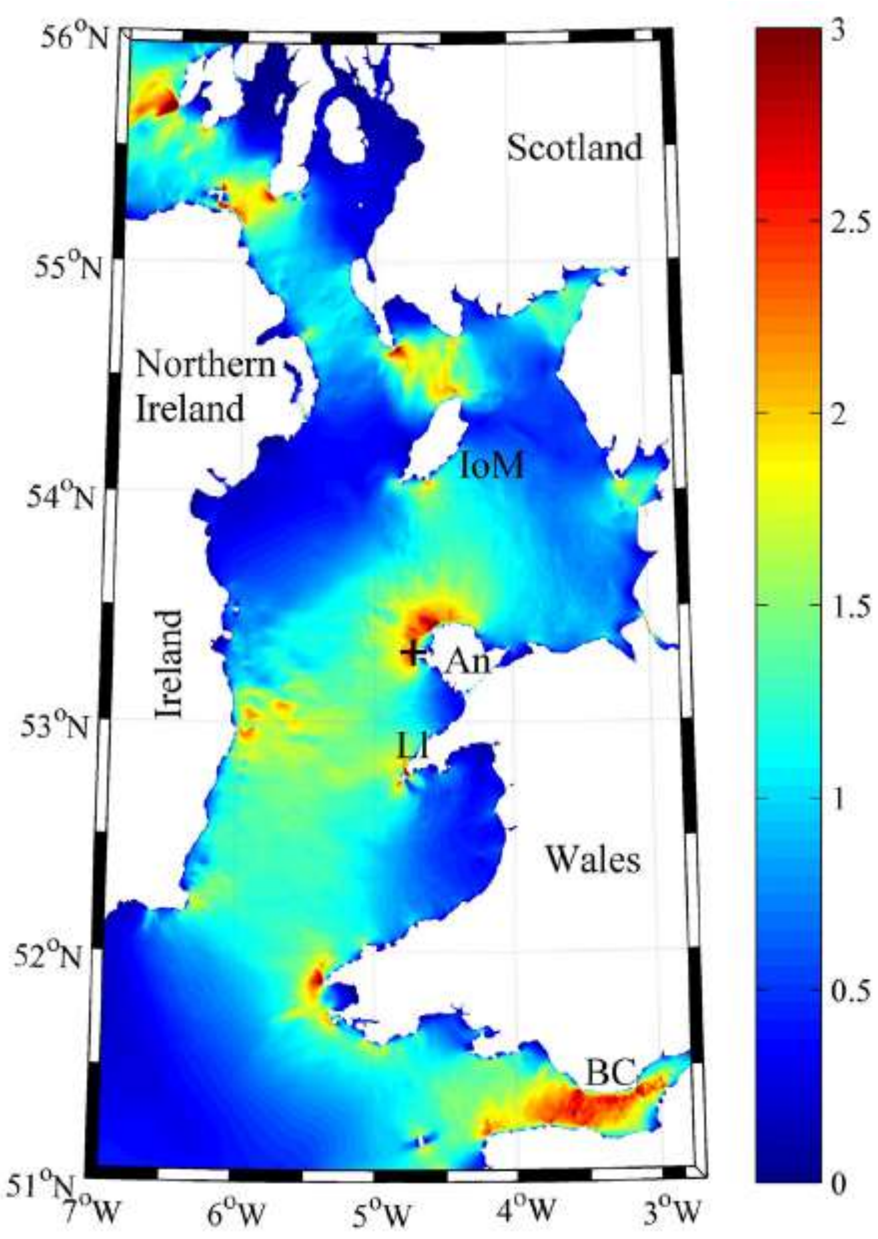

Figure 18 Peak spring tide current velocity (m/s) in the Irish Sea (From: Lewis et al. (2015))

3.5.2.1 Wind Regime

The wind regime indicates a propensity towards a southerly direction with wind speeds less than 20 m/s.

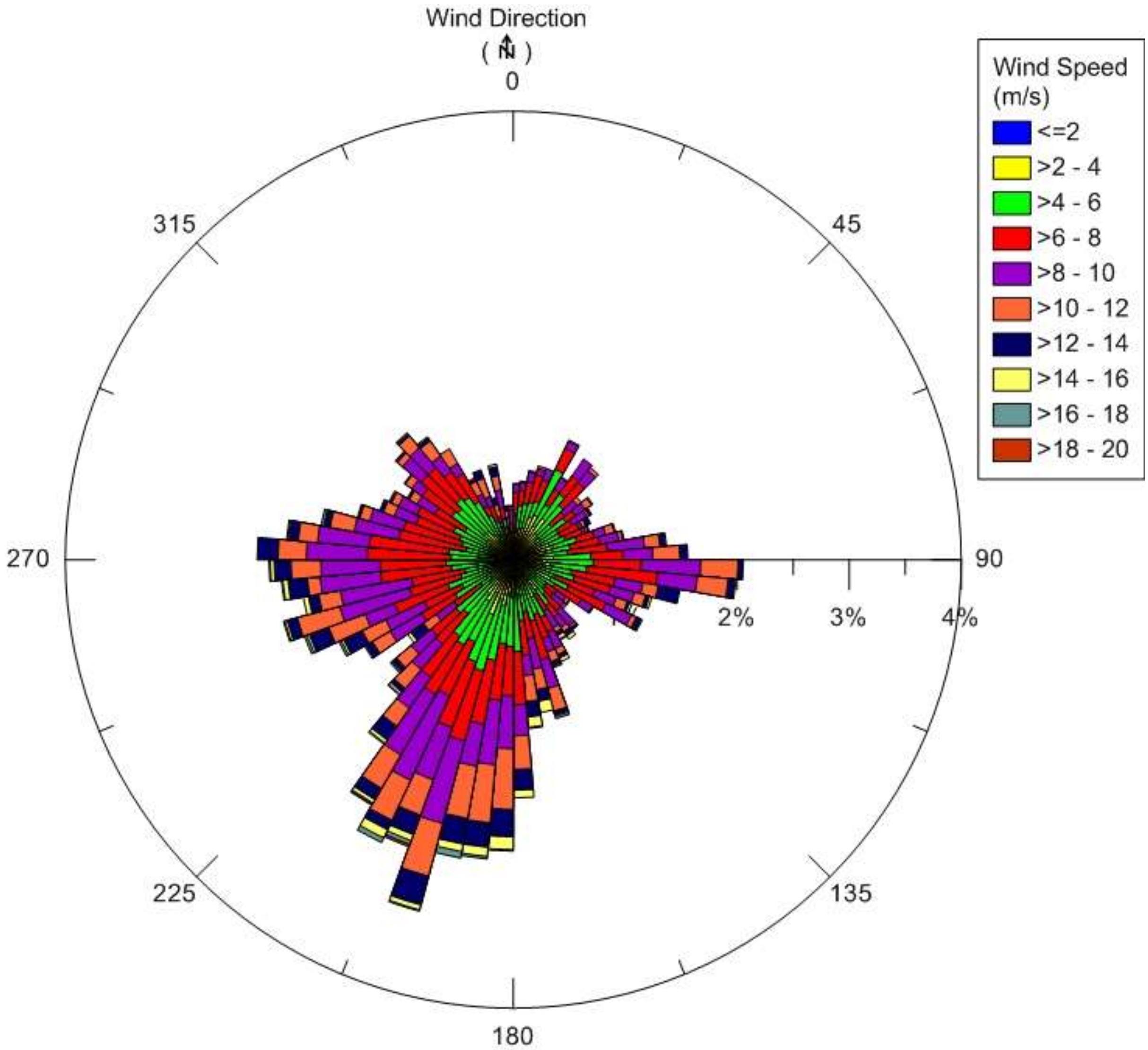

Figure 19 Wind rose for M2 Buoy 2013

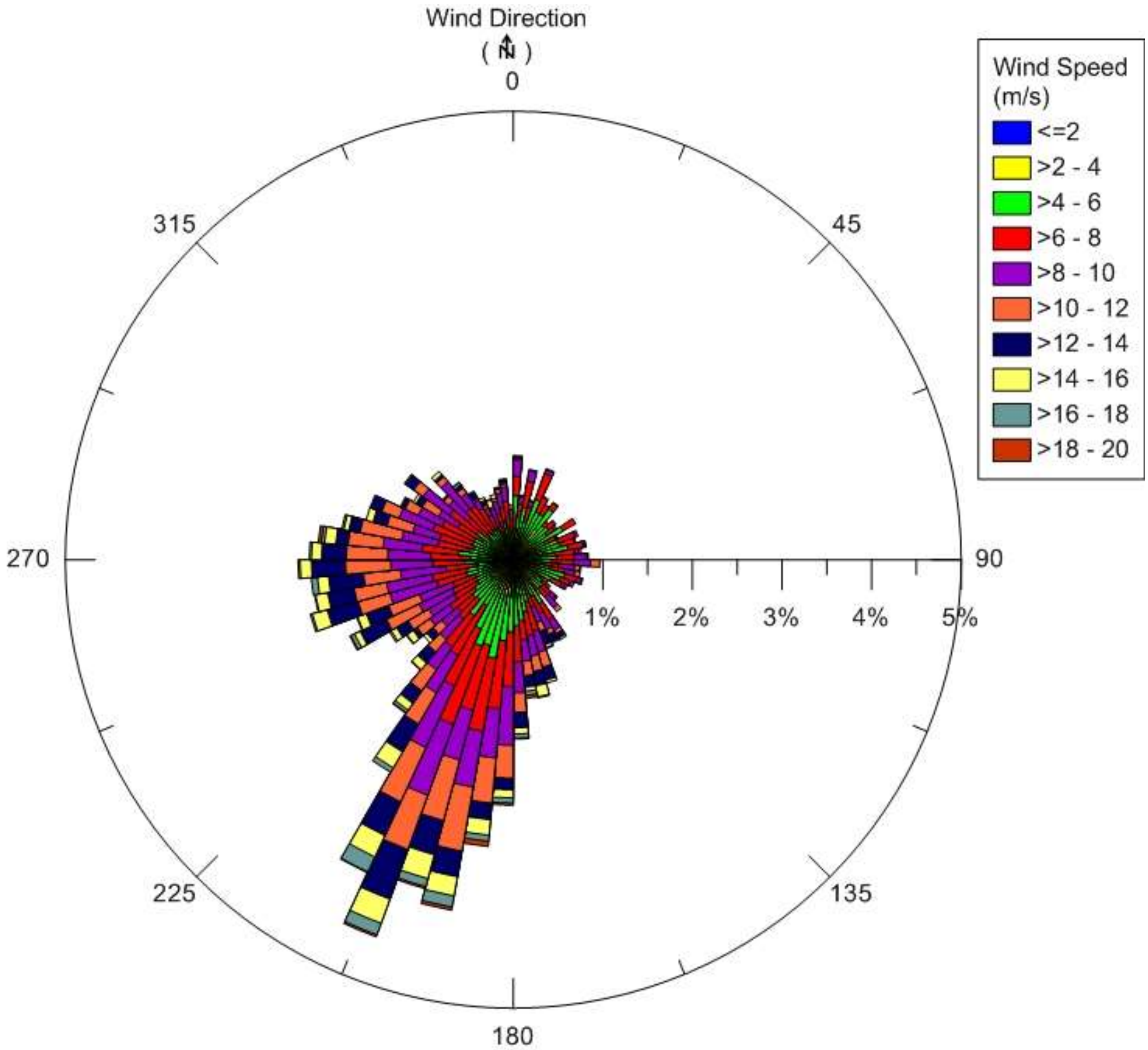

Figure 20 Wind rose for M2 Buoy 2015

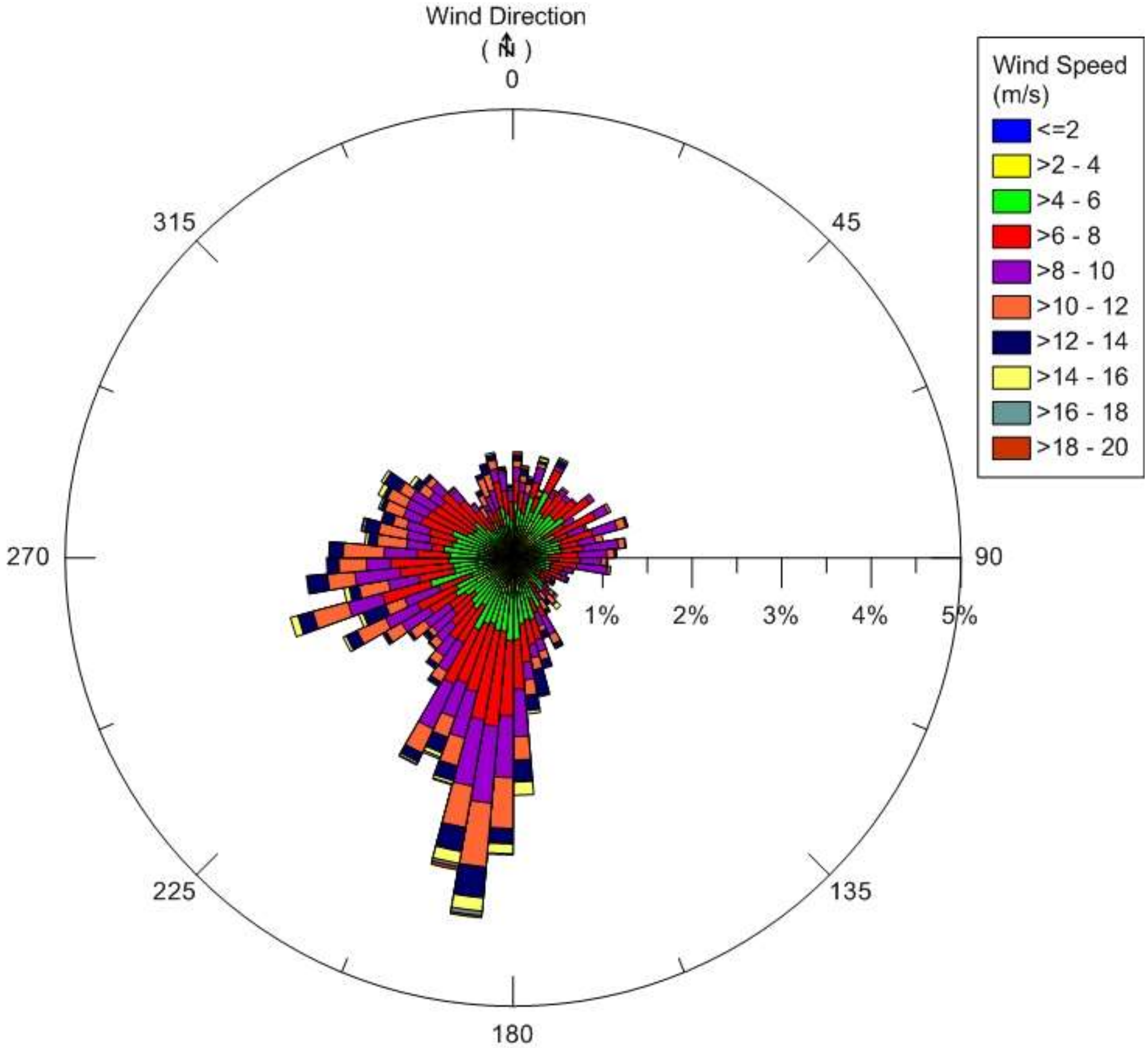

Figure 21 Wind rose for M2 Buoy 2016

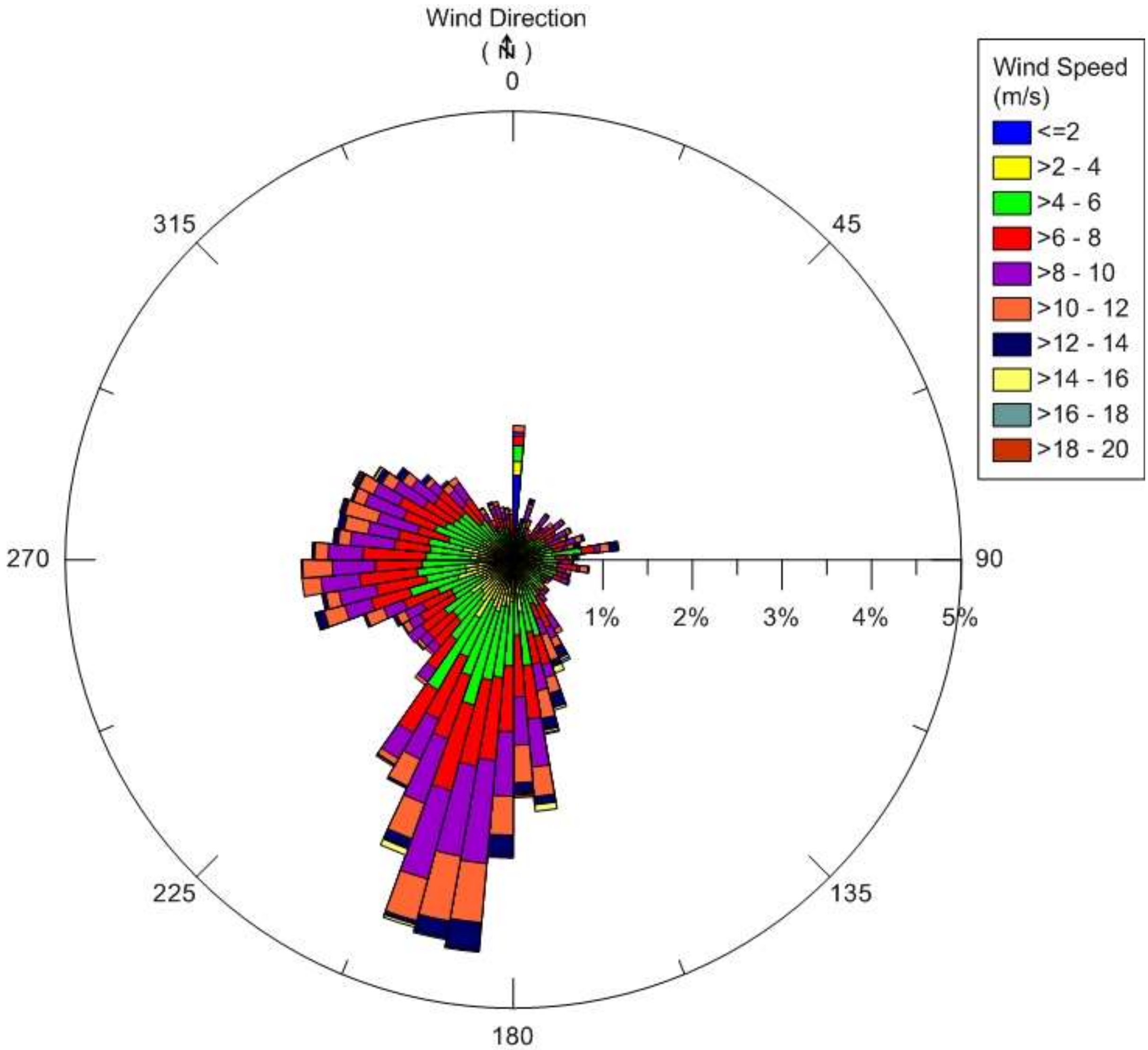

Figure 22 Wind rose for M2 Buoy 2017

3.5.2.2 Wave Regime

Wave data also needs to be analysed to determine whether there is a wave induced scour component or in fact the wave agitation may impede scour from developing. A critical factor will be the wave directionality. To determine the relative contribution of the waves, it is necessary to plot out the wave roses and examine the wave scatter data.

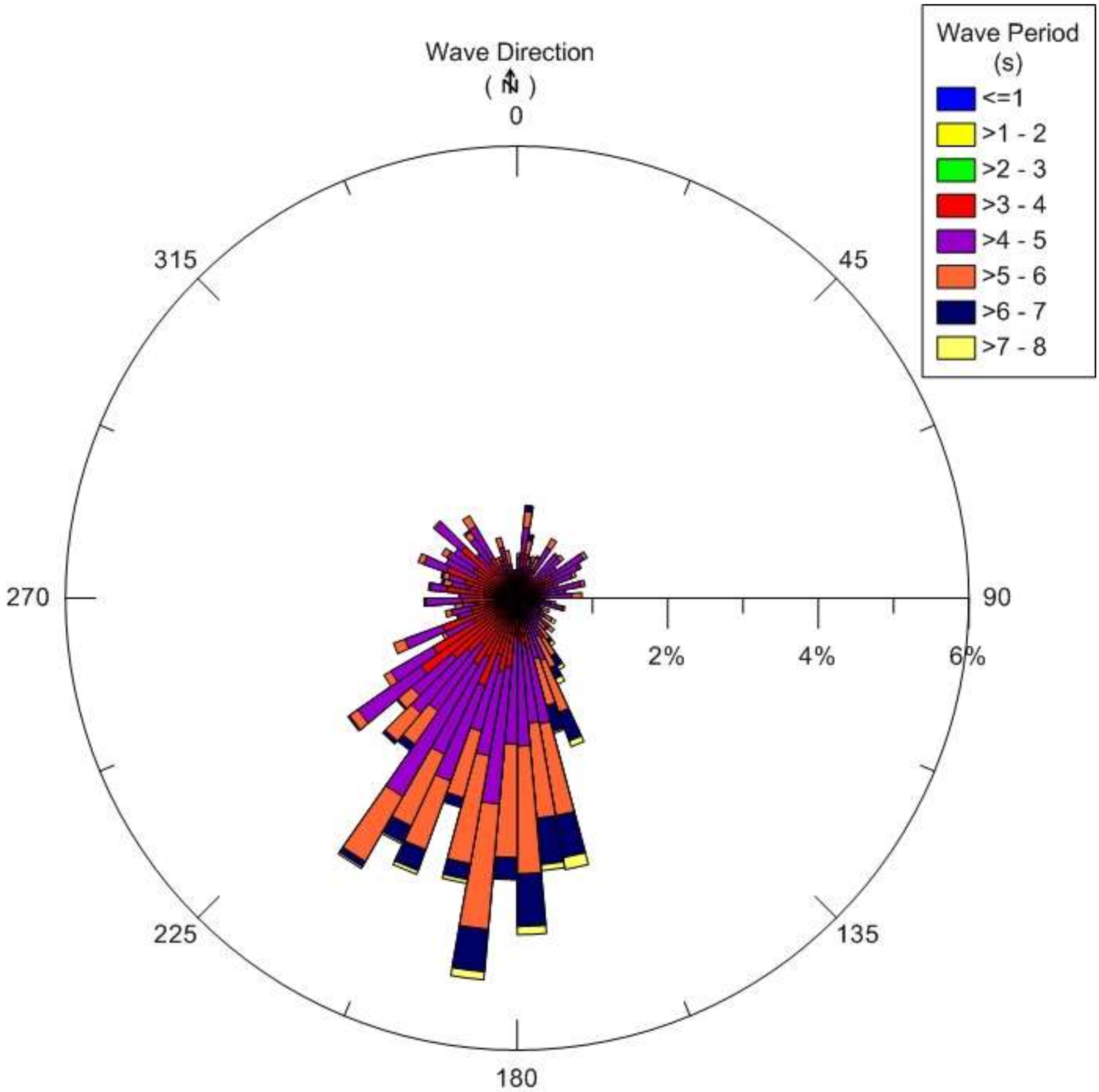

Figure 23 Wave direction and period from M2 buoy 2013

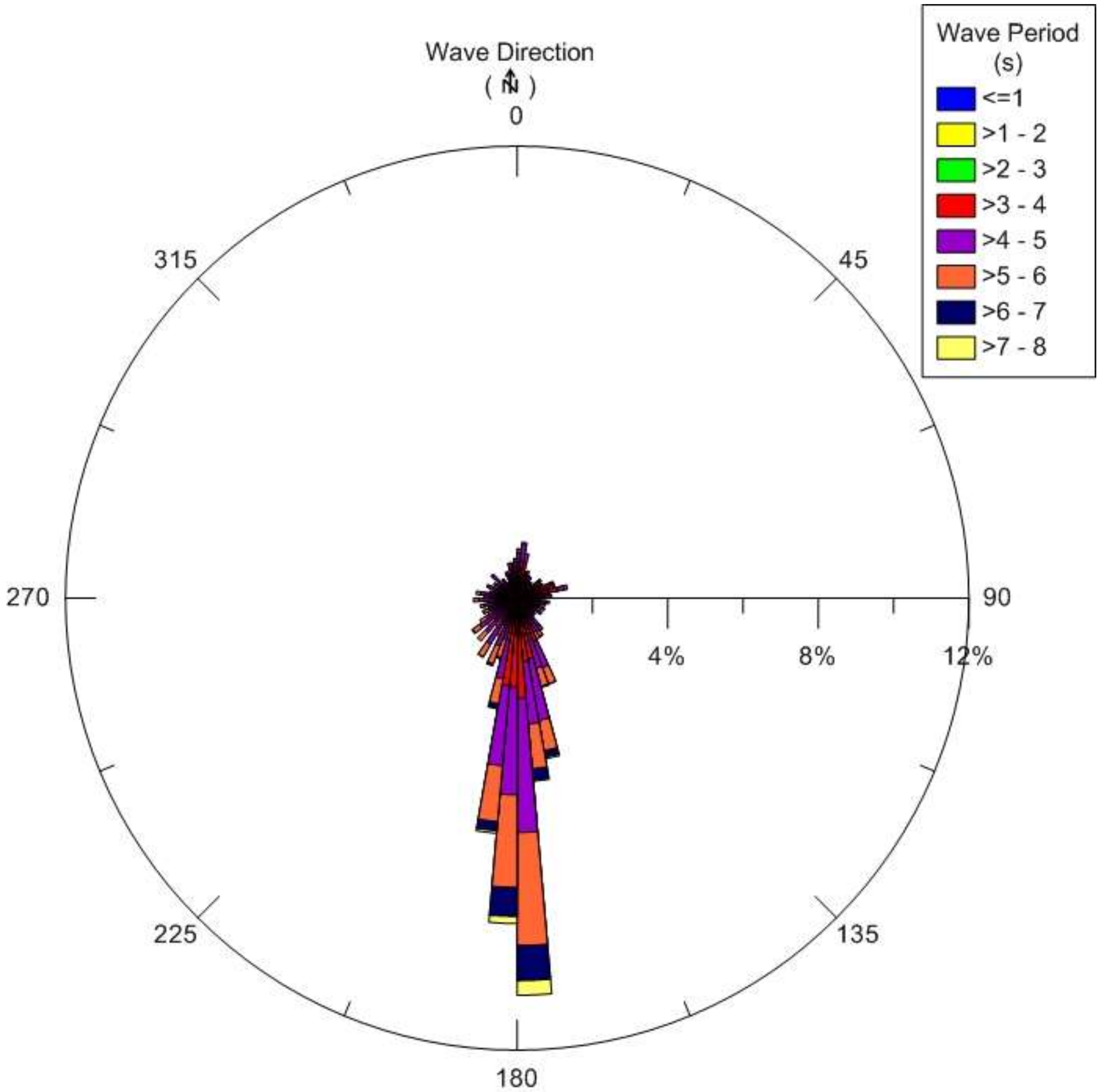

Figure 24 Wave direction and period from M2 buoy 2015

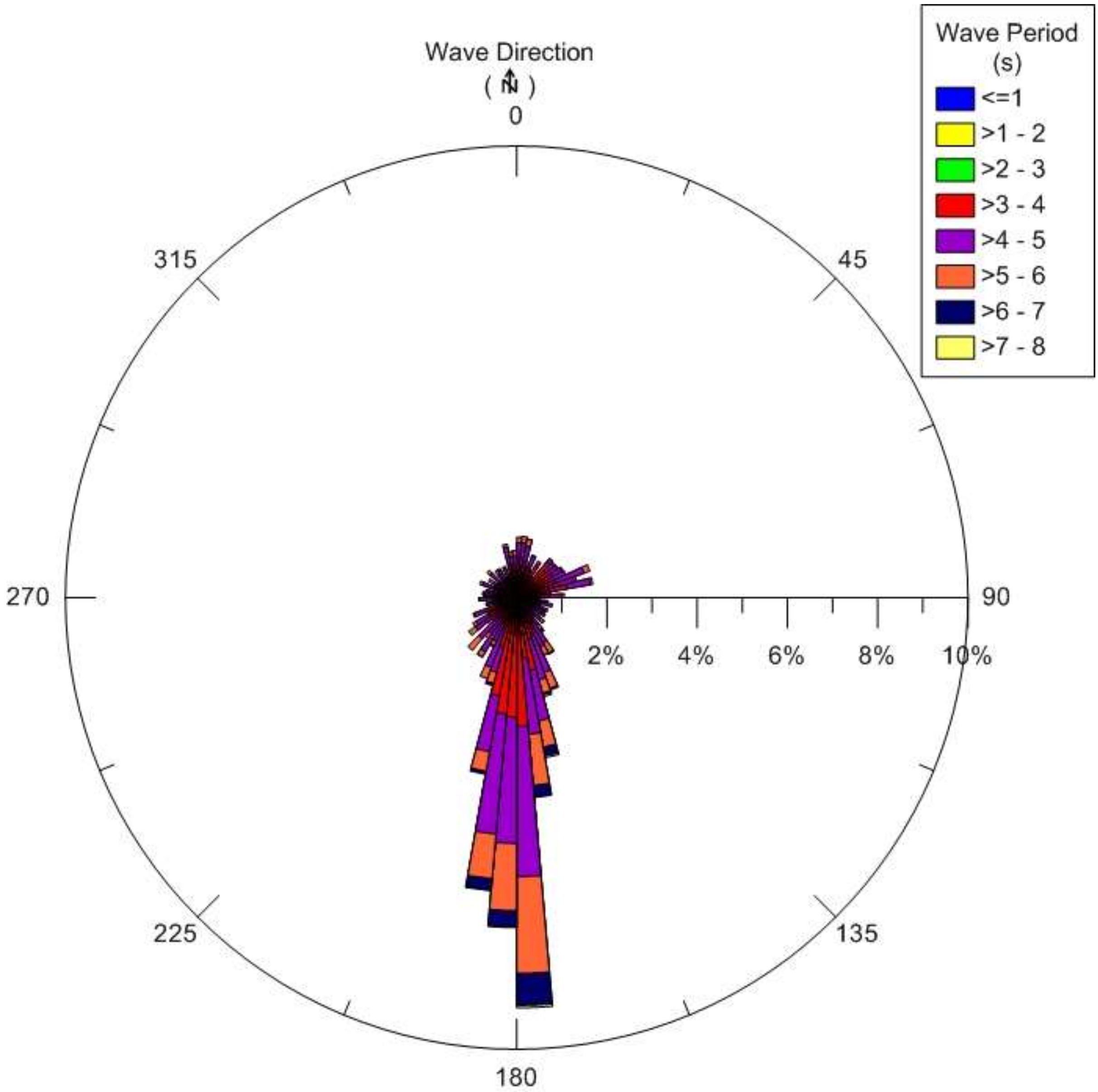

Figure 25 Wave direction and period from M2 buoy 2016

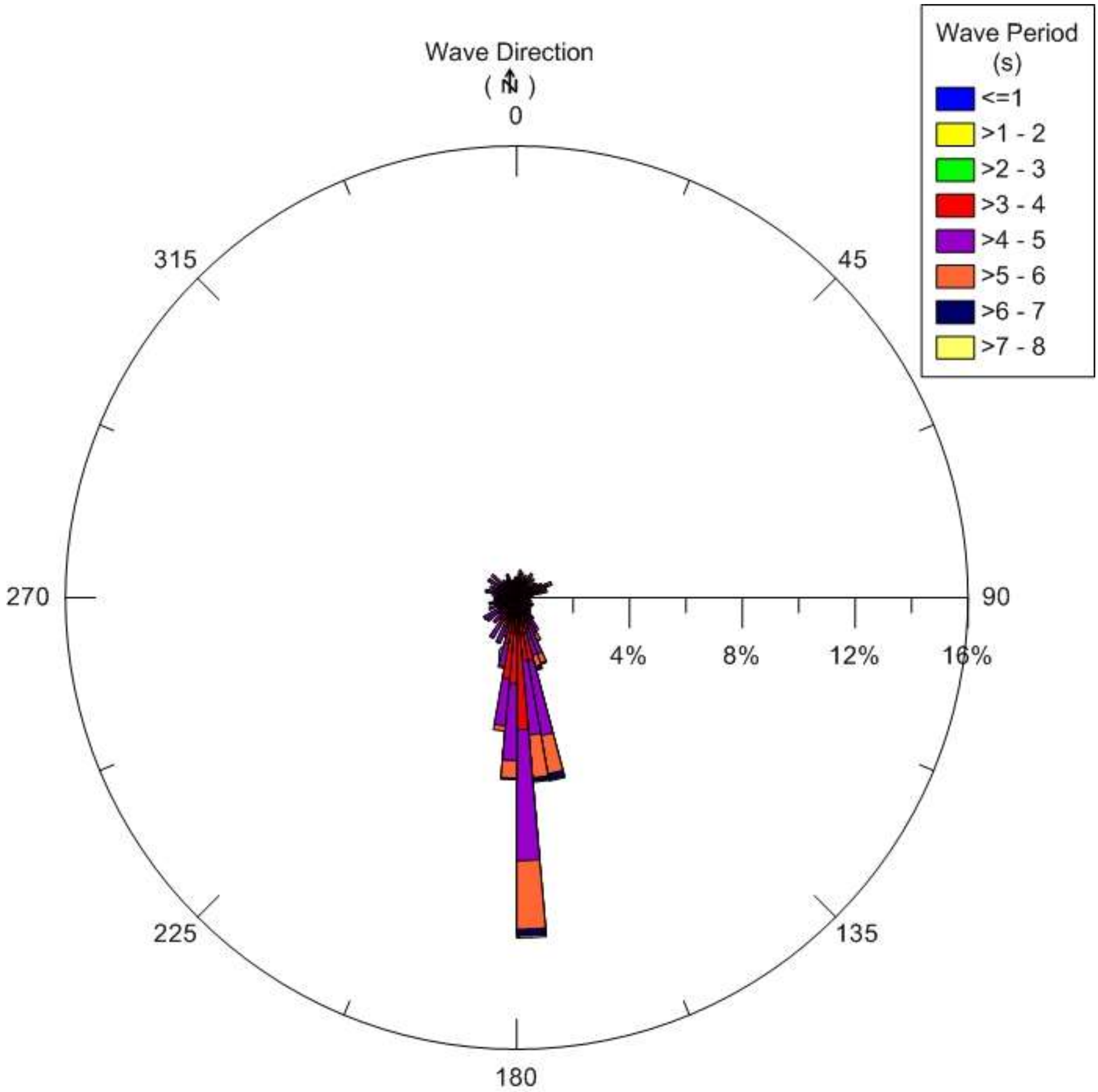

Figure 26 Wave direction and period from M2 buoy 2017

The data suggests there is a slight wind-wave misalignment, but not significant in augmenting scour conditions. From this data, we could garner relevant parameters to input into numerical equations with which to predict and characterise scour in the area, including wave height and wave period (Table 4 -
Table 7).

Table 4 Annual average wave height data from M2 Buoy

Year	Value (m)
2013*	1.44
2014**	1.34
2015	1.2
2016	1.1
2017	1.1
2018***	1.73

*No data for Jan - Jul
**No data for Feb – Jul
***Jan – Mar only

Table 5 Seasonal average wave height data from M2 buoy

Year	Period	Value (m)
2013	Jan - Mar	n/a
	Apr - Jun	n/a
	Jul - Sept	0.8
	Oct - Dec	1.6
2014	Jan - Mar	1.73
	Apr - Jun	n/a
	Jul - Sept	0.85
	Oct - Dec	1.46
2015	Jan - Mar	1.48
	Apr - Jun	0.89
	Jul - Sept	0.81
	Oct - Dec	1.66
2016	Jan - Mar	1.5
	Apr - Jun	0.84
	Jul - Sept	0.88
	Oct - Dec	1.19
2017	Jan - Mar	1.35
	Apr - Jun	0.84
	Jul - Sept	0.89
	Oct - Dec	1.5
2018	Jan - Mar	1.73

Table 6 Annual average wave period data from M2 buoy

Year	Value (s)
2013*	4.4
2014	4.3
2015	4.3
2016	4.2
2017	4.1
2018***	4.9

*No data for Jan - Jul
**No data for Feb – Jul
***Jan – Mar only

Table 7 Seasonal average wave period data from M2 buoy

Year	Period	Value (s)
2013	Jan - Mar	n/a
	Apr - Jun	n/a
	Jul - Sept	4
	Oct - Dec	4.6
2014	Jan - Mar	4.8
	Apr - Jun	n/a
	Jul - Sept	3.8
	Oct - Dec	4.4
2015	Jan - Mar	4.4
	Apr - Jun	4
	Jul - Sept	3.9
	Oct - Dec	4.8
2016	Jan - Mar	4.5
	Apr - Jun	4
	Jul - Sept	4
	Oct - Dec	4.1
2017	Jan - Mar	4.4
	Apr - Jun	3.9
	Jul - Sept	4
	Oct - Dec	4.4
2018	Jan - Mar	4.9

3.5.3 Sediment properties

Based on particle–size analysis of core samples particle size distribution (PSD) curves were generated (Figure 28 - Figure 34) to extract key particle size values including median (D50) as well as D60 and D10 (Table 8). In this study, median PSD values derived from core analysis (upper 3 meters) were felt to be more robust and representative of seabed conditions than grab sample (upper centimetres).

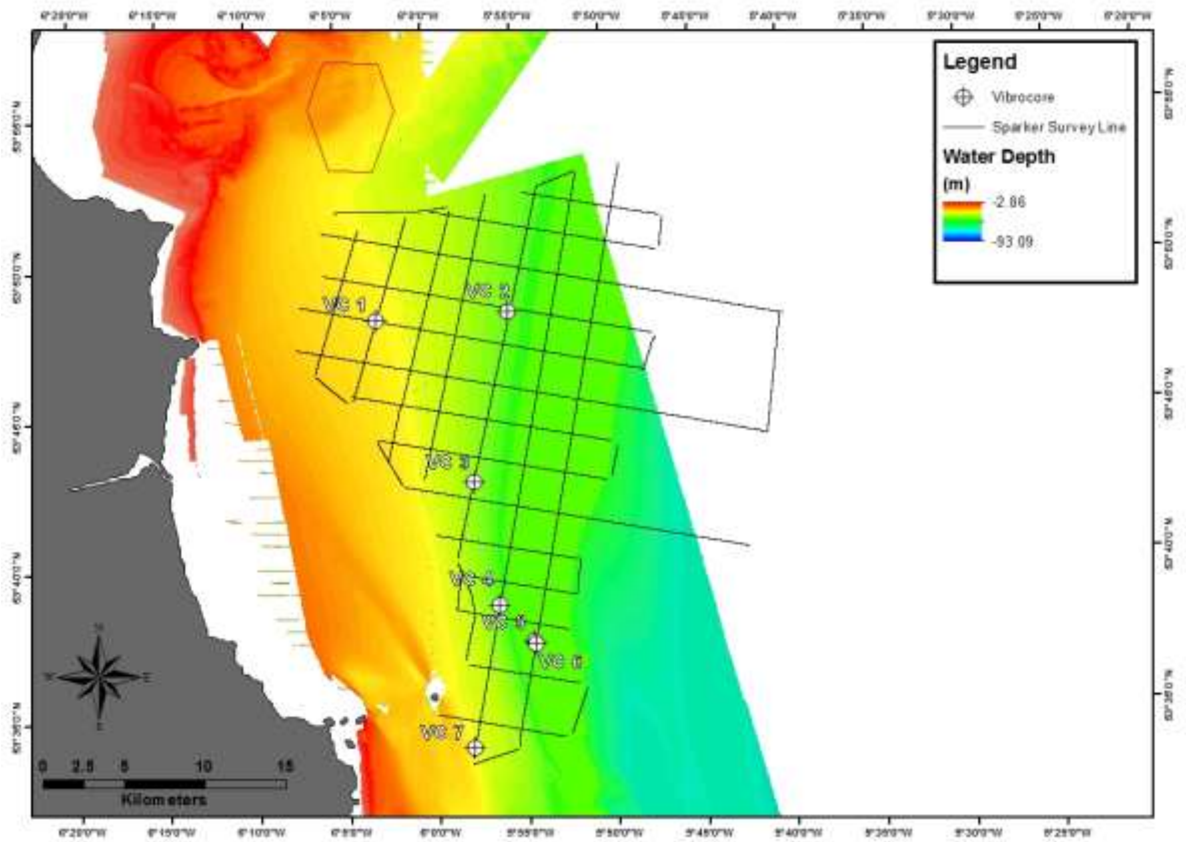

Figure 27 Vibrocore locations (VC)

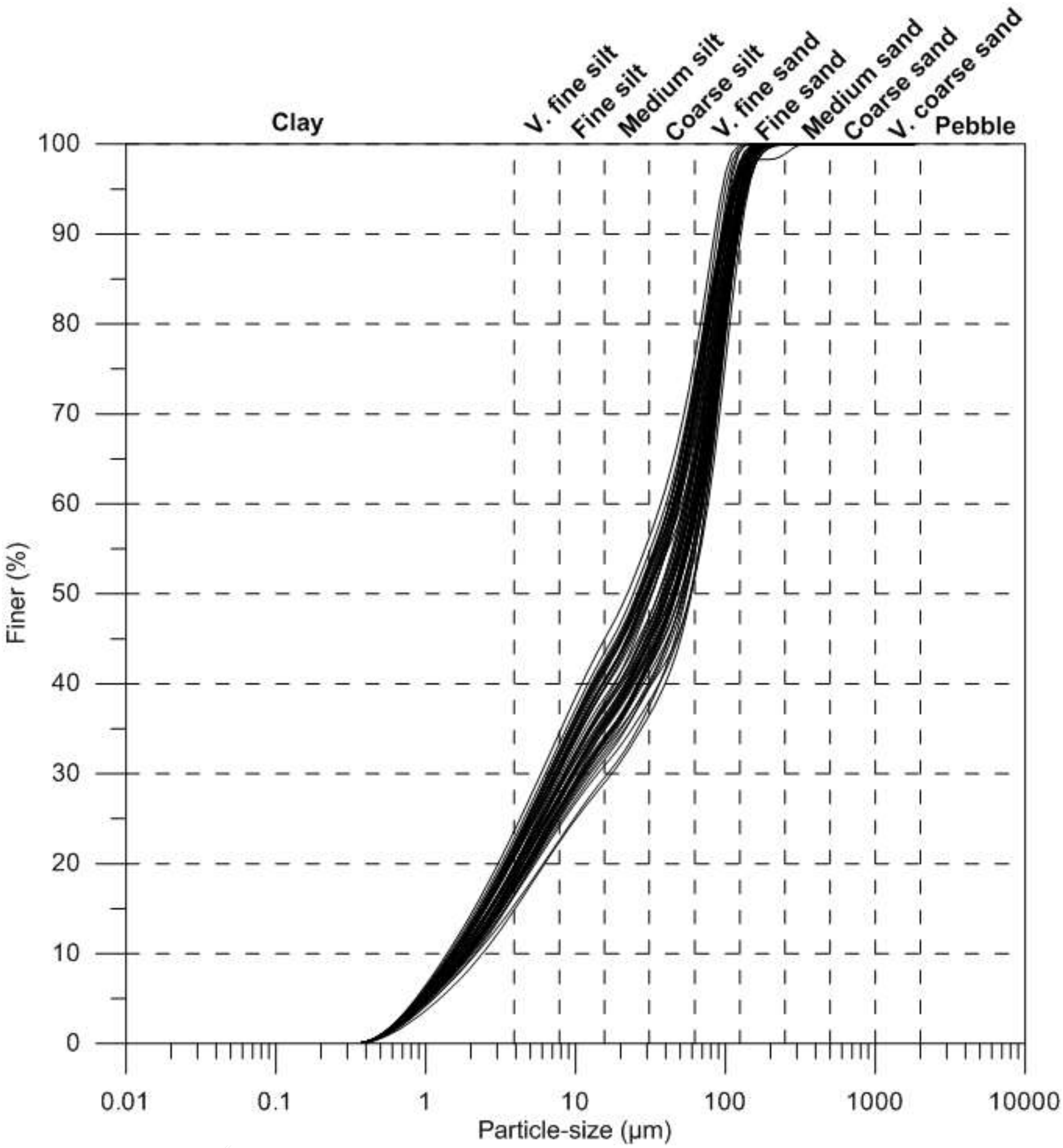

Figure 28 PSD curves of point samples from core VC 1a

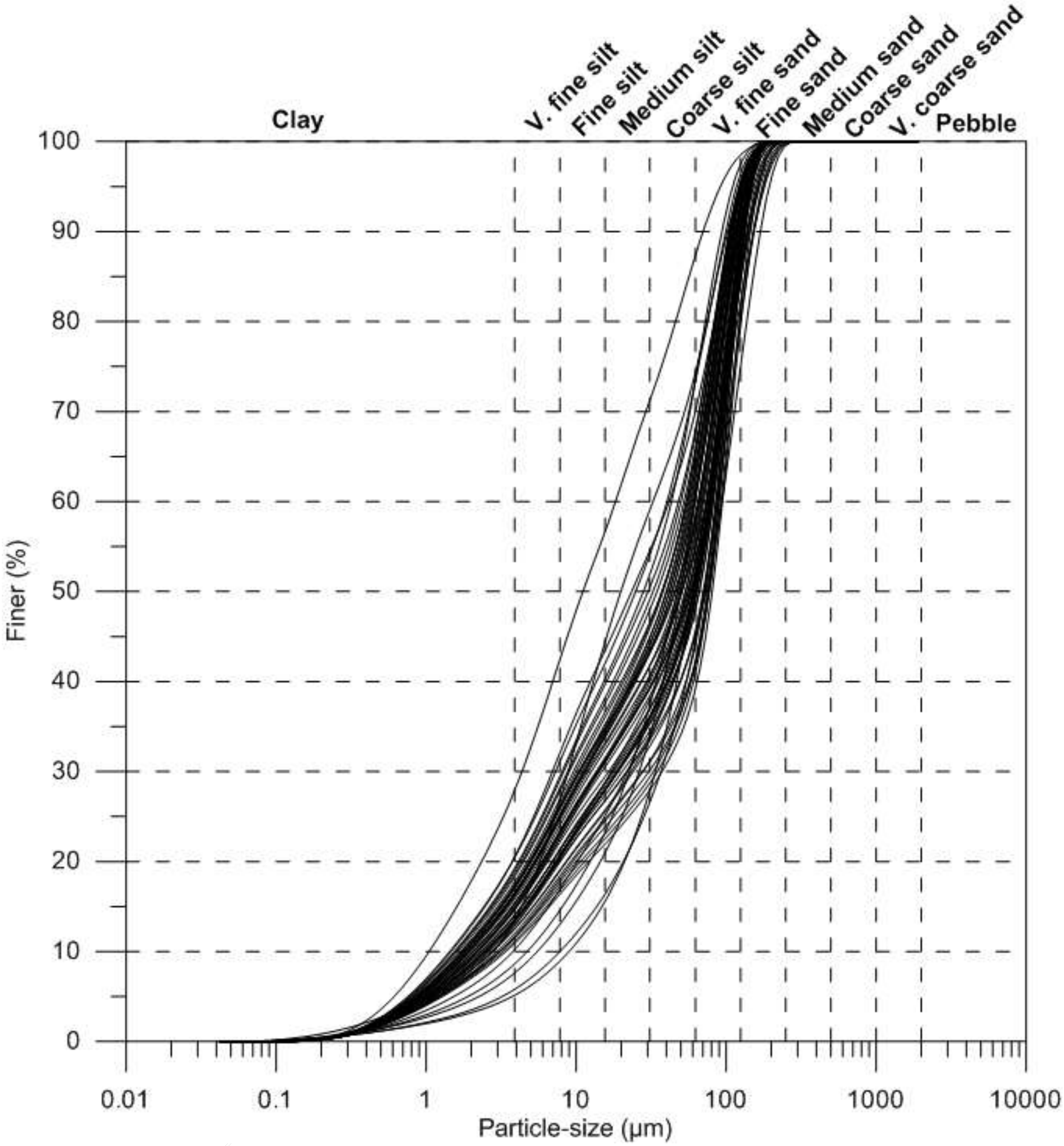

Figure 29 PSD curves of point samples from core VC 1b

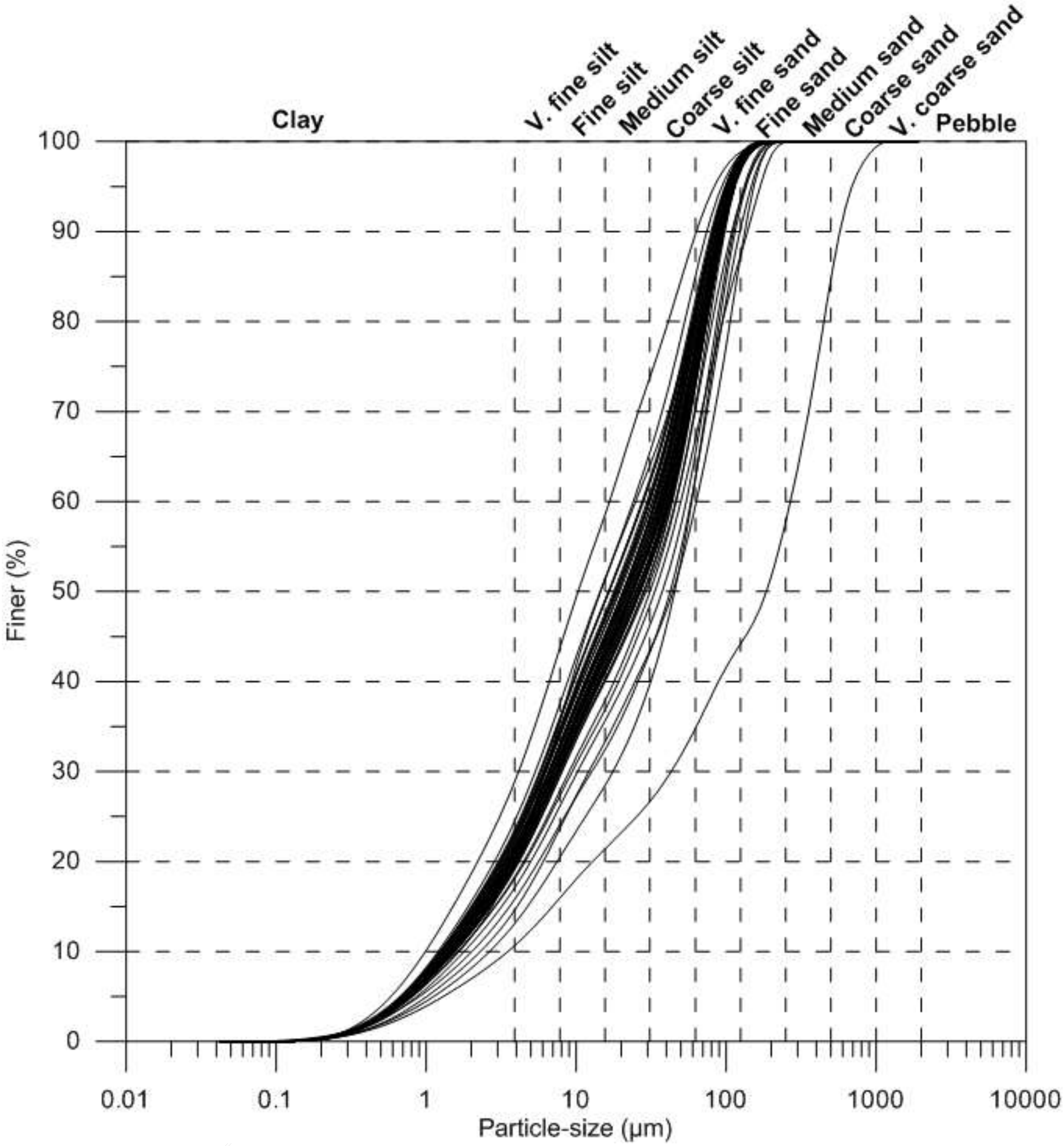

Figure 30 PSD curves of point samples from core VC 2

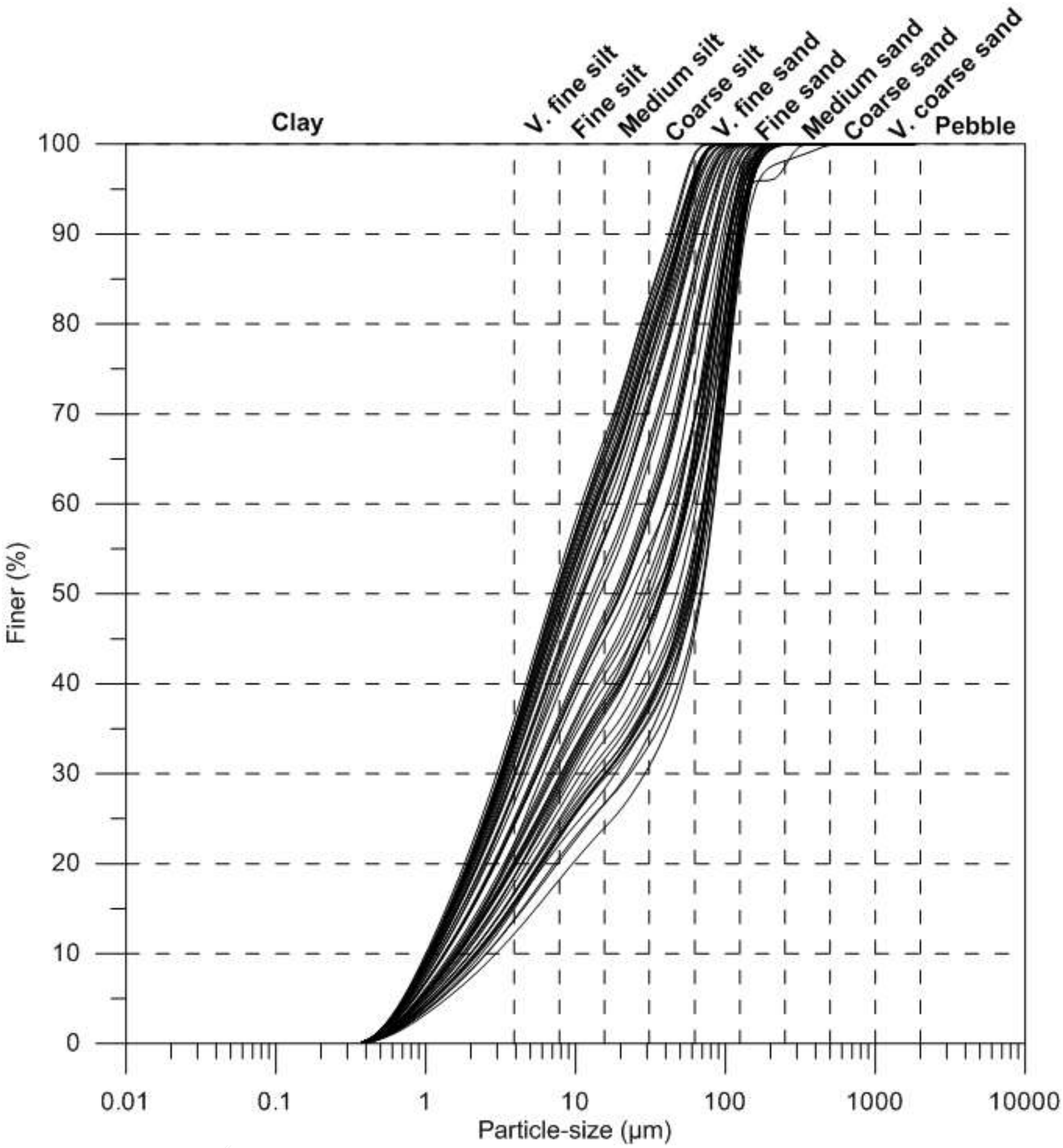

Figure 31 PSD curves of point samples from core VC 3a

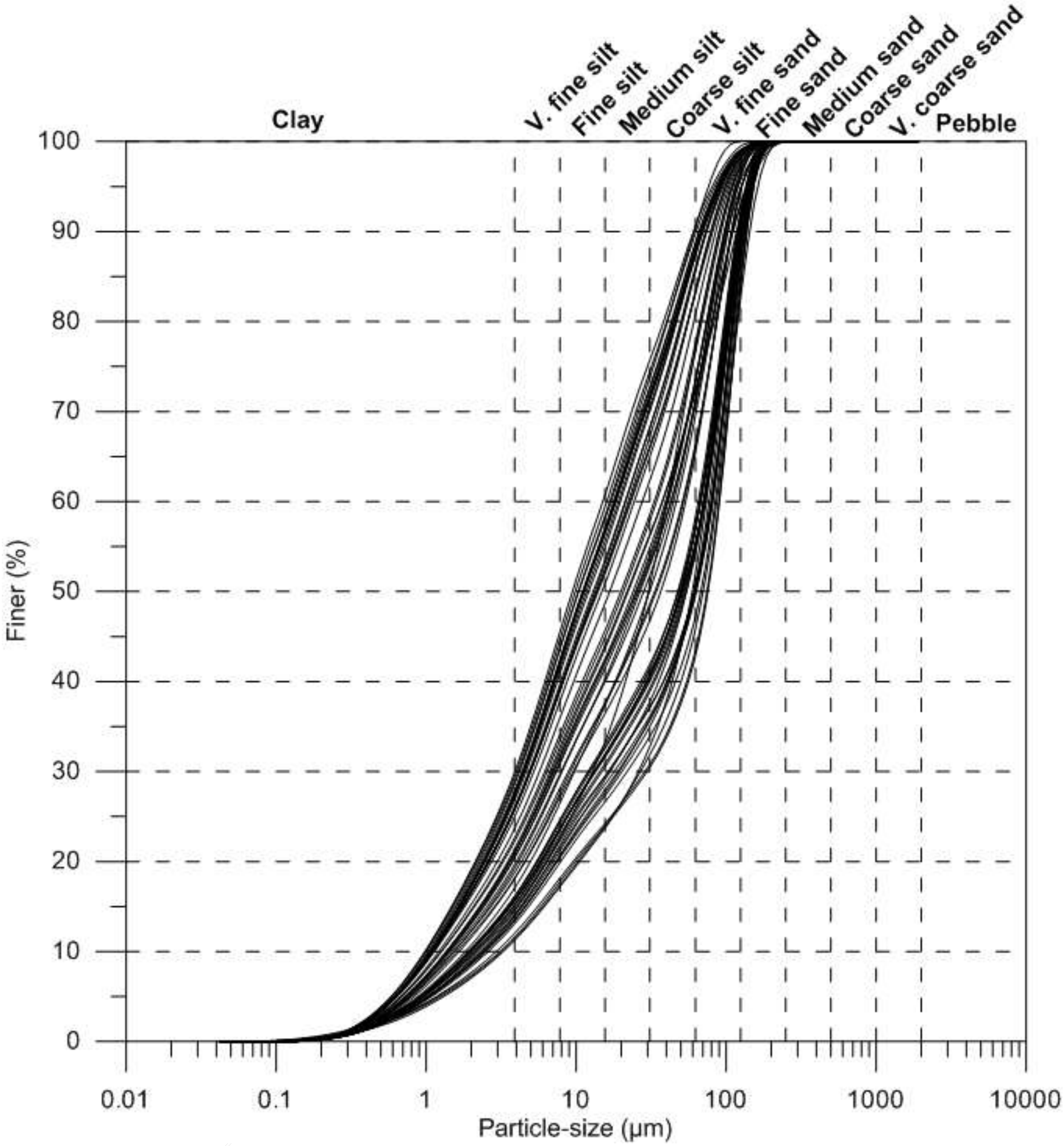

Figure 32 PSD curves of point samples from core VC 3b

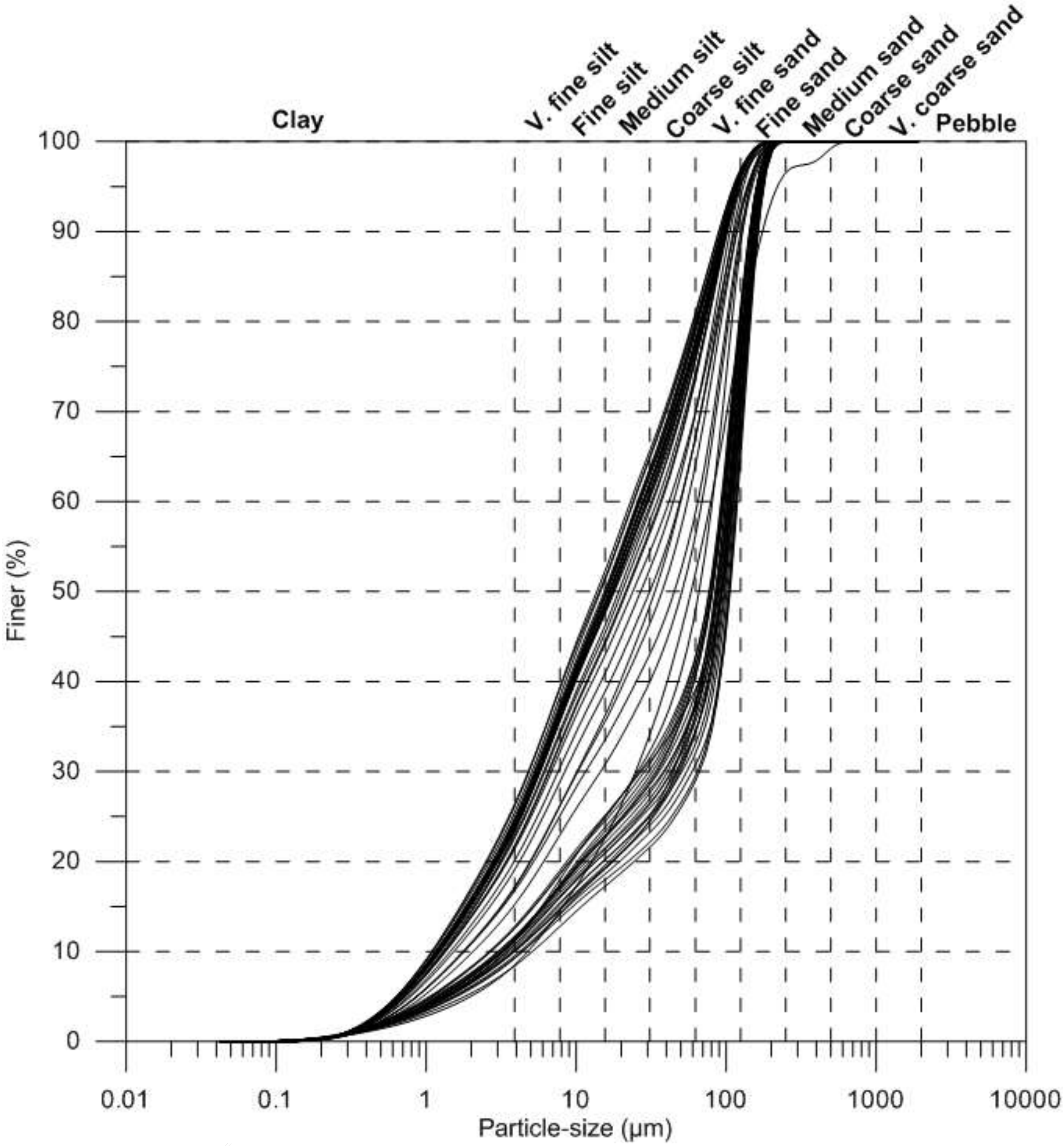

Figure 33 PSD curves of point samples from core VC 4a

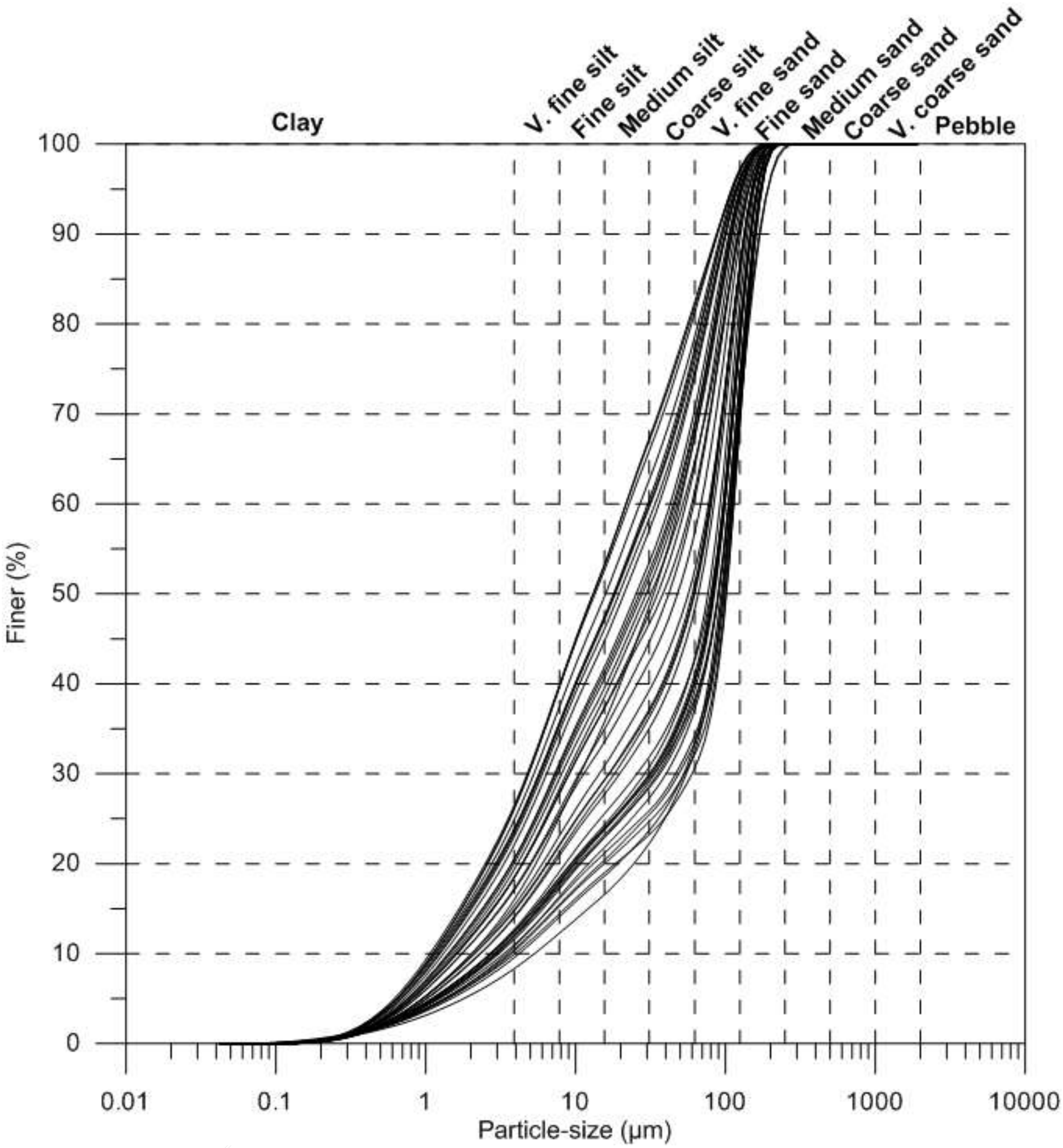

Figure 34 PSD curves of point samples from core VC 4b

Table 8 PSD values derive from PSA analysis

Core ID	D50 (µm)	D60 (µm)	D10 (µm)
VC1a	109	121	6
VC1b	65	81	2.6
VC2	25	41	1.7
VC3a	59	78	2.4
VC3b	60	80	2.5
VC4a	109	121	6
VC4b	100	120	3.9

3.5.4 Foundation geometry

The foundation geometry plays a pivotal role in the process of scour formation and in that regard, the key parameters include the diameter and height of the foundation. For the purposes of this study, the foundation has assumed to comprise a monopile with a diameter between 6 and 10m, representative of monopile geometries needed to support next generation turbines for offshore wind turbines between 2020 and 2030.

3.6 Geotechnical Assessment

In total, 17 Cone Penetration Tests (CPTs) were undertaken across the site as part of the Developing Geotechno-stratigrphies (Leg 2) survey (cruise CE14001) (Figure 35). The CPT traces penetrated from between 3.12m below mudline (bml) to a maximum penetration depth of 30.05m bml.

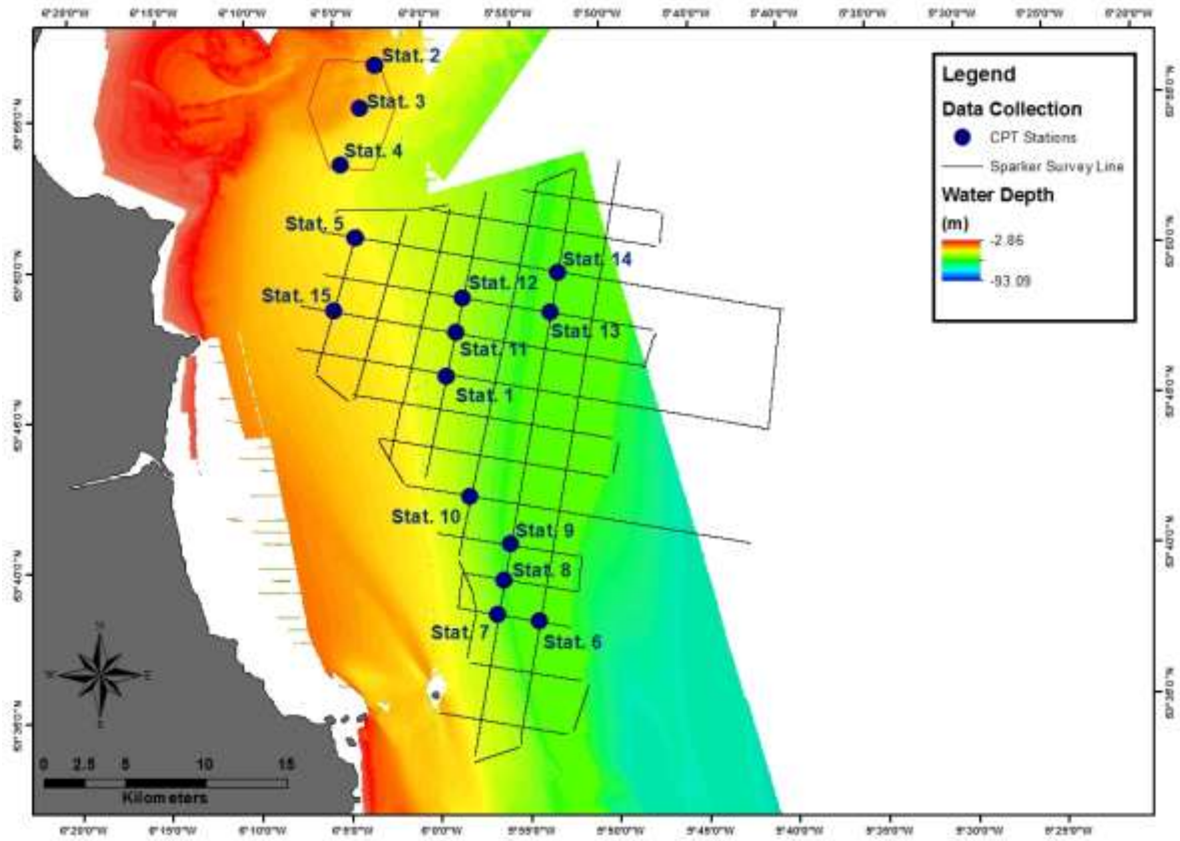

Figure 35 Site investigation location plan

The CPT trace, tip resistances are shown in Figure 36 below where two distinct groups of traces are evident, (i) CPTs that were terminated within the first 5 meters and (ii) those that extended to deeper depths. The CPTs that terminated in the shallower deposits typically showed more variability and higher values with the tip resistance, qT, reaching values between 5 and 10MPa. This is suggestive of shallow granular deposits (sands/gravels). The deeper CPTs show a more consistent behaviour with very low CPT tip resistances (<1MPa) to significant depths. It is worth noting that the data quality required some pre-screening and no pore pressures or friction measurements are available for many of the shallow traces. This means the shallow traces cannot be plotted on classification charts and is difficult to examine the material behaviour in significant detail from the CPT data. The remaining traces, where full data is available, were used to derive classification charts illustrating the material behaviour. These charts are shown as Figure 36 which shows the data over the full depth of the CPT pushes (left hand image) and also concentrates on the upper 3m (right hand image), which is most relevant to scour analysis. These classification charts are based on calibrated data from around the world where CPT data has been undertaken beside borehole data, which has then facilitated a number of zones of material behaviour to be established. The Robertson chart adopted in this study uses 9 zones of material behaviour based on normalised values of Friction Ratio and normalised cone resistance (Qt). The descriptions of each zone are provided below the classification chart. As can be seen from the Charts, the dominant material behaviour across the range of measurements is that of Zone 3 "*Clays to Silty Clays*", the second most dominant zone is #1, "Sensitive, fine grained". When focusing in on the first three meters, which are of most relevance to the present scour study (see Figure 38), it is apparent that the most significant scatter occurs over the top meter, where some silts and clay mixtures are observed alongside some intermittent sands/gravels. Note, due to the nature of the formulation used to normalise the CPT cone resistance, where the denominator is dependent on the in-situ stresses, the very shallow data plotted in the classification charts are least reliable – therefore some of the observed scatter may be due to the normalisation procedures and low effective stresses in the first 200 to 300mm below mudline. Below the first meter, (1-3m bml), the fine grained Clays to Silty Clays dominant the behaviour.

Focussing on the fine-grained material, it is possible to derive a profile of undrained shear strength using a correlation and an assumed NkT factor for similar materials. Adopting an NkT factor of 15 yields the undrained shear strength profile, which is shown in Figure 39. This normalisation also relies on the vertical effective stress, which can be derived from the bulk unit weight (density) of the material, which for the silty Clays considered at this site a value of 16kN/m3 is deemed appropriate. Also shown on Figure 39 is the vertical effective stress multiplied by a constant factor of 0.3, which for a normally consolidated silty Clay could represent a reasonable first estimate of the undrained shear strength. It is clear from the data, that the factored effective stress significantly overestimates the undrained shear strength profile correlated from the CPT data. The CPT data yields a near constant undrained shear strength measurement of 10kPa, which is independent of depth. Given the low values of undrained shear strength and the constant profile, it is possible that this deposit is in fact underconsolidated.

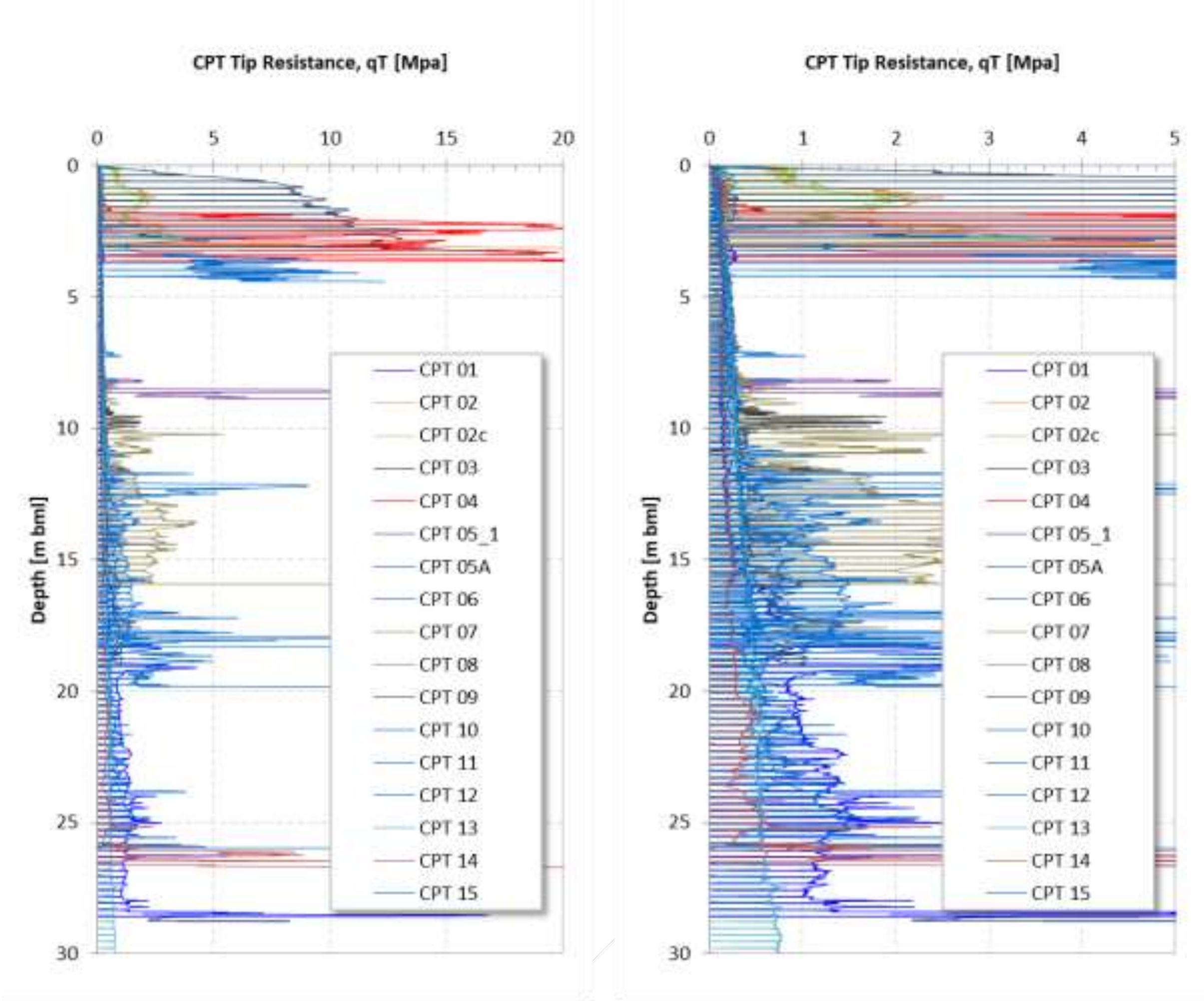

Figure 36 CPT tip resistance, qT (two different horizontal scales shown)

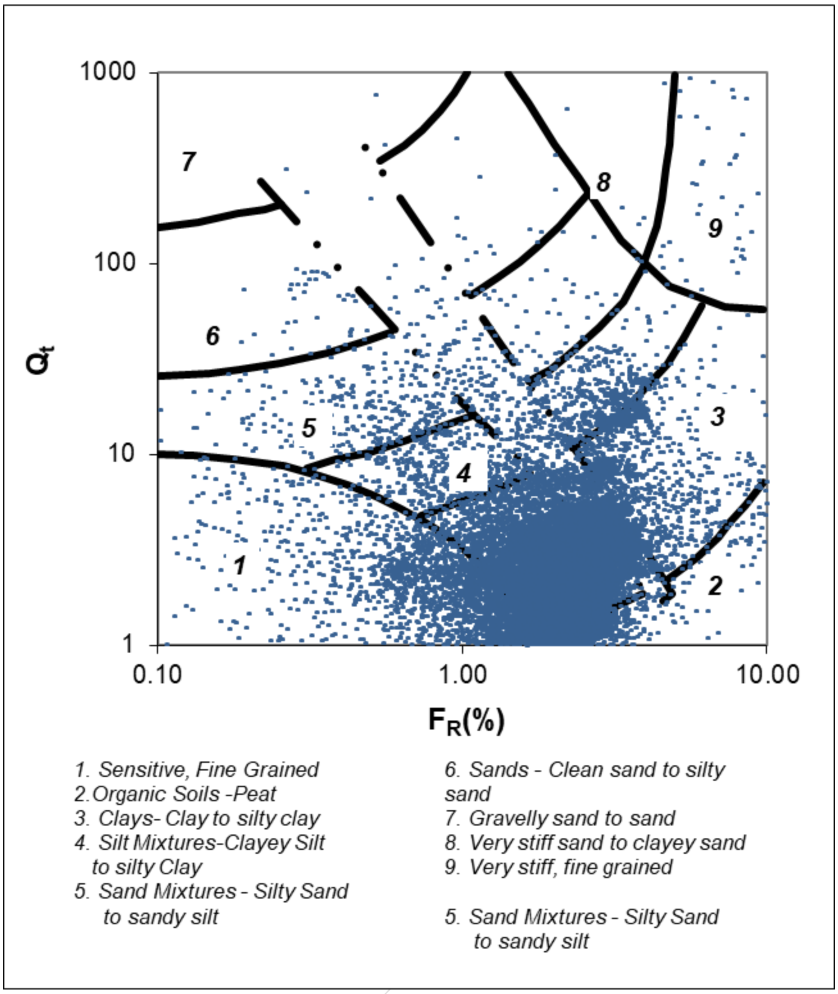

Figure 37 Robertson classification chart (for all available data)

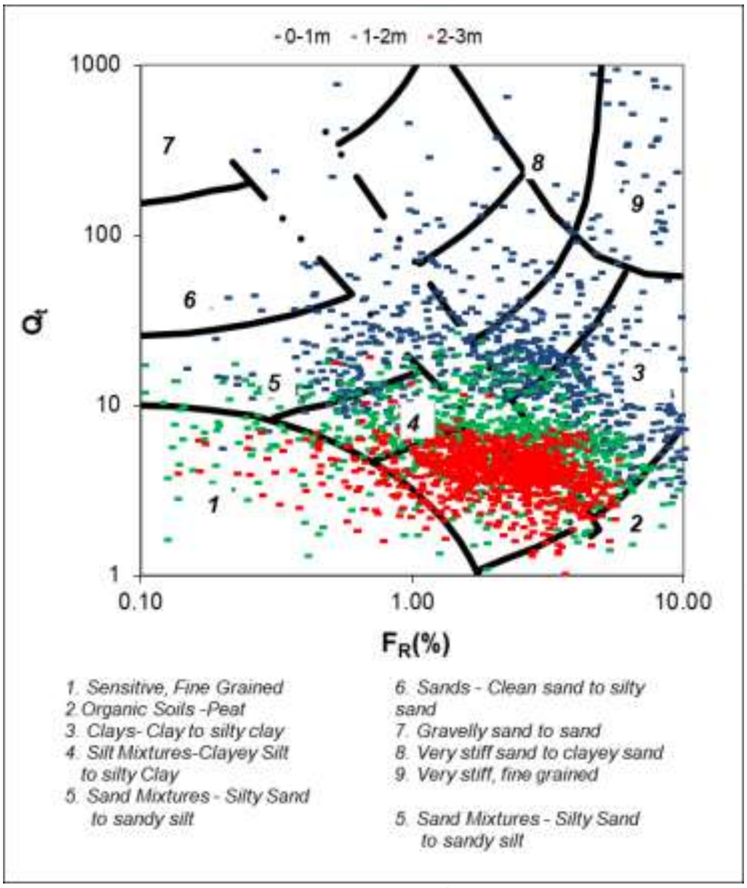

Figure 38 Robertson classification chart (for initial 3m below mudline)

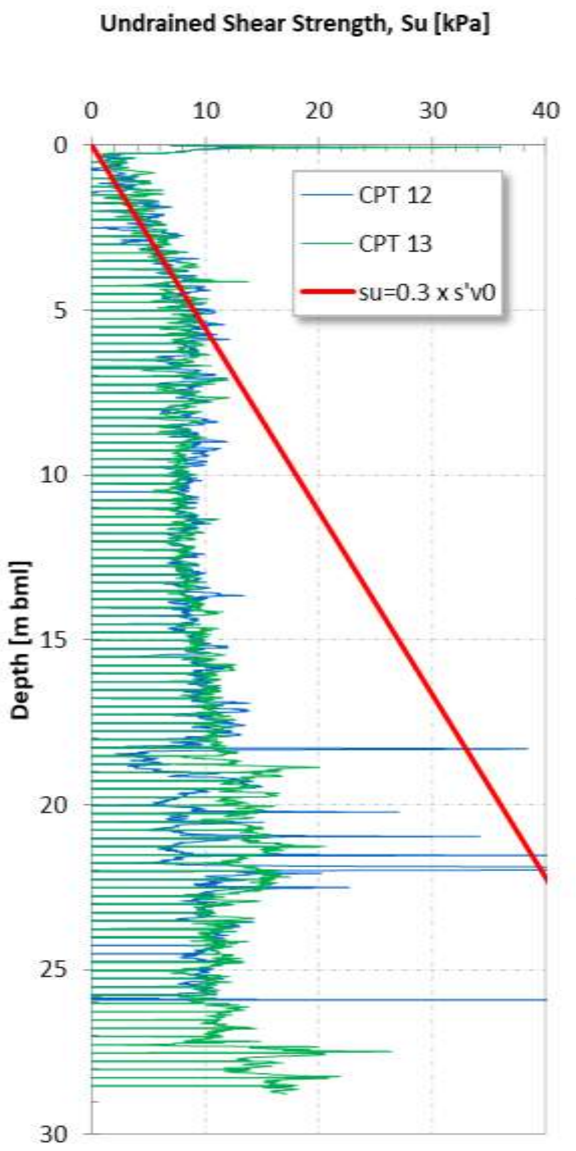

Figure 39 Undrained shear strength (CPT 13 and 14)

3.7 Scour Analysis

A preliminary scour assessment was carried out according to the deterministic approach outlined by Whitehouse (1998). This involved the input of site data in the procedures described in Section 2.2 to determine the susceptibility of the seabed to wave- and/or current-induced scour. The analysis took into account the seasonal variability of the wave climate condition in the broader WISMB area (Table 9), as well as, spatial distribution of water depth and sediment size as obtained during previous ground truthing campaign at different core locations (Table 10).

Table 9 Seasonal averages for wave climate parameters (based on wave data from M2 buoy)

Year	Time of year	Wave Period (s)	Wave Height (m)
2013-2018	Jan - Mar	4.6	1.56
	Apr - Jun	4	0.86
	Jul - Sept	3.9	0.85
	Oct - Dec	4.5	1.48

Table 10 D50 sediment-size and water depth at core locations

Location	d50 (µm)	Water depth (m)
VC1a	62	29.5
VC1b	65	29.5
VC2	25	40
VC3a	59	36.4
VC3b	50	36.4
VC4a	109	41
VC4b	100	41

In order to assess the sediment mobility potential in the WISMB area, the values of critical bed shear stress, τ_{cr}, were first calculated at different core locations. The results were then compared against the wave-induced bed shear stress values, τ_w, to inform the susceptibility of the seabed to scour due to wave effects. The impact of currents was subsequently incorporated in the analysis by back-calculating the minimum (depth-averaged) current velocities, $\overline{U}_{cr}$, required to mobilise the sediments.

3.7.1 Critical bed shear stress

The threshold bed shear stress values (due to wave and/or current effects) to induce sediment mobility at various core locations are provided in Table 11. The assessment takes into account the median sediment size and the sediment density at various locations.

Table 11 Minimum bed shear stress required for sediment mobilisation

Location	Critical bed shear stress (N/m2)
VC1a	0.054
VC1b	0.056
VC2	0.022
VC3a	0.051
VC3b	0.043
VC4a	0.094
VC4b	0.086

3.7.2 Scour potential due to wave effects

In order to assess the impact of waves on the scour potential, the wave data from the M2 buoy was used to calculate the wave–driven near bed orbital velocities, U_w. The resulting near bed velocities were then converted to the corresponding wave related bed shear stress values, τ_w (Table 12), which allowed comparison against the critical shear stress values, τ_{cr} (Table 11). The analysis suggests that, often, the wave-induced bed shear stress (τ_w) by itself is sufficient to exceed the critical shear stress threshold (τ_{cr}).

Table 12 Wave-induced bed shear stress

Location	Wave-induced bed shear stress, τw (m/s)			
	Jan – Mar	Apr - Jun	Jul – Sept	Oct - Dec
VC1a	0.139	0.045	0.042	0.124
VC1b	0.142	0.046	0.043	0.127
VC2	0.048	0.014	0.013	0.043
VC3a	0.091	0.028	0.026	0.081
VC3b	0.084	0.025	0.023	0.074
VC4a	0.099	0.029	0.027	0.087
VC4b	0.094	0.028	0.025	0.083

3.7.3 Scour potential due to current effects

The effect of current velocity was considered in the analysis by back-calculating the values of depth-averaged current velocity ($\bar{U}^*$) required for the current bed shear stress (τ_c) to exceed τ_{cr}. The results of back-analysis is summarised in Table 13, where the minimum required current velocity (to initiate scour) is seen to vary between 0.18 and 0.34 m/s.

Table 13 Minimum depth averaged current speed necessary for sediment mobility, excluding wave effects

Location	Min. Current speed, Ū*, necessary to exceed threshold bed shear stress, without the presence of waves (m/s)
VC1a	0.263
VC1b	0.268
VC2	0.181
VC3a	0.261
VC3b	0.243
VC4a	0.343
VC4b	0.331

3.7.4 Scour potential due to combined wave-current effects

The minimum current speed necessary to induce sediment mobility is reduced once the impact of waves is incorporated in the analysis. Table 14 summarises the thresholds for depth-averaged current velocity to initiate sediment mobility with the presence of waves.

Table 14 Minimum depth averaged current speed necessary for sediment mobility, at the presence of wave effects

Location	Min. Current speed, Ū*, necessary to exceed threshold bed shear stress, with the presence of waves (m/s)			
	Jan – Mar	Apr - Jun	Jul – Sept	Oct - Dec
VC1a	0.000	0.107	0.124	0.000
VC1b	0.000	0.115	0.131	0.000
VC2	0.000	0.105	0.113	0.000
VC3a	0.000	0.176	0.184	0.000
VC3b	0.000	0.156	0.164	0.000
VC4a	0.000	0.285	0.291	0.094
VC4b	0.000	0.272	0.278	0.063

Figure 40 shows the reduction in threshold depth-averaged current velocities (necessary to initiate sediment mobility) due to the inclusion of wave effects. It can be seen that at the presence of waves can eliminate the need for contribution of currents to the initiation of seabed mobility during the months of October-March at nearly all core locations, while reducing the required current velocity between 15% and 60% between the months of April-September. In addition, it can be observed that the contribution of waves to the sediment mobility become less prominent as we move from VC1 location in the northern part of WISMB area toward VC4 in the southern part.

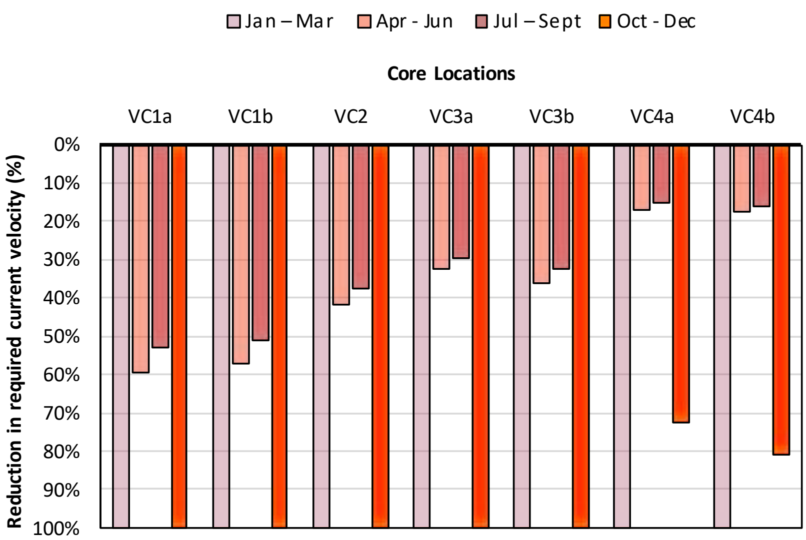

Figure 40 Reduction in threshold current velocities required for mobilisation of seabed sediments due to the presence of waves.

Figure 41 shows the impact of seasonal variability on the threshold current velocities required to initiate scour. The results imply that the seabed in the WISMB area is likely to undergo scour in the period from October to March (at nearly all core locations) due to the impact of waves with minimal or no contribution from current velocities. In the period from April to September, however, a minimum depth-averaged current velocity may be required in order to initiate scour. It can be observed that the required current velocity in this period varies between 0.1 and 0.29 m/s. In addition, a generally increasing trend can be observed as we move between locations VC1 to VC4, showing correlation with water depth (as the water depth increases the contribution of waves become less dominant and higher current velocities are required to mobilise the sediments).

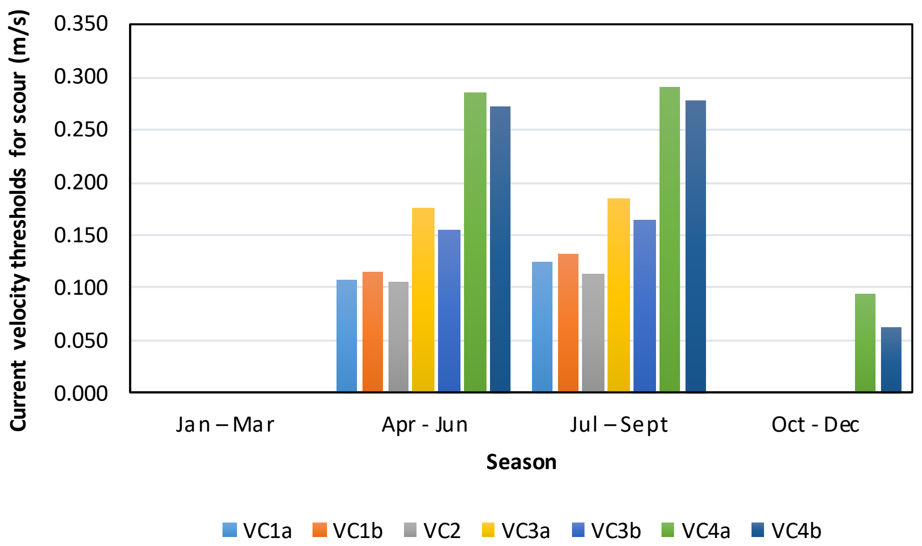

Figure 41 Required current velocity to induce seabed mobilisation in the WISMB area - Seasonal variability

In the preceding analysis, τ_{cr} represents the ambient (i.e. pre-installation) conditions at the seabed. To determine the threshold of scour due to installation (introduction of obstacles on the seabed), a bed shear stress amplification factor (*M*) shall be used (i.e. τ_{cr}/M). The introduction of this factor can significantly reduce the critical shear stress threshold (τ_{cr}), suggesting that the insertion of a foundation structure (e.g. monopole) would have a significant impact on inducing sediment mobility and scour. The amplification factor can vary depending on the shape and size of the structure. A preliminary assessment based on an upper and lower bound estimates of M, showed that the presence of waves alone can be sufficient to induce scour in the proximity of any seabed structure (irrespective of seasonal conditions), while the threshold current velocity to initiate scour can be reduced between 50% and 67% depending on the geometry/size of the seabed obstacle.

The details of calculations for the threshold bed shear stress, as well as the bed shear stress induced due to the action of waves and/or currents are provided in Appendix A.

4 Summary and Conclusions

The sediments of the Western Irish Sea Mud Belt can be divided, generally, into two units: a lower, highly heterogeneous, glacial deposit and a homogenous, fine-grained marine deposit. The latter of which was the primary focus of this study with respect to scour susceptibility. The fine-grained marine sediments are found at the surface and to a depth of between 0.8 and 26.5 mbsl. The sediments appear to be under-consolidated with relatively low shear strength. At the surface, sediments show a general trend of fining northward across the stud area.

Previously, it was suggested that the current speeds in the WISMB were insufficient to mobilise sediment and initiate scour without obstruction (Callaway et al., 2009; Holmes & Tappin, 2005). However, the analysis in Section 3.7 suggests that wave induced bed stress are sufficient to generate sediment mobility without the necessity of relatively strong tidal currents (Table 12).

The presence of obstacles on the seabed in the WISMB can generate significant amounts of scour (Section 3.3) with scour signatures revealing variations in localised seabed hydrodynamics, which, very often, are at odds with generalised regionalised modelled output (Figure 17). This suggests that local phenomena could have a strong effect on hydrodynamics and, hence, sediment mobility and scour. In this instance, the development of a seasonal gyre in the WISMB could be significant in variation in WISMB seabed hydrodynamics. Analysis in Section 3.7 suggests that the presence of wind turbine foundations would have a significant effect on lowering sediment mobility thresholds.

After previous qualitative studies (notably Callaway et al. (2009) and Caston (1975)), this study was the first attempt at quantifying the scour potential of sediments in the WIMSB. Based on this summary, we conclude the following:

1. Sediments in the WIMSB are generally fine-grained and geotechnically relatively weak;
2. These sediments are generally not mobile within the area but can be susceptible to scour when seabed obstacles perturb the hydrodynamic regime;
3. The hydrodynamic regime in the WIMSB is more complicated than outlined in previous regional models with seasonal, local phenomena (e.g. a gyre) potentially having a strong effect;
4. There is significant scope for utilising shipwreck scour signatures in verifying future modelling efforts;
5. Wave induced bed shear stresses may play a more important role in seabed sediment mobility than previously noted by previous authors, reducing the necessity of (relatively) strong current velocities to initiate sediment mobility.

To these conclusions, we add the following caveats:

1. Due to the lack of information in the WIMSB, the metocean data used in this study involved a degree of spatial extrapolation, and therefore, may involve fully represent the site condition;
2. Grain-size parameters based on core analysis were taken from a limited geographic distribution across the study site and may not be fully representative of ground condition.

3. While the current study provides valuable insights into the potential for sediment mobility in the WIMSB area, the scour susceptibility predictions shall still be viewed as first estimates due to the limited site data available and the preliminary methodology adopted. It is therefore expected that the findings may be subject to alterations upon the availability of more accurate site specific data and the adoption of detailed scour modelling techniques.

5 Guidelines and Recommendations

As an initial attempt at assessing sedimentary mobility, the flow chart presented by Whitehouse (1998) (Figure 9) proved a useful tool and guideline. Using readily available data and straightforward calculations, it offers the user an easy to follow method with which to generate a basic understanding of the potential for sediment mobility that incorporates the significant environmental factors of sediment, waves and currents. We would recommend adapting this method at an early stage of any sediment mobility or scour assessment. Furthermore, Whitehouse (1998) also offers a more thorough guide to a probabilistic approach in considering the likelihood of sediment being mobilised around a completed structure.

As identified in the summary, the shortcoming in the application of this method came from the paucity of site-specific metocean data. Generally, understanding regarding the hydrodynamic regime of the WISMB is suffering from a paucity of information. Therefore, we make the following recommendations:

1. Execution of a full metocean survey to include data collection pertaining to site specific wave regime and seabed current conditions;
2. Repeat MBES surveys at selected shipwreck sites would add much valued information regarding scour development from which key understandings about scour processes could be garnered;
3. A specific hydrodynamical modelling exercise of the WISMB using this information, and cognisant of localised phenomena, would be of great value in future morphodynamical modelling and scour assessment efforts;
4. A greater density of core coverage with particle-size analysis across the WISMB is necessary to extend the coverage of this study and verify some of the findings with respect to the influence of grain-size variation in scour susceptibility.
5. With the availability of further metocean and grain-size data, we recommend the application of other scour assessment calculations identified in this study to compare with the results of the method by Whitehouse (1998).

Acknowledgments

The authors are most grateful to Prof. Andy Wheeler of University College Cork for permission to use the ISMA and GOST data as part of this study. We are also grateful to Charise McKeon of GSI for supplying shipwreck MBES data.

References

Belderson, R. H. (1964). Holocene sedimentation in the western half of the Irish Sea. *Marine Geology*, *2*(1963), 147–163.

Belderson, R. H., & Stride, A. H. (1966). Tidal current fashioning of a basal bed. *Marine Geology*, *4*, 237–257.

BGS. (2015). Geology of the seabed and shallow subsurface : The Irish Sea, 42.

Breusers, H. N. C., Nicollet, G., & Shen, H. W. (1977). Local scour around cylindrical piers. *Journal of Hydraulic Research*, *15*(3), 211–252.

Callaway, A., Smyth, J., Brown, C. J., Quinn, R., Service, M., & Long, D. (2009). The impact of scour processes on a smothered reef system in the Irish Sea. *Estuarine, Coastal and Shelf Science*, *84*(3), 409–418. https://doi.org/10.1016/j.ecss.2009.07.011

Caston, G. F. (1975). Igneous Dykes and Associated Scour Hollows of the North Channel, Irish Sea. *Marine Geology*, *18*, 77–85.

Coughlan, M., Wheeler, A. J., Dorschel, B., Lordan, C., Boer, W., Gaever, P. va., … Mörz, T. (2015). Record of Anthropogenic Impact on the Western Irish Sea Mud Belt. *Anthropocene*, (0). https://doi.org/http://dx.doi.org/10.1016/j.ancene.2015.06.001

Det Norske Veritas. (2007). *Design of Offshore Wind Turbine Structures*.

Det Norske Veritas. (2014). DNV-OS-J101 Design of Offshore Wind Turbine Structures.

Dickson, C., & Whatley, R. C. (1993). The Biostratigraphy of a Holocene borehole from the Irish Sea. In *Proceedings of 2nd European Ostracodologists Meeting* (pp. 145–148). Glasgow: British Micropalaeontological Society, London.

Dobson, M. R., Evans, W. E., & James, K. H. (1971). The sediment on the floor of the southern Irish

Sea. *Marine Geology*, *11*, 27–69.

Folk, R. L., & Ward, W. C. (1957). Brazos River Bar: a study in the significance of grain size parameters. *Journal of Sedimentary Petrology*, *27*(1), 3–26.

Hill, A. E., Brown, J., & Fernand, L. (1997). The summer gyre in the Western Irish Sea: Shelf sea paradigms and management implications. *Estuarine, Coastal and Shelf Science*, *44*, *Supple*(0), 83–95. https://doi.org/http://dx.doi.org/10.1016/S0272-7714(97)80010-8

Holmes, R., & Tappin, D. R. (2005). *DTI Strategic Environmental Assessment Area 6, Irish Sea, seabed and surficial geology and processes, British Geological Survey Commissioned Report, CR/05/057*.

Horsburgh, K. J., Hill, A. E., Brown, J., Fernand, L., Garvine, R. W., & Angelico, M. M. P. (2000). Seasonal evolution of the cold pool gyre in the western Irish Sea. *Progress in Oceanography*, *46*(1), 1–58. https://doi.org/http://dx.doi.org/10.1016/S0079-6611(99)00054-3

Jackson, D. I., Jackson, A. A., Evans, D., Wingfield, R. T. R., Barnes, R. P., & Arthur, M. J. (1995). *United Kingdom offshore regional report: the geology of the Irish Sea*. London: British Geological Survey.

Johnson, L. R. (1983). The transport mechanisms of clay and fine silt in the north Irish Sea. *Marine Geology*, *52*(1–2), 33–41. https://doi.org/10.1016/0025-3227(83)90017-8

Kershaw, P. J. (1986). Radiocarbon dating of Irish Sea sediments. *Estuarine, Coastal and Shelf Science*, *23*(3), 295–303. https://doi.org/http://dx.doi.org/10.1016/0272-7714(86)90029-6

Kirby, R., Parker, W. R., Pentreath, R. J., & Lovett, M. B. (1983). *Sedimentation studies relevant to low-level radioactive effulent dispersal in the Irish Sea. Part III. An evaluation of possible mechanisms for the incorporation of radionuclides into marine sediments*.

Komar, P. D., & Miller, M. C. (1973). The threshold of sediment movement under oscillatory water waves. *Journal of Sedimentary Petrology*, *43*(4), 1101–1110. https://doi.org/10.1306/74D7290A-2B21-11D7-8648000102C1865D

Lewis, M., Neill, S. P., Robins, P. E., & Hashemi, M. R. (2015). Resource assessment for future generations of tidal-stream energy arrays. *Energy*, *83*(March), 403–415. https://doi.org/10.1016/j.energy.2015.02.038

Lunne, T., Robertson, P. K., & Powell, J. J. M. (1997). *Cone Penetration Testing In Geotechnical Practice*. London: Blackie Academic & Professional.

Matutano, C., Negro, V., López-Gutiérrez, J. S., & Esteban, M. D. (2013). Scour prediction and scour protections in offshore wind farms. *Renewable Energy*, *57*, 358–365. https://doi.org/10.1016/j.renene.2013.01.048

Mitchell, P. I., Condren, O. M., Leo, L., & Mcmahon, C. A. (1999). Trends in plutonium , americium and radiocaesium accumulation and long-term bioavailability in the western Irish Sea mud basin. *Journal of Environmental Radioactivity*, *44*, 223–251.

Olbert, A. I., Dabrowski, T., Nash, S., & Hartnett, M. (2012). Regional modelling of the 21st century climate changes in the Irish Sea. *Continental Shelf Research*, *41*, 48–60. https://doi.org/http://dx.doi.org/10.1016/j.csr.2012.04.003

Pantin, H. M. (1977). Quaternary sediments of the northern Irish Sea. In C. Kidson & M. Tooley (Eds.), *The Quaternary History of the Irish Sea* (pp. 27–54). Liverpool: Seel House.

Robinson, I. S. (1979). The tidal dynamics of the Irish and Celtic Seas. *Journal of Geophysical Research*, *56*, 159–197.

Sumer, B. M., & Fedose, J. (2002). *The mechanics of scour in the marine environment*. Singapore: World Scientific.

Sumer, B. M., Fredose, J., & Christensen, N. (1992). Scour around vertical pile in waves. *Journal of Waterway, Port, Coastal and Ocean Engineering*, *8*(1), 15–31.

Sumer, B. M., & Fredsoe, J. (2002). *The mechanics of scour in the marine environment*. Singapore: World Scientific.

Uehara, K., Scourse, J. D., Horsburgh, K. J., Lambeck, K., & Purcell, A. P. (2006). Tidal evolution of the northwest European shelf seas from the Last Glacial Maximum to the present. *Journal of Geophysical Research*, *111*. https://doi.org/10.1029/2006JC003531

Van Landeghem, K. J. J., Uehara, K., Wheeler, A. J., Mitchell, N. C., & Scourse, J. D. (2009). Post-glacial sediment dynamics in the Irish Sea and sediment wave morphology: Data–model comparisons. *Continental Shelf Research*, *29*(14), 1723–1736. https://doi.org/http://dx.doi.org/10.1016/j.csr.2009.05.014

Wheeler, A. J., & Party, S. (2009). *Irish Sea Marine Assessment (ISMA)* (Vol. Cruise Rep).

Wheeler, A. J., & Party, S. (2014). *Developing Geotechno - stratigraphies (Leg 2)*.

Whitehouse, R. (1998). Scour at Marine Structures: A Manual for Practical Applications.

https://doi.org/10.1680/sams.26551

Whitehouse, R. J. S., & Harris, J. M. (2014). Scour Prediction Offshore and Soil Erosion Testing. In *Proceedings of the OMAE2014 - ASME 2014 33rd International Conference on Ocean, Offshore and Arctic Engineering*. San Francisco, California. https://doi.org/10.1115/OMAE2014-24271

Whitehouse, R. J. S., Harris, J. M., Sutherland, J., & Rees, J. (2011). The nature of scour development and scour protection at offshore windfarm foundations. *Marine Pollution Bulletin*, *62*(1), 73–88. https://doi.org/10.1016/j.marpolbul.2010.09.007

Whitehouse, R. J. S., Harris, J., Sutherland, J., & Rees, J. (2008). An assessment of field data for scour at offshore wind turbine foundations. *4th International Conference on Scour and Erosion Tokyo*, (November), 329–335.

Whitehouse, R. J. S., Sutherland, J., & Harris, J. M. (2011). Evaluating scour at marine gravity foundations. *Proceedings of the Institution of Civil Engineers-Maritime Engineering*, *164*(4), 143–157. https://doi.org/DOI 10.1680/maen.2011.164.4.143

Williams, S. J., Kirby, R., Smith, T. J., & Parker, W. R. (1981). *Sedimentation studies relevant to low level radioactive effulent dispersal in the Irish Sea. II. Sea bed morphology, sediments and shallow sub-bottom stratigraphy of the eastern Irish Sea. Report No. 120, Institute of Oceanographic Sciences (Unpublished m*.

Yuan, F., Bennell, J. D., & Davis, A. M. (1992). Acoustic and physical characteristics of gassy sediments in the western Irish Sea. *Continental Shelf Research*, *12*(10), 1121–1134.

APPENDIX A

DETAILS OF SCOUR ASSESSMENT CALCULATIONS

Table 15 Details of calculation of critical bed shear stress

Core Location	D50 (µm)	Ѳcr	g (m/s2)	Sediment Density (kg/m3)	Water Density (kg/m3)	Critical bed shear stress (N/m2)
VC1a	62	0.0905	9.8	2000	1026	0.054
VC1b	65	0.0905	9.8	2000	1026	0.056
VC2	25	0.0905	9.8	2000	1026	0.022
VC3a	59	0.0905	9.8	2000	1026	0.051
VC3b	50	0.0905	9.8	2000	1026	0.043
VC4a	109	0.0905	9.8	2000	1026	0.094
VC4b	100	0.0905	9.8	2000	1026	0.086

Table 16 Details of calculation of current-induced bed shear stress

Core Location	D50 (µm)	Water Depth (m)	Critical shear stress (N/m2)	Drag coefficient	Water Density (kg/m3)	Threshold current velocity, Ū* (m/s)
VC1a	62	29.5	0.054	0.0008	1026	0.263
VC1b	65	29.5	0.056	0.0008	1026	0.268
VC2	25	40	0.022	0.0006	1026	0.181
VC3a	59	36.4	0.051	0.0007	1026	0.261
VC3b	50	36.4	0.043	0.0007	1026	0.243
VC4a	109	41	0.094	0.0008	1026	0.343
VC4b	100	41	0.086	0.0008	1026	0.331

Table 17 Minimum depth averaged current speed necessary for sediment mobility, at the presence of wave effects

Core Location	D50 (µm)	Time of year	Wave Period (s)	Wave Height (m)	Water Depth (m)	Wave Length (m)	Wave Number	Wave Orbital Velocity (m/s)	z0 (m)	Amplitude of the orbital wave motion (m)	Wave friction factor	Water Density (kg/m3)	Wave-induced bed shear stress (N/m2)
VC1a	62	Jan - Mar	4.6	1.56	29.5	78.2	0.080	0.201	0.000062	0.147	0.007	1026	0.139
	62	Apr - Jun	4.0	0.86	29.5	68.0	0.092	0.089	0.000062	0.057	0.011	1026	0.045
	62	Jul - Sept	3.9	0.85	29.5	66.3	0.095	0.084	0.000062	0.052	0.012	1026	0.042
	62	Oct - Dec	4.5	1.48	29.5	76.5	0.082	0.185	0.000062	0.132	0.007	1026	0.124
VC1b	65	Jan - Mar	4.6	1.56	29.5	78.2	0.080	0.201	0.000065	0.147	0.007	1026	0.142
	65	Apr - Jun	4.0	0.86	29.5	68.0	0.092	0.089	0.000065	0.057	0.011	1026	0.046
	65	Jul - Sept	3.9	0.85	29.5	66.3	0.095	0.084	0.000065	0.052	0.012	1026	0.043
	65	Oct - Dec	4.5	1.48	29.5	76.5	0.082	0.185	0.000065	0.132	0.007	1026	0.127
VC2	25	Jan - Mar	4.6	1.56	40.0	91.1	0.069	0.135	0.000025	0.099	0.005	1026	0.048
	25	Apr - Jun	4.0	0.86	40.0	79.2	0.079	0.057	0.000025	0.036	0.009	1026	0.014
	25	Jul - Sept	3.9	0.85	40.0	77.2	0.081	0.053	0.000025	0.033	0.009	1026	0.013
	25	Oct - Dec	4.5	1.48	40.0	89.1	0.071	0.124	0.000025	0.088	0.005	1026	0.043
VC3a	59	Jan - Mar	4.6	1.56	36.4	86.9	0.072	0.154	0.000059	0.113	0.008	1026	0.091
	59	Apr - Jun	4.0	0.86	36.4	75.5	0.083	0.066	0.000059	0.042	0.013	1026	0.028
	59	Jul - Sept	3.9	0.85	36.4	73.7	0.085	0.062	0.000059	0.038	0.013	1026	0.026
	59	Oct - Dec	4.5	1.48	36.4	85.0	0.074	0.141	0.000059	0.101	0.008	1026	0.081
VC3b	50	Jan - Mar	4.6	1.56	36.4	86.9	0.072	0.154	0.000050	0.113	0.007	1026	0.084
	50	Apr - Jun	4.0	0.86	36.4	75.5	0.083	0.066	0.000050	0.042	0.012	1026	0.025
	50	Jul - Sept	3.9	0.85	36.4	73.7	0.085	0.062	0.000050	0.038	0.012	1026	0.023
	50	Oct - Dec	4.5	1.48	36.4	85.0	0.074	0.141	0.000050	0.101	0.007	1026	0.074
VC4a	109	Jan - Mar	4.6	1.56	41.0	92.2	0.068	0.131	0.000109	0.096	0.011	1026	0.099
	109	Apr - Jun	4.0	0.86	41.0	80.2	0.078	0.054	0.000109	0.035	0.019	1026	0.029
	109	Jul - Sept	3.9	0.85	41.0	78.2	0.080	0.051	0.000109	0.032	0.020	1026	0.027
	109	Oct - Dec	4.5	1.48	41.0	90.2	0.070	0.119	0.000109	0.085	0.012	1026	0.087
VC4b	100	Jan - Mar	4.6	1.56	41.0	92.2	0.068	0.131	0.000100	0.096	0.011	1026	0.094
	100	Apr - Jun	4.0	0.86	41.0	80.2	0.078	0.054	0.000100	0.035	0.018	1026	0.028
	100	Jul - Sept	3.9	0.85	41.0	78.2	0.080	0.051	0.000100	0.032	0.019	1026	0.025
	100	Oct - Dec	4.5	1.48	41.0	90.2	0.070	0.119	0.000100	0.085	0.011	1026	0.083

Table 18 Minimum depth averaged current speed necessary for sediment mobility, at the presence of wave effects

Core Location	D50 (µm)	Time of year	Wave Period (s)	Wave Height (m)	Water Depth (m)	Water Density (kg/m3)	Critical shear stress (N/m2)	Wave-induced Bed shear stress (N/m2)	Threshold current velocity, Ū* (m/s)
VC1a	62	Jan - Mar	4.6	1.56	29.5	1026	0.054	0.139	0.000
	62	Apr - Jun	4.0	0.86	29.5	1026	0.054	0.045	0.107
	62	Jul - Sept	3.9	0.85	29.5	1026	0.054	0.042	0.124
	62	Oct - Dec	4.5	1.48	29.5	1026	0.054	0.124	0.000
VC1b	65	Jan - Mar	4.6	1.56	29.5	1026	0.056	0.142	0.000
	65	Apr - Jun	4.0	0.86	29.5	1026	0.056	0.046	0.115
	65	Jul - Sept	3.9	0.85	29.5	1026	0.056	0.043	0.131
	65	Oct - Dec	4.5	1.48	29.5	1026	0.056	0.127	0.000
VC2	25	Jan - Mar	4.6	1.56	40.0	1026	0.022	0.048	0.000
	25	Apr - Jun	4.0	0.86	40.0	1026	0.022	0.014	0.105
	25	Jul - Sept	3.9	0.85	40.0	1026	0.022	0.013	0.113
	25	Oct - Dec	4.5	1.48	40.0	1026	0.022	0.043	0.000
VC3a	59	Jan - Mar	4.6	1.56	36.4	1026	0.051	0.091	0.000
	59	Apr - Jun	4.0	0.86	36.4	1026	0.051	0.028	0.176
	59	Jul - Sept	3.9	0.85	36.4	1026	0.051	0.026	0.184
	59	Oct - Dec	4.5	1.48	36.4	1026	0.051	0.081	0.000
VC3b	50	Jan - Mar	4.6	1.56	36.4	1026	0.043	0.084	0.000
	50	Apr - Jun	4.0	0.86	36.4	1026	0.043	0.025	0.156
	50	Jul - Sept	3.9	0.85	36.4	1026	0.043	0.023	0.164
	50	Oct - Dec	4.5	1.48	36.4	1026	0.043	0.074	0.000
VC4a	109	Jan - Mar	4.6	1.56	41.0	1026	0.094	0.099	0.000
	109	Apr - Jun	4.0	0.86	41.0	1026	0.094	0.029	0.285
	109	Jul - Sept	3.9	0.85	41.0	1026	0.094	0.027	0.291
	109	Oct - Dec	4.5	1.48	41.0	1026	0.094	0.087	0.094
VC4b	100	Jan - Mar	4.6	1.56	41.0	1026	0.086	0.094	0.000
	100	Apr - Jun	4.0	0.86	41.0	1026	0.086	0.028	0.272
	100	Jul - Sept	3.9	0.85	41.0	1026	0.086	0.025	0.278
	100	Oct - Dec	4.5	1.48	41.0	1026	0.086	0.083	0.063